Design and Development of a Radiation Protection Assistant Robot

Jahan Zeb

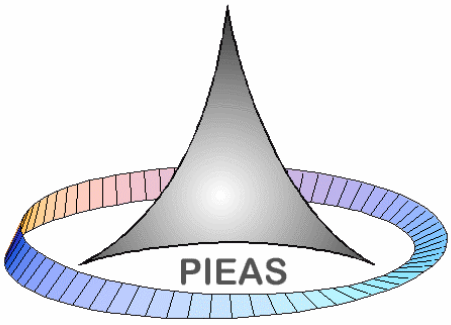

Department of Electrical Engineering

Pakistan Institute of Engineering & Applied Sciences

Islamabad-45650, Pakistan

November 2009

Design and Development of a Radiation Protection Assistant Robot

Jahan Zeb

Submitted to Pakistan Institute of Engineering & Applied Sciences in partial fulfillment of the requirements for the degree of

Doctor of Philosophy

Department of Electrical Engineering
Pakistan Institute of Engineering & Applied Sciences
Islamabad-45650, Pakistan

November 2009

Declaration

I declare that all material in this thesis which is not my own work has been identified and that no material has previously been submitted and approved for the award of a degree by this or any other university.

Signature: 

Author's Name: Jahan Zeb

It is certified that the work in this thesis is carried out and completed under our supervision.

Supervisor :

Dr. Nasir Ahmad,
Chief Scientist,
PIEAS, Islamabad.

Co-Supervisor :

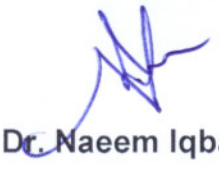

Dr. Naeem Iqbal,
Principal Engineer,
Department of Electrical Engineering,
PIEAS, Islamabad.

Dedicated to my father

Mr. Zafar Ullah Khan (Late)

(May his soul live in eternal peace!)

ACKNOWLEDGEMENTS

All praises are for almighty ALLAH, the most beneficent, the most merciful, WHO endowed me with the strength to finish this work. My humble respect to the Holy Prophet (Peace Be Upon Him) who emphasized to seek knowledge from cradle to grave.

I feel elevated in expressing my gratitude to my supervisor Dr. Nasir Ahmed and co-supervisor Dr. Naeem Iqbal for their help, guidance and valuable suggestions to complete this challenging project in Pakistan.

I am thankful to Dr. Syed Salman Ahmad, Chief Scientist and Dr. Waheed Arshed Deputy Chief Scientist, PINSTECH for the much-needed help and support for higher studies and for the experimentation at Secondary Standard Dosimetry Laboratory (SSDL) of Health Physics Division, PINSTECH. The help provided by Mr. Khalid Mehmood, Principal Scientist and the assistance of Mr. Anees Ahmed Farooqi, Senior Scientific Assistant and Mr. Zia Khurshid, Scientific Assistant-I during the work, is appreciated.

I am grateful to Mr. Farooq Rashid, Principal Scientist, PINSTECH for his help and technical support at every step of this project from designing to fabrication. This project could not have been completed without his help. Gratitude is due to Mr. Abdul Hameed Principal Engineer, Applied Physics Division, PINSTECH is happily acknowledged. The help provided

by Mr. Naveed Rai, Senior Scientist, PAEC and Mr. Akram Naz, Principal Scientist, Equipment Maintenance Division, PINSTECH and his team for the fabrication of PCBs is acknowledged.

I would like to thank Mr. Wazir Ali Wassan Junior Engineer General Service Division (GSD), PINSTECH and other members of GSD for fabricating the mechanical parts of RPAR.

The assistance provided by Mr. Khalid Mehmood Baig and Mr. Inam-ul-Haq GSD, PIEAS for fabricating the mechanical parts of RPAR is acknowledged.

My special thanks are due to my friends and colleagues Dr. Muhammad Munir, Dr. Rameez-ul-Islam, Dr. Muhammad Wasim, Dr. Talat Iqbal, Dr. Umar Karim Mirza and Dr. Abdul Jabbar for the encouragement and help they provided me. The useful discussions with Dr. Nadeem Qaiser and Dr. Muhammad Jaudet Department of Electrical Engineering, PIEAS on various aspects of the project RPAR are appreciated.

The opportunity provided by Pakistan Atomic Energy Commission and the financial support extended by PIEAS are gratefully acknowledged.

Above all, my special and warmest appreciations are for my wife, Dr. Uzma Khan and my daughters Ismah Zeb, Mah Noor and Maleeha Zeb who bore me during tense days of my Ph.D studies.

Last but not the least; I am thankful to all my relatives, friends and well–wishers.

Jahan Zeb

CONTENTS

CONTENTS

Chapter 7: RADIATION EFFECTS ON ELECTRONICS AND ROBOTS

Chapter 8: RADIATION HARDENING STUDY OF RPAR

Chapter 9: COST ANALYSIS OF RPAR

Chapter 10: WIPE TESTING OF SEALED RADIATION SOURCES USING RPAR

CONTENTS

Chapter 11: CONCLUSION AND FUTURE RECOMMENDATIONS

LIST OF FIGURES

LIST OF FIGURES

LIST OF FIGURES

LIST OF TABLES

Symbol	Meaning (common units)
Ø	diameter. (cm)
J	Jacobian.
$\theta(t)$	m-vector of joints variables.
$r(t)$	n-vector of Cartesian variables.
$f(\cdot)$	Continuous non-linear function whose structure and parameters are known for a given manipulator.
d_i	translation or the offset along z_i from the x_{i-1}, i = 1 to 4.
θ_i	rotation in degree about z_i of x_{i-1} into x_i in the right-hand sense.
α_i	rotation or twist in degree about axis x_{i-1} of z_{i-1} into z_i in the right-hand sense.
b_i	displacement along x_{i-1} from z_{i-1} to z_i.
h	Waist height. (cm)
e	Shoulder length. (cm)
f	Elbow length. (cm)
s_1	$\sin\theta_1$
c_1	$\cos\theta_1$
c_{23}	$c_2c_3 - s_2s_3 = \cos(\theta_2 + \theta_3)$
s_{23}	$s_2c_3 + s_3c_2 = \sin(\theta_2 + \theta_3)$
P_x	final Gripper origin position, x component.
P_Y	final Gripper origin position, y component.
P_Z	final Gripper origin position, z component.
N_A	Avogadro's Number.
A	atomic mass of the target atom/nucleus.
ρ	density. (g/cm^3)
σI	cross section for the given interaction.
ϕ	incident particle flux. ($particles/cm^2.s$)
ϕo	uncollided flux. ($particles/cm^2.s$)
x	depth of penetration. (cm)
μ	attenuation coefficient. (cm^{-1})
ΔV_{th}	threshold-Voltage shift. (V)
$f_{i+1,i}$	resulting force exerted on link *i +1* by *i* at point O_i.
$f_{i,i-1}$	resulting force exerted on link *i* by *i-1* at point O_{i-1}.
f_i^*	inertia force exerted at the centre of mass of link *i*.
g	acceleration of gravity.
m_i	mass of link *i* .
${}^iI_i$	inertia matrix of link *i* about its centre of mass and expressed in the *i*th link frame.
$n^*_{i+1,i}$	resulting moment exerted on link *i +1* by *i* at point O_i.

$n^*_{i,i-1}$	resulting moment exerted on link *i* by *i-1* at point O_{i-1}.
n^*_i	inertia moment exerted at the centre of mass of link *i*.
p_i	Position vector of the origin of the *i*th link frame with respect to the base link frame, $p_i = \overline{O_0 O_i}$.
p_{ci}	Position vector of the centre of mass of the *i*th link frame with respect to the base link frame, $p_{ci} = \overline{O_0 C_i}$.
r_i	Position vector of the origin of the *i*th link frame with respect to the (*i-1*)th link frame, $r_i = \overline{O_{i-1} O_i}$.
r_{ci}	Position vector of the centre of mass of the link *i* with respect to the *i*th link frame, $r_{ci} = \overline{O_i C_i}$.
v_i	absolute linear velocity of the origin O_i.
v_{ci}	absolute linear velocity of the centre of mass of link *i*.
$\dot{v}_i$	absolute linear acceleration of the origin O_i.
$\dot{v}_{ci}$	absolute linear acceleration of the centre of mass of link *i*.
z_i	Unit vector pointing along the z_i-axis.
ω_i	absolute angular velocity of link *i*.
$\dot{\omega}_i$	absolute angular acceleration of link *i*.

PUBLICATIONS

(a) RESEARCH PAPERS

(i) Jahan Zeb, Farooq Rashid, Naeem Iqbal and Nasir Ahmed,
"Design and Development of Mobile Robot for Radiation Protection Assistance", IJCSNS, International Journal of Computer Science and Network Security, Vol.7, No.4, April, 2007, pp.99-106.

(ii) Jahan Zeb, Farooq Rashid and Naeem Iqbal,
"Kinematics Study and Workspace Analysis of an Articulated Robotic Arm of a RPAR", Mehran University Research Journal of Engineering & Technology, Vol. 26, No.2, April, 2007, pp.191-200.

(iii) Jahan Zeb, Farooq Rashid, Naeem Iqbal and Nasir Ahmed,
"Wipe Testing of Sealed Radiation Sources using a Radiation Protection Assistant Robot", Nuclear Technology & Radiation Protection, Vol. XXIV, No. 2, Sept. 2009, *(In press).*

(b) CONFERENCE PRESENTATION

(i) Jahan Zeb, Nadeem Qaiser, Naeem Iqbal and Nasir Ahmed
"Kinematics Modeling of the Arm of a Radiation Protection Assistant Robot", *Proceedings, 9th International Multi-topic IEEE-INMIC conference*, Karachi, December 2005, pp 89-94, 2005.

(ii) Jahan Zeb, Farooq Rashid, Naeem Iqbal and Nasir Ahmed
"A Simple and Low Cost Radiation Protection Assistant Robot for Multipurpose Tasks", *Proceedings, National Conference on Information and Communication Technologies (NCICT-2007),* Bannu, June 2007, pp 81-87, 2007.

(c) IN PREPARATION

(i) Torque responses due to the movement of links in a two degree of freedom articulated robotic arm

(ii) Radiation Hardening study of radiation protection assistant robot.

ABSTRACT

Robots are playing quite a useful role in many industries. In nuclear industry, robots protect radiation workers from receiving radiation doses while working in highly active areas. They also improve the quality of work and demonstrate profitability in nuclear industry.

The aim of this project was to design and develop a Radiation Protection Assistant Robot (RPAR) for assisting radiation workers in a radioactive environment for routine work as well as in emergency situation. During an emergency situation, where higher doses are likely to be received, RPAR can be used effectively to perform various tasks, such as radiation mapping, sampling and handling radioactive waste/materials.

To accomplish these tasks a mobile robot having 4 Degree-Of-Freedom (DOF) articulated robotic arm was designed and developed using locally available components and indigenous resources. The mechanical segments, i.e. gripper, wrist, elbow, shoulder and waist were developed at Pakistan Institute of Engineering & Applied Sciences (PIEAS) and Pakistan Institute of Nuclear Science & Technology (PINSTECH). The main platform was developed to carry on-board computer, rechargeable battery, controlling electrical and electronics modules/circuits. The electronic modules have been developed using components available in local market. These modules include H-bridge, relay logic, parallel port interface and limit switch modules. Control panel and remote console are developed to control and operate the RPAR. An embedded controller card was also developed to determine the positions of various links of RPAR.

RPAR weighs 55.6 kg. It is powered by a 12 V DC rechargeable dry battery. Its maximum payload capacity and reach are 2.1 kg and 1.04 m, respectively. It can be controlled by a wired remote control or an off-board PC via wireless Ethernet.

Three Software namely RPARSOFT, RPAR-DEMO and SEDAS were designed and developed using Visual Basic 6.0. RPARSOFT was developed to operate the RPAR from the keyboard of an off-board computer. The RPAR-DEMO was developed to self check the electrical and electronic modules of RPAR, whereas, SEDAS was designed for the embedded controller card to determine the real time position of wrist, elbow, shoulder and waist of RPAR.

Kinematics studies, Dynamics analysis, manipulator Jacobian and work space analyses were performed to study the performance and range of the robot. Repeatability range and payload capacity of RPAR was measured. Radiation hardening study has also been carried out to check the stability and reliability of the commercial components in the field of gamma radiation. The modules were found working satisfactorily before and after irradiating them up to a dose of 9 Sv.

The objectives have been achieved successfully.

CHAPTER
ONE

INRODUCTION

1.1 INTRODUCTION

Nuclear Technology plays a vital role in the rapid development of industry, agriculture and medical sciences. A minor accident at a nuclear installation is several times more hazardous than an ordinary accident mainly because of radiation hazards. Radiation is also problematic in nuclear industry for rescue worker in contaminated or radiation area (Iborra et al; 2003). To prevent the human worker from unwanted radiation exposure, it is therefore, necessary to develop equipment, tools and particularity robots or robotic devices to assist radiation workers in radiation-environment. Among the main applications of robots and robotic devices is automation of repeatedly precise work for mass-production and working in the areas where human access is limited due to environmental constraints

such as chemicals and nuclear radiation. Due to this reason, robots are very useful supporting tools in many industries including nuclear industry. Robotics in the nuclear industry should be able to replace human operator not only to comply with the ALARA (As Low As Reasonably Achievable) principle applied to radiation protection, but also in order to guarantee technological support and to improve the working conditions as well as the quality of the tasks performed (Desbats et al; 2004). Usually quality of the work and profitability are the motivations to switch over from a regular mass-production work to an automated system.

With the advancement in solid-state electronics, different types of controller modules with high radiation stability for robotic system are available and are intensively used in nuclear and other industries. There are specially designed service robots and robotic devices for a limited task (Byrd 1995). These commercially available robotic devices are normally very expensive and their repair requires sophisticated tools and workshop facilities.

The national and international regulatory authorities and radiation protection agencies emphasize that the radiation dose for a radiation worker should not exceed 20 mSv per year (IAEA 1996). Due to this low dose regulation, more workers have to be employed to accomplish a single job. Once the maximum dose limit is reached the worker has to stop working immediately. The implementation of radiation protection regulations costs an estimated amount of $500,000 per man-Sv (Marian and Rowan; 1987).

Robotic systems, appropriately hardened against the deleterious effects produced by ionizing radiations, can offer a cost-effective solution in the performance of these functions. In the nuclear industry a "rule-of-thumb" is that a robotic system is a viable alternative to human worker if its equivalent cost is less than $10K/person-rem eliminated (Bennett and Posey; 1997). Hence, it is quite necessary to introduce robots and robotic

devices to execute job assigned in radiation area not only to compensate these expenses, but also to reduce the number of required highly skilled technical manpower as low as possible. It is obvious that a dollar spent on robot, is returned in double, because of radiation safety (Nucl. Eng. Int. 1990). Therefore, the use of robots and robotic devices in nuclear industry can play a vital role in reducing the risk of hazardous radiation exposure to meet the concept of ALARA (Kathren 1980).

Robots also find applications in nuclear reactors. For example, it is essential to shut down a nuclear reactor to allow necessary human intervention near the reactor core for inspections and maintenance work. Besides, due to factors such as corrosion, stress and aging etc. of a nuclear installation, its safety equipment and controlling components demand increase in inspection frequency and at a deeper level. Some robotic devices are used for fuel shuffling/replacement and removal of faulty parts and components of the reactor core. The use of robot automation helps to shorten the maintenance time and hence provides safety from radiation. The robotic devices reducing the number of radiation workers eventually reduce the use of protective wares and generation of radioactive wastes. It can easily work in a hazardous environment in any emergency situation and protect the human workers from putting their life and health in risk. Furthermore, at least a remotely controlled system (semi-automatic) is often the only way to enter in a dangerously high radiation dose area to meet any emergency.

With the rapid depletion of the fossils fuel resources, the demand of nuclear energy is increasing. For instance, Pakistan has planned to double its nuclear power generation in the next ten years, which may cause the risk of repeated radiation exposure to radiation workers. Such problems can be eliminated by the use of devices such as Radiation Protection Assistant Robot (RPAR) in nuclear industries. However, in nuclear industry, safety of the radiation workers is of major importance. This is necessary to make the

nuclear installation risk free and as safe as possible. Even with strict quality controls and design specifications, the frequency of inspections and maintenance has to be increased due to many factors. On the other hand due to technical and economical reasons, the shutdown period of a nuclear reactor cannot be prolonged. Further more, it is worth mentioning that most of the nuclear installations have limited workspaces. In an emergency situation, the narrow working space obstructs the radiation workers to work freely within a restricted area and time. Hence, the limitations increase the risk of unwanted radiation exposure. It is quite difficult to meet the required dose limits due to the workspace and time limitations. Therefore, robotics is the only solution and compensation for these expenses by reducing the number of human radiation workers to meet the concept of ALARA. Similarly, the robots and robotic devices can perform their task satisfactorily for longer period, till the completion of the job, without the risk of unwanted exposure due to radiations.

In this study, the objective was to design and develop a simple and inexpensive mobile robotic device capable of assisting radiation workers in a medium level of ionizing radiation environment where human can not perform for longer durations. This multipurpose Radiation Protection Assistant Robot (RPAR) was designed for effective use for tasks such as radiation mapping, air sampling, shifting and transportation of hot irradiated samples etc. Its intended use was also to pick and carry the accidentally dropdown irradiated sample and handling of liquid and dispersible solid waste such as contaminated ion-exchanger resin etc. Another use was for Wipe-Testing of sealed radiation sources that otherwise delivers reasonable higher radiation exposure to the workers. It is hoped that with the help of this robot, radiation workers can accomplish a task without having any exposure to hazardous environment for longer durations.

1.2 RELATED WORK: ROBOTS IN NUCLEAR INDUSTRIES

Robots are becoming an integral part of nuclear industries and several robots were designed, developed and are in use. Mostly the robots are developed for dedicated jobs, which means that they are not running continuously but only when they are needed. Repair and inspection robots are good examples of such robots. Since these robots are not permanently kept in radiation field, so their radiation hardening is a minor concern. On the other hand, a robot whose aim is to manipulate radiation equipment or to survey on a daily basis will require high radiation tolerant components. Some of the robots used in the nuclear industry are briefly described here.

1.2.1 Surveillance and Routine Monitoring Robots

A Semi-Intelligent Mobile Observing Navigator (SIMON) is a mobile surveillance and monitoring robot developed in 1990. This robot was first used at Savannah River site of Department of Energy (DOE), USA in 1990 (Weber and Vanecek; 1990). The SIMON was designed to avoid the need of human inspection in a nuclear facility. The SIMON was used to measure and transmit radiation, temperature and televised views of the area in real time. The SIMON successfully detected 20 spots of beta contamination that were undetected by human survey (Nucl. Eng. Int. 1996). Equipment used with SIMON includes radiation detectors, temperature sensors and a camera mounted on a telescopic mast. SIMON navigates into a room by either following a programmed path or it was controlled manually to perform its monitoring task. A total dose radiation hardness of 200 Gy (20 krad) was achieved at a reasonable cost using this design approach. SIMON received a US patent in 1994.

A Mobile Automated Characterization System (MACS) was designed in 1996 as the second generation of SIMON robot (Nucl. Eng. Int. 1996). The goal of this robot was to

develop a contamination map of nuclear facility being subjected to decontamination and decommissioning purpose. MACS was capable to perform decontamination task automatically and in a reliable manner as compared to radiation workers equipped with portable detectors. The MACS was equipped with sensitive detectors and transmits information in real time to the host station.

Later on another Autonomous Robotic Inspection Experimental System (ARIES) robot was developed by University of South Carolina, USA for the DOE (Byrd and Pettus; 1996). The DOE stores several thousands of steel drums containing Low Level radioactive wastes. These drums were stacked and stored in long aisles. The weekly inspection of the packaging integrity was required. This work was tedious and long term exposures were to be avoided, although the radiation levels were not hazardous to workers. The goal of ARIES was to perform visual inspection of each drum and prevent the radiation worker from getting unnecessary radiation exposure during the job.

Another Stored Waste Autonomous Mobile Inspection (SWAMI) robot for such jobs (Hazen 1994) was also developed for DOE. These two robots were having similar capabilities; however ARIES was more sophisticated and modern. ARIES used the K3A mobile platform manufactured by Cybermotion.

1.2.2 Steam Generator Inspection and Maintenance Robots

The Consolidation Edison Combined Inspection and Lancing (CECIL) robot was designed for steam generator maintenance (Malaugh and Monaghan; 1994). The buildup of sludge on the secondary side of steam generator reduces its thermal efficiency. This accumulation decreases the power output of the power plant and cost millions of dollars. CECIL is designed to clean the bottom part of steam generator. The Foreign Object Search and Retrieval (FOSAR) robot was also designed to search and retrieve foreign

objects in the steam generator (Murchie and Reinhardt; 1995). The robots called Upper bundle In Bundle (UBIB) and Upper Bundle Hydraulic Cleaning (UBHC) were introduced in 1996 (Reinhardt et al; 1997). These robots offer a considerably increased cleaning and inspection efficiency compared to the CECIL system.

There were several mechanical arms that were mainly used for steam generator inspection or maintenance. ROSA I, II & III were remotely controlled maintenance and inspection robots. ROSA-III was a mechanical arm that can be equipped with tools for general purpose work. It was used for steam generator operations through the manhole port to reduce personnel exposure. ROSA-III was developed by Westinghouse Electric. The COBRA system was specifically designed to increase maintenance productivity and to reduce personnel exposure when workers access the inside of steam generator (Nucl. Eng. Int. 1992). It was lightweight electric manipulators that use to inspect and repair the lower tube sheet. COBRA was developed by B & W Nuclear Service in 1992.

1.2.3 Reactor Vessel Inspection Robots

Inspection of reactor vessels is carried out on periodic basis to fulfill specific regulations. The goal is usually to look for cracks and to probe the welds visually with an ultrasonic probe. These operations imply several challenges. First, all the operations are accomplished underwater since the reactor is completely flooded. Secondly, all the equipment in the reactor has to be taken out prior to inspection. This means the reactor is out of service during the maintenance period. The third challenge is the accessibility of the welds. Early design of reactor vessel did not include any inspection guidelines, nor provided an easy access to sensitive part of the vessel. The inspection of Boiling Water Reactor (BWR) vessels is often much more challenging then the Pressurize Water Reactor (PWR) inspections because of their highly complex internal structure. The Advance

Ultrasonic Testing (A-UT) machine is an innovative method that revolutionized the reactor vessel inspections. This robot does not have a central mast but has a small base held to the vessel wall by four suction cups. This A-UT robot scans the vessel and then swims or moves to its next location using its eight wheels and six thrusters. It uses several lasers to determine its orientations and its position inside the vessel.

The Ultrasonic Reactor Scanner Un-like Aris (URSULA) robot was developed in 1995. It was one of the most highly developed systems (Glass et al; 1999). In URSULA three suction cups were used to attach itself to the vessel wall while six- Degree-of-Freedom (DOF) arms scanned the welds with an ultrasonic module. URSULA was so small that it can enter the reactor through personnel hatch and two units can work together in the vessel, offering considerable time savings.

1.2.4 Pipe Inspection Robots

PWR and BWR have pipes that also need inspection of their welds. Two types of pipe inspection are available depending on the access possibility; welds from the inside or the outside of the pipe. In BWR, small gaps are another problem beside radiation. Some times the gap is smaller than 30 cm. Robots specially designed to access and inspect these welds are used. Pipe crawlers are widely used for inside inspection of pipes. These robots use tracks, wheels or thrusters to navigate deep in the pipe. The tasks performed by these robots are the visual inspection of the pipe with CCD camera (Wiesman 1992), scanning with ultrasonic transducers and radiation mapping (Schreiner, 1994). These robots are often flexible and can be as small as 5.08 cm of diameter.

1.2.5 Underwater Inspection Robots

Gamma rays can be shielded with water at very low cost. Thus, nuclear power plants operations are performed under water for this reason. Many robots are therefore designed to operate underwater. In the past, long poles and telescopic arms were used to perform visual inspection and to retrieve small objects (Gebel and Fontcuberta; 1994). This method is not only costly, but also causes personnel exposure (Willis et al; 1999). One of the first submersible robots used in nuclear industry was the Mini Rover (Rizzo 1991). It was used in 1987, in Salem- I for underwater reactor core inspection (Rosen 1999). The Phantom 500 robot is the biggest submersible made by Deep Ocean Engineering Inc. It is capable of visual inspection but can also retrieve small objects in a reactor core and perform simple ultrasonic testing. Toshiba has developed a very small (1.5 cm diameter 20 cm long) Remotely Operated Vehicle (ROV), that navigates under water to inspect BWR core internals (Kimura et al; 1995).

1.2.6 Handling and Processing of Radioactive Waste Robot

Manipulators are playing essential role in nuclear industry. They are used in many disciplines to process repetitive and delicate work. They replaced the human arm where the radiation level compromises the safety of the personnel. For a long time the manipulation of hazardous material has been executed by a master-slave system. The advantages of this system are its simplicity and affordability. The shortcomings are a low payload, narrow workspace and limited distance between operator and shielded radiation area. Teleported systems have been developed to avoid such problems. In such systems, the symmetry of movement is not reproduced mechanically but electrically. For radioactive environments, the requirements for a teleported robot are a good sealing of the parts to avoid contamination, the installation of a forced feedback system, an acceptable level of radiation

hardness, a good payload/mass ratio, a higher reliability and modularity for easier maintenance and an easy integration into embedded equipment. The installation of radiation hardened force feedback system is very important when upgrading a commercial manipulator to its nuclear equivalent. The Nuclear Engineered Advance Telerobot (NEATER) 760 developed by AEA Technology is a modification of the commercial PUMA 762 robot (Abel and Watson; 1990 and Fryatt 1994). The onboard electronics of the PUMA was redesigned to a tolerance level of 10^6 Gy of total dose. The maximum load of the NEATER robot is 20 kg at a maximum reach of 1.4 m. The similar robot has been used by French CEA for the modifications of a STRAUBLIRX 90 robot (Desbats et al; 1999). The CEA also developed a BD 250 dexterous arm to meet unique requirements in the nuclear industry. The BD 250 is a 7-DOF mechanical arm. The payload is 25 kg, while the mass of robot is 75 kg; the payload to mass ration is very good. The total length of the robot is 1.4 m and the arm can be introduced into a 25 cm diameter fitting. The on-board electronics and the force feedback sensors are radiation resistant up to 10 kGy.

1.2.7 Decontamination and Decommissioning Robot

Despite of regular care and maintenance of the equipment in a nuclear facility, it may happen that radioactive contaminants are spilled and must be removed. Also, some facilities and hardware need to be decontaminated during operations. Mostly, the spill is small enough and does not give too much ionizing dose to the worker. However, the needs to reduce personnel exposure according to the ALARA concept are pushing the use of robotics for cleaning and decontamination work. Conventional, general-purpose robot or custom made actuators as well as cleaning robots are used depending on the cleaning needs and the contaminated facility geometry. A master slave manipulator was specifically designed to cleanup a flooded radiation waste area at Nine Mile Point1. The robot

removed all the contaminated materials and decontaminated the area to acceptable levels. A robot called Tethered Remote Operating Device (TROD) consisting of a remote manipulator Gamma 7F with six DOF and 2 m reach was used. It was manufactured by RedZone robotics (Gerriets 1992). The Gamma 7F manipulator was hydraulically powered and controlled by an operator; its radiation resistance was greater than 10^5 Gy. The TROD system accomplished many tasks including removing debris and barrels as well as decontaminating walls and floor. The use of TROD was efficient and saved between 1180 and 1960 man mSv of personnel exposure.

The ANDROS Mark VI robot was used at the Susquehanna nuclear power plant to clean up radioactive tank nozzles (Boughman and Jones; 1992). Remotec manufactures the ANDROS robot, which included six tracks, a manipulator arm with a 16 kg maximum load and two video cameras. The tracks allowed the ANDROS to move on an uneven ground. No radiation hardening was required since the dose rate in the tank was as low as 0.03 to 0.05 Gy h^{-1}. The operator controlled the ANDROS via a long flexible cable. Two robots; Scarab IIA and Scavenger were used together for a cleaning operation. About one cubic meter of spent resin tank was spilled in a pump room of Waterford-3 plant (Nucl. Eng. Int. 1998). The radiation level on the floor was up to 1 $Sv.h^{-1}$. A two-robot strategy was applied. First the Scarab IIA gathered the waste at the lowest point of the room. Secondly a water nozzle spray was used by Scarab robot to slurry the waste while the Scavenger robot vacuumed the floor. The waste was then evacuated to a shielded container in adjacent room.

1.2.8 Tank Cleanup Robot

Tank cleanup robots are used to handle highly toxic and highly radioactive waste. This waste is generated by the production of nuclear weapons with the chemical processing

used in separation facilities. The waste is normally stored in single shell concrete tanks for a short period of time. Such tanks are located at the production sites owned by the DOE (e.g., Hanford Site, Oak Rdge Reservation, Savannah River Site, etc). These tanks have been in use much longer than originally planned and many of these tanks are now leaking and are creating a major threat to the environment (Houssay 2000). Such tanks do not meet today's requirement for toxic and radioactive storage. The waste contained in the single shell tanks has to be removed and stored in more appropriate storage. The removal of the waste is challenging for many reasons. First, the waste is extremely toxic, corrosive and radioactive, and is sometimes inflammable as well as explosive. Secondly the tanks access is limited to only tank risers as small as 45.72 cm in diameter. Third, the inside of tanks is sometimes filled with pipes and equipment that limits the maneuverability inside the tank. This equipment consists of cooling pipes, thermocouples and other monitoring devices. Finally, the consistency of the waste is very complex. Tanks contain liquid, soft and hard sludge. The composition of each tank is different; sometimes a crust is formed on the top layer of waste. The chemical composition of the waste, its radiation activity and temperature must also be determined as well as the sludge consistency and depth.

The DOE has developed remote tools that perform visual inspection, ultrasonic testing and sampling. The easiest way to monitor the inside of a tank is to lower a video camera through the 12.7 cm diameter of one of the tank risers. This method has been used in cooled waste tanks at the Savannah River site (Anderson et al; 1992).

The Remote Tank Inspection (RTI) system is a five DOF manipulator attached to a telescopic mast, which is lowered vertically from a 30.48 cm tank-riser (Griebenow et al; 1992). The vertical mast can go as deep as 1250 cm below the ground level and the arm has a reach of 180 cm. Several end effectors can be attached to the manipulator to accomplish a wide variety of missions (Griebenow et al; 1991). The visual inspector end effecter

consists of two cameras, two lights and a light positioning system. The setup using the RTI system was tested in 1991 in a mock-up facility and was the basis of a Light Duty Utility Arm (LDUA) that was developed in the first half of the nineties at the DOE Hanford site (Jaquish et al; 1991 and Burks et al; 1991). An improvement was made in LDUA and called as Modified Light Duty Utility Arm (MLDUA). It is an eight DOF hydraulic arm (Glassell et al; 1999). Its reach in the tank has a radius of 503 cm and has a maximum payload of 90.72 kg. The MDLUA was efficient and reliable but has the drawback of being bulky, heavy and costly. The Houdini system is a mobile robot that is inserted into the tank in a folded position through tank raisers (Schemf 1994). Once on the tank floor Houdini is automatically deployed. It consists of a mobile platform moved by two parallel tracks. The Houdini system offers greater access to the internal part of the tank and an improved efficiency with light weight and versatile equipment.

1.2.9 Decommissioning Robots

Many nuclear facilities completed in 40's and 50's are completing their lifetime and decommissioning effort is a priority and challenging job. The reduction of employee exposure as well as cost reduction requires the uses of remote tools for contaminated parts (Bares 1995). Main job in decommissioning is to remove the core elements. The rest of the building can be decommissioned in classical way. The classical decommissioning strategy is to dismantle large structure from top to bottom, and then transport the components for more smaller pieces and packaged. For example the dismantling of the Niederuichbach power plant in Germany followed the following steps: dismantling of upper neutron shield, removal of pressure tube units, dismantling of lower neutron shield, dismantling of moderate vessel and dismantling of thermal shield (Orwantschke 1995).

The decommissioning of the CP-5 research reactor at the Argonne National Laboratory in 1997 was carried out by Dual Arm Work Module (DAWM) system (Noakes; 1999 and Cox 1999). It consists of two Schilling Titan II mounted on a five Degree-of-Freedom articulation platform. The DAWM module can be installed on a ground mobile vehicle called Rosie, or on a platform suspended to an overhead crane. This configuration was used in CP-5 reactor and renamed the Dual Arm Work Platform (DAWP). The DAWP undertook the complete dismantling of the reactor. Its operation also involved cutting of the metallic parts and removal of the graphic blocks and lead bricks. The DAWM and DAWP included five on-board computers. Several cameras provided a good view of the manipulator operation. The electronics did not have a radiation-hardening requirement. A similar system was planned for the remote dismantling of a spent fuel reprocessing facility in Karlsruhe, Germany (Hendrich et al; 1999). The system was called Manipulator Carrier System (MCS). The mechanical arm was two electromechanical master slave manipulator (EMSM) having eight Degree-of-Freedom, 100 kg payload and a reach of 280 cm. This equipment was improved after realistic tests in a mock-up facility were carried out from 1995 to 1997. The actual demolition was carried out in 2003.

A German firm Mak System Gmbh has designed a manipulator vehicle that was radiation resistant up to 10kGy from ^{137}Cs by using of Tungsten shielding (Nucl. Eng. Int. 1994). This vehicle called SMF has six axis hydraulic arms with a maximum payload of 250 kg and has a reach of 300 cm. The end effectors of this arm can be a gripper as well as any required decommissioning tool. The SMF robot has been available since March 1994 from Kerntechnische Hilfsdienst Gmbh in Germany.

1.2.10 Robot for Post Accident Operations

When an unexpected problem occurs in a radiation environment, it becomes a potential hazard. The Chernobyl accident on April 26th 1986 has stressed the need for robots intervention in case of nuclear accidents. The first robots that were sent to Chernobyl failed because of a lack of radiation hardness and their tethers stuck in the rubble. The Russians were first to design a robot especially for the Chernobyl accident. The Mobot-ChHV was on site as soon as August 1986 and successfully cleared the roof (Batanov 1999). It was equipped with electromechanical actuators and did not have any on-board electronics. In the following years many robots have been developed and have accomplished a wide variety of tasks at Chernobyl (Ivanov et al; 1999). Among them were a video inspection robot, a boring and drilling robot, a dust and air cleaning robot and a few dismantling robots. The latest robot "Pioneer", designed to explore the inside of Chernobyl sarcophagus was the result of US-Russian collaboration (Slifko et al; 1999). Pioneer used a fully electric track based platform. It carried a remote viewing system, concrete sampling drill and a manipulator arm etc. The original goal of this robot was to take concrete sampling of walls and floor. The Pioneer has the same six DOF arm as the ANDROS Mark V-A robot and has a maximum payload of 45 kg and a reach of 168 cm. The control electronics of Pioneer was not onboard but in the central station to avoid radiation damage. However, the viewing system, the drilling tool and the mechanical arm control electronics were installed onboard. A Tungsten shielding box provided a total radiation hardening up to 10 kGy to the onboard electronics. The control console was equipped with monitors, switches, joysticks and graphic user interface for easy operation. The maximum distance between the operator and the robot was 500 m.

1.3 THESIS ORGANIZATION

Need of robotics in Pakistan and applications of robotics in nuclear industry have been discussed in this chapter to identify the purpose and motivation behind conducting this research. The next three chapters are devoted to the discussion about the design and development of RPAR. The mechanical considerations are discussed in Chapter 2 while Chapter 3 and 4 are devoted to electrical/electronic and software development of RPAR, respectively. In Chapter 5, an effort has been made to study the Kinematics, Jacobean and workspace analysis of RPAR. Dynamical analysis of RPAR is carried out in Chapter 6. Radiation Hardening of Robots is briefed in Chapter 7. The Radiation Hardening study of RPAR is discussed in Chapter 8. Cost analysis of RPAR is presented in Chapter 9 and application of RPAR for the wipe testing of sealed radiation sources is described in Chapter 10. The last chapter provides conclusions and future projects with RPAR.

The specifications of RPAR is placed in the appendix-A.

CHAPTER

TWO

DESIGN AND DEVELOPMENT: MECHANICAL

2.1 INTRODUCTION

The main objective of the work described in this thesis is to develop a general purpose robot that could operate in radiation environment using components available in the local market. This chapter describes the design requirements, the design approach and mechanical design considerations of Radiation Protection Assistant Robot (RPAR) being developed in this work.

2.2 DESIGN REQUIREMENTS

Although the robot was designed as general purpose device, however, the specific problem for which the RPAR was manufactured was to assist the radiation workers for shifting of irradiated samples in a sealed Aluminum container from the shelf of hot cell to a lead container trolley placed inside the reactor building in PINSTECH. A schematic

diagram with dimensions of the hot cell is shown at Fig. 2.1. The neutron irradiated samples are contained in the Aluminum container is called as "Rabbit" (ø 2 cm × 10 cm) with minimum required weight of 20 g. The design parameters of the articulated arm were calculated to accomplish this task.

2.3 THE APPROACH

Development of RPAR involved many challenging tasks in mechanical, electrical, electronics, control, software and radiological areas. The design of RPAR articulated robotic arm was primarily centered on creating motions similar to that of human's arm. As such, link length, joint position and centers of gravity were designed to correspond to that of human's arm. The link lengths were also adjusted as to drop or pick an object from the floor or Hot cell.

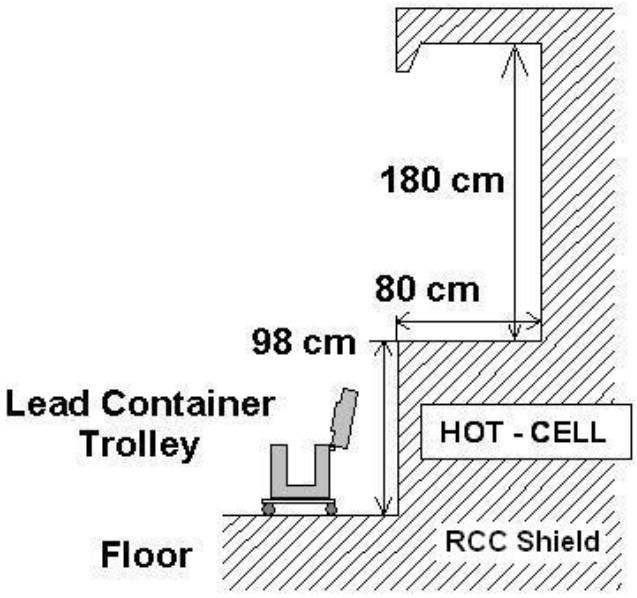

Fig. 2.1: Schematic diagram of hot cell.

Positioning and orientations of the joint actuators were determined by the axis through which the joints were required to rotate and the shapes and the volume of the space available to mount the actuators. In addition to these criteria, weight saving was also a major issue. The conventional car wiper DC motors were used to actuate the articulated robotic arm and mobile platform. The material used in the construction of the articulated robotic arm and platform must be as light as possible or modified in a way that it becomes lighter and washable. Perhaps the greater limiting factor of all was cost. While it has not directly effected component selection for the mechanical frame of the robotic arm, it has limited the power/weight ratio of the joint actuators. Therefore this provided many challenges to the mechanical design of the robot.

2.4 MECHANICAL DESIGN CONSIDERATION

The Radiation Protection Assistant Robot (RPAR) comprises of a cubical tri-wheeled platform and Four Degree of Freedom (4-DOF) serial type articulated robotic arm (Fig. 2.2). The RPAR is powered by 12 V, 17 AH rechargeable onboard battery. Total length of articulated robotic arm is four feet attached to a three feet high mobile cubical platform. The RPAR with a total mass of 55.6 kg and 2.1 kg payload can move with maximum speed of 24.4 cm/s. This payload to mass ratio is very good.

The RPAR is activated by seven 12V DC motors, connected to various mechanical arrangements in different segments and all motors are controlled by independent modules for diverse types of motions and functions. Two motors control the horizontal movement of RPAR or differential wheel driving systems. These motor can move the RPAR left, right, forward and backward. While four motors are used to produce 3-dimensional movement of four DOF serial type articulated robotic arm. One motor is used for opening-closing mechanism of end effector or gripper.

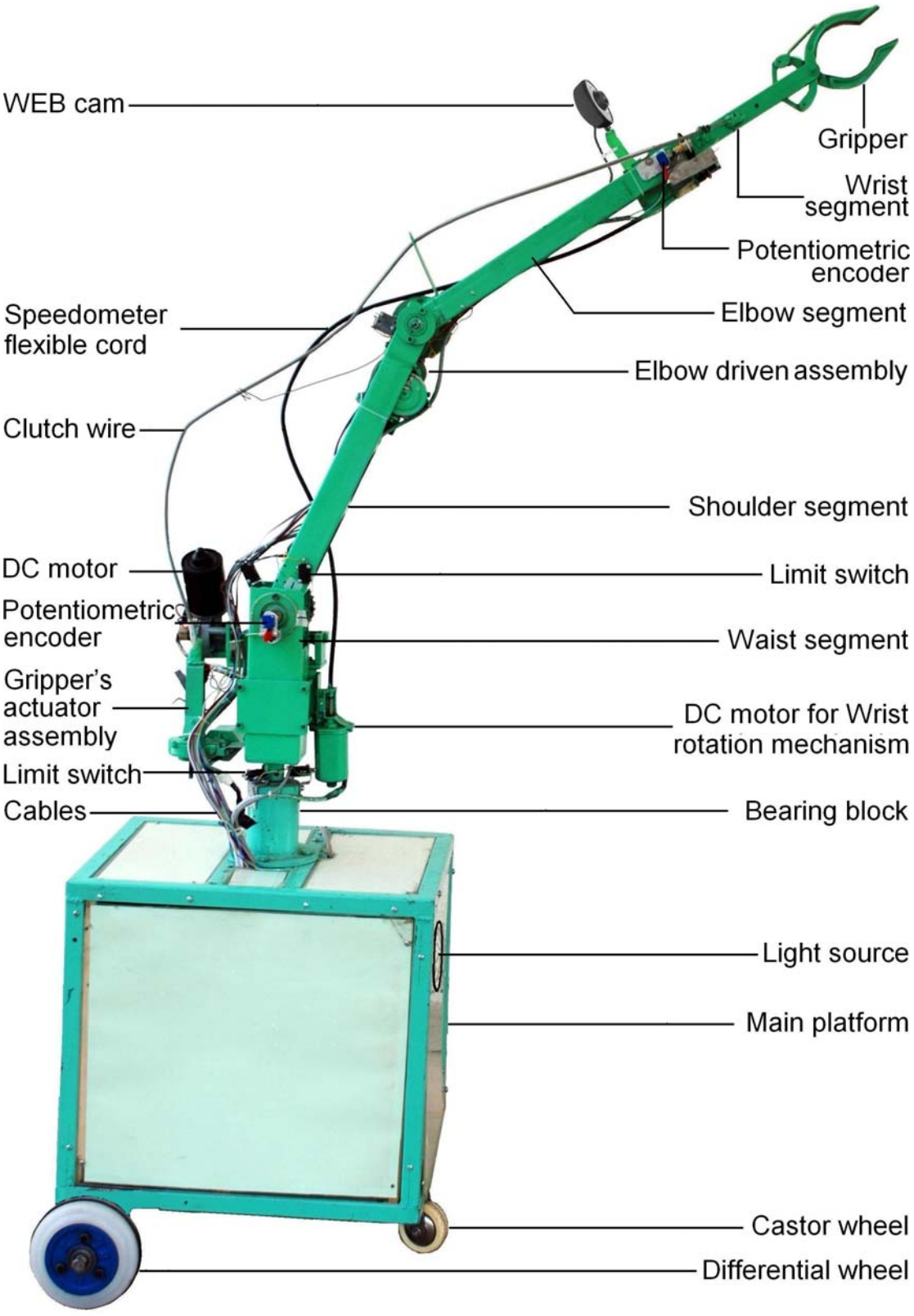

Fig. 2.2: Radiation Protection Assistant Robot (RPAR).

The RPAR consists of following six major mechanical components/segments.

1. Cubical Platform
2. Waist segment
3. Shoulder segment
4. Elbow segment
5. Wrist segment
6. Gripper

Each segment has specific dimensions, properties, functions and independent controlling mechanism and circuitry. The driver modules and electronics circuitry of all the motors are installed inside the Cubical Platform.

2.4.1 Cubical platform

The Cubical platform consists of following components:

1. Cubical platform; (dimensions Length (L) = 51 cm, Width (W) = 38 cm and Height (H) = 46 cm).
2. Waist 12 V DC motor & mounting assembly
3. Worm gear module
4. Bearing block assembly.
5. Onboard electronics which is comprised of ;
    a. Control Panel
    b. Relay Logic Modules (RLM) for Waist
    c. RLM for Shoulder
    d. H-Bridge Module (HBM) for Elbow

e. HBM for Wrist motion

f. RLM for Gripper Open-Close mechanism

g. RLM for left wheel motor

h. RLM for right wheel motor

i. Robot-Computer interfacing modules

6. On-board computer
7. 17 AH, 12 V DC rechargeable battery
8. Two 12 V DC motors for differential wheel system
9. Lead jacket filled with mineral oil

The moving cubical platform is a welded frame of 2.5 cm square mild steel (MS) box pipes (16 SWG). The material MS box pipe is preferred on other lighter material such as Aluminum because of its rigidity, easy machining, availability and fabrication. The only disadvantage of this material is its weight. The cubical platform is the biggest part of RPAR. All the electronics and electrical components including, controlling circuit such as H-bridge modules, Relay Logic modules, Parallel Port Interfacing module I & II and a 12 V DC rechargeable battery is mounted inside this platform. The battery charging connector is provided at the base of the platform to connect the RPAR with the charging unit.

The tri-wheeler configuration gives a precisely controlled mobility to RPAR platform. Two hard neoprene rubber wheels (ø15 cm) are directly fixed to two independently controlled 12 V DC car wiper motors to provide a differential wheel driving systems to the platform. The fixation of rubber wheel to the wiper motor is shown in Figs. 2.3 and 2.4.

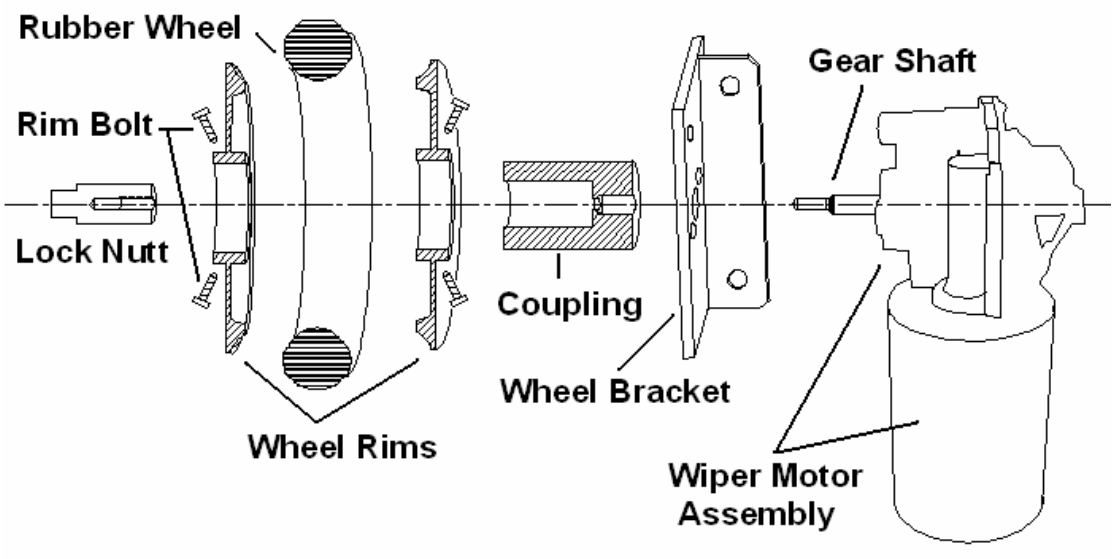

Fig. 2.3: Exploded view of a differential wheel assembly.

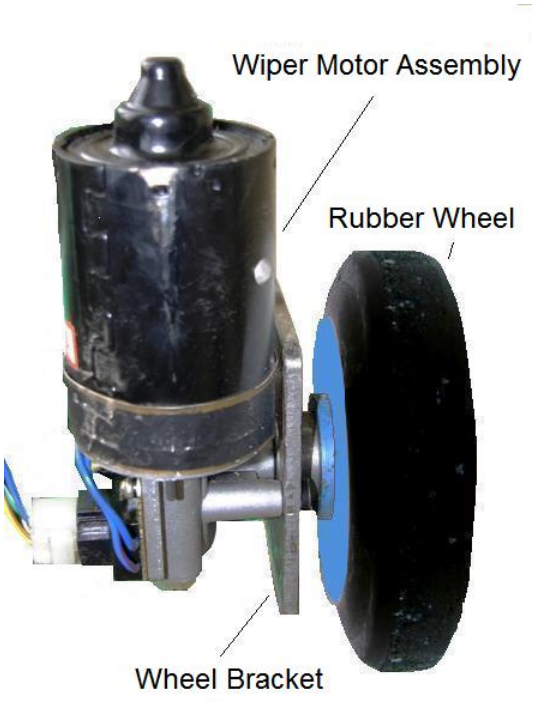

Fig. 2.4: Motorized differential wheel.

The third wheel is a caster wheel (Ø 8.0 cm). The waist of the articulated robotic arm is fixed over an extended shaft, on the upper portion of a bearing block assembly. This bearing block assembly is fixed in the middle of the top surface of the RPAR platform. This bearing block is supported with two balls-bearings (6203ZZ) fitted at its both ends. The lower extended portion of the bearing block shaft is attached with a worm gear assembly (gear ratio = 1:30). The worm of this assembly is directly coupled to the DC wiper motor shaft as shown in Fig. 2.5. This system is used to move the whole robotic arm or waist segment in clockwise or anticlockwise direction. The designed worm gear assembly has two worm gears systems, i.e. one inside the wiper motor and other is main gear module. The double worm gears configuration gives good controllable movements and high torque output yield.

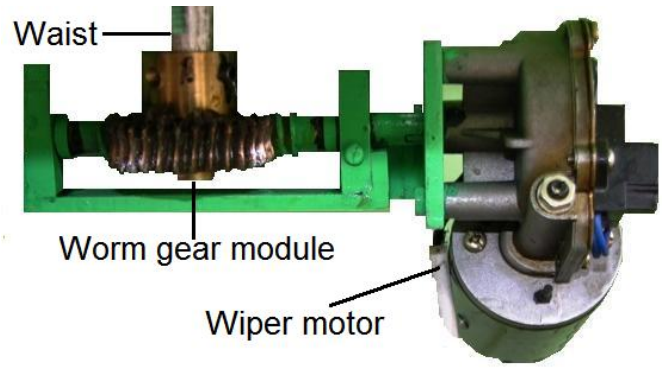

Fig. 2.5: Waist rotating system.

The commercial grade greases and lubricants used in the DC motors bearing and in gear system quickly decompose under radiation fields and produce ceasing and other problems in controllability and uniform movements (Houssay 2000). Due to these reasons, the wiper motors and geared motors were degreased thoroughly with kerosene oil to

remove commercial grease and lubrication oil. After degreasing and drying, the bush bearings were soaked with 10% colloidal graphite solution (Neulube No. 2) in isopropyl alcohol obtained from Newman Tools Inc. (Canada). The "Neulube No. 2" paste was applied directly to all moving parts including shafts, gears, worm gears and flexible cords used in the construction of RPAR. The colloidal graphite is called as Dried-Lubricant and has excellent radiation resistance property (Newman 2007). Also the ordinary electrical wires in the DC motors were replaced with high quality rubber coated wires because of high radiation stability. A double walled (0.2 cm lead sheet) jacket filled with mineral oil was used to protect onboard (slave) computer (Laptop: Dell Latitude D510), electronic controlling modules and interfacing cards from radiation damage. The double walled 0.2 cm apart lead jacket filled with mineral oil reduces the dose rate of 0.5 MeV gamma rays by 1.5 times, hence protected from x-rays and gamma radiations. The mineral oil provides a high hydrogen content medium for neutron absorption. This is especially important with higher energy neutrons, where the low atomic number elements must be used to moderate the neutrons. The mineral oil also provides a minimal amount of gamma shielding (Premier 2007).

2.4.2 Waist Segment

The Waist segment consists of the following components;

1. Waist body (dimension; L = 7.62 cm, W = 7.62 cm and H = 40.6 cm)
2. Shoulder moving mechanism system
3. Shoulder pivot mechanism
4. Two 6203ZZ bearings and a coupling shaft

The Waist segment is fixed on a bearing block assembly shaft Ø 1.7 cm × 21 cm coming out from the upper portion of the bearing block assembly with the help of 2 × 8M countersink screws. The bearing block assembly is 11 cm long and 7.6 cm in diameter cylinder having two ball bearings 6203ZZ at its both ends. The shaft is supported by these two ball bearings. The waist worm wheel is attached to the lower end of this shaft. The Waist segment is manufactured from welding two MS box pipes having a dimension of L = 7.62 cm, W= 3.81 cm and H = 40.6 cm. The upper end of Waist is reinforced with the help of MS sheet (16 SWG) having a dimension of 7.62 cm (L) × 8 cm (W) to hold the torque action and weight of articulated arm and payload. The Shoulder movement mechanism, Gripper clutch arrangement and DC motor for the rotational mechanism of Wrist are attached on this segment. The pivot joint of the Waist and the Shoulder is provided with a set of worm gear (gear ratio = 1 : 28). The Shoulder moving mechanism is shown in Figs. 2.6 and 2.7.

The sweep movement of the waist is limited within 195° range with the help of two micro-switches. This range is sufficient to obtain required working area coverage. The Shoulder position-measuring-rotary-encoder and limit switches are also attached on the Waist segment.

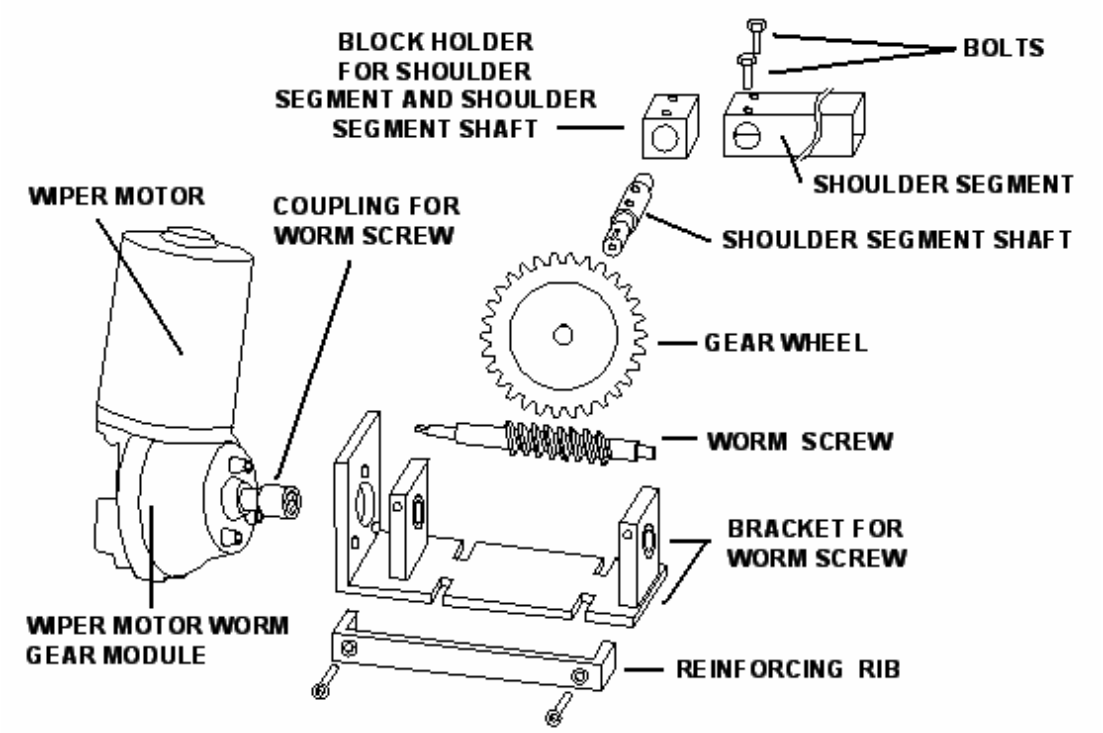

Fig. 2.6: Exploded view of a Shoulder rotation assembly.

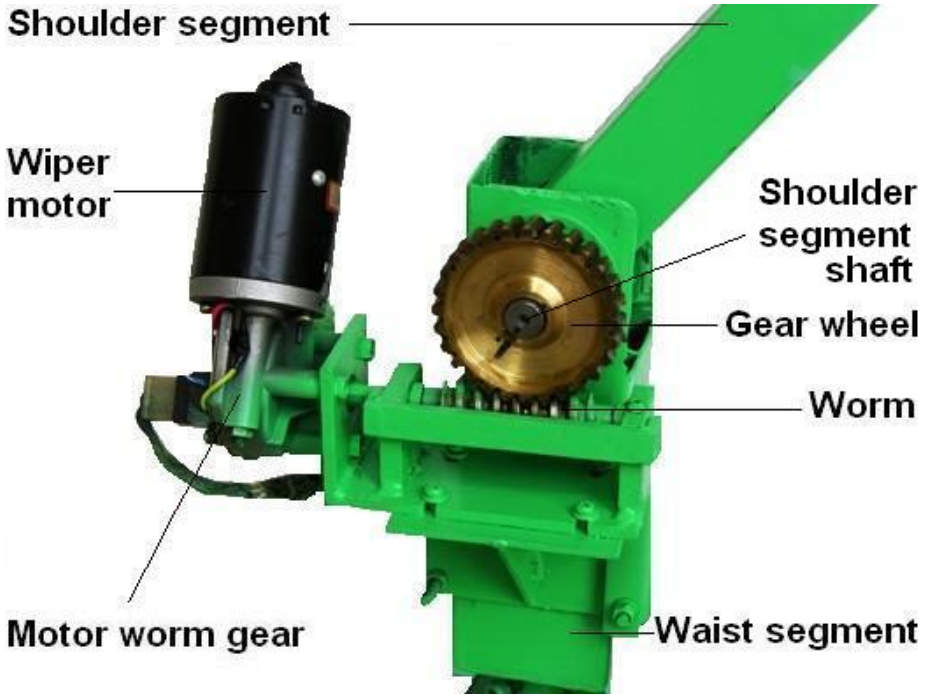

Fig. 2.7: Worm geared Shoulder rotation assembly.

2.4.3 Shoulder Segment

The Shoulder segment consists of following components:

1. Shoulder segment (dimension; L = 5.1 cm, W = 5.1 cm and H = 46.1 cm)
2. Pivot Shaft (dimension; Ø 1.7 cm × 14.5 cm)
3. Elbow moving mechanism
4. Two 6203ZZ bearings and housings

The Shoulder segment is fixed to the upper portion of Waist segment with the help of Shoulder segment pivot Shaft. The Shoulder is attached to this pivot shaft with the help of two 8M countersink screws. This pivot shaft coupled to the worm wheel has been supported by two ball bearings 6203ZZ attached at the both reinforced ends of Waist with the help of 6203ZZ ball bearing housing. A brass gear wheel is fixed at one end of the pivot shaft, so that when gear wheel rotates, the shoulder moves up and down. The Shoulder segment is manufactured from MS box pipe (22 SWG). To make Shoulder segment lighter in weight, slots have been made on the upper and lower sides of the box pipe. The cutting is made in such a way that the strength of pipe is not affected. Also, two extra pieces of MS sheet (16 SWG) having a dimension of 5.1 cm (L) × 8 cm (W) are welded to reinforce the both ends of Shoulder segment so that it can hold the weight and torque of Elbow and Wrist segments and gripped load. The 6200ZZ ball bearing housing is fixed to the terminal end of Shoulder segment. The Elbow segment is attached with the Shoulder segment with the help of Elbow segment pivot shaft (Ø 1 cm × 11.6 cm). The Elbow is attached to this pivot shaft with the help of two 8M countersink screws. This pivot shaft is supported by two ball bearings 6200ZZ attached at the both reinforced ends of Shoulder. The gear ratio in spur gears module is 1: 7.5. The Elbow rotation assembly is shown in Figs. 2.8 and 2.9.

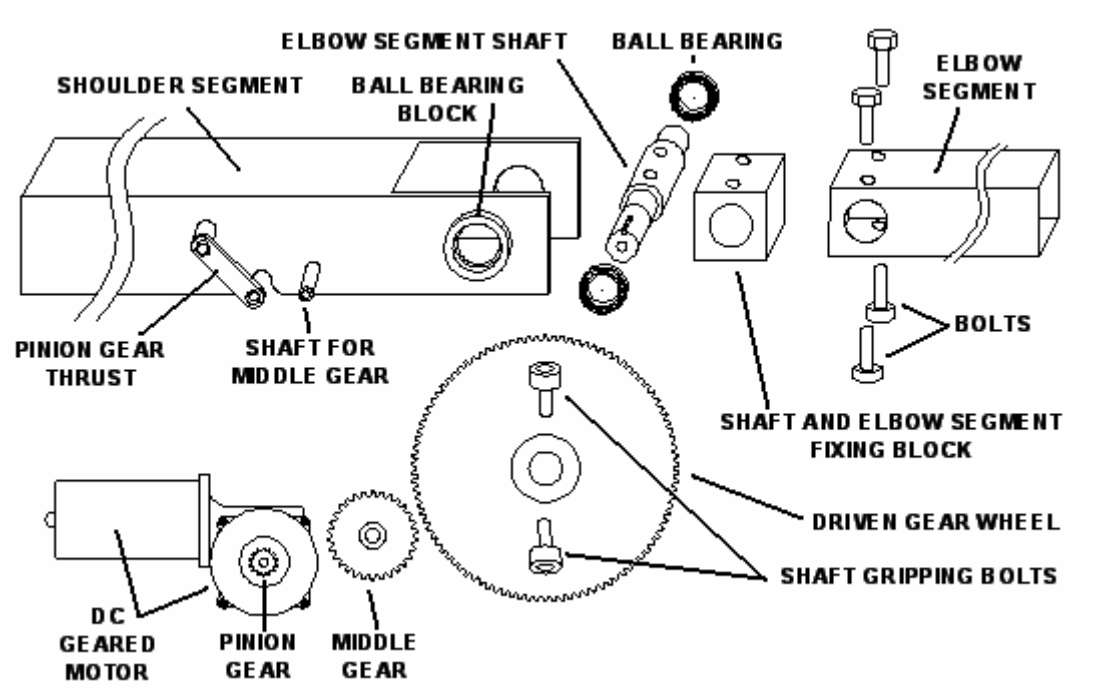

Fig. 2.8: Exploded view of Elbow rotation assembly.

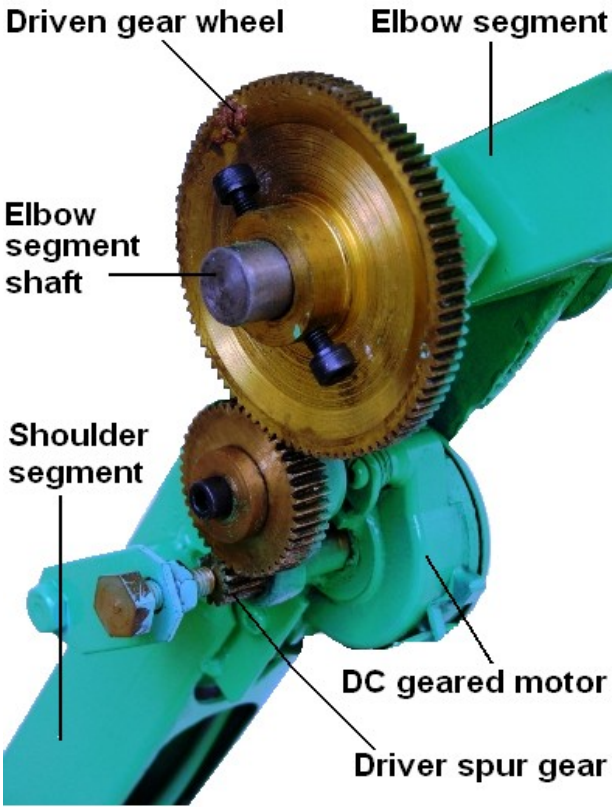

Fig. 2.9: DC geared motor with spur gear in Elbow module assembly.

The Elbow segment or spur gear module is driven by a DC worm geared motor (12 V DC**,** 1.2 A) fixed inside the Shoulder segment box pipe. Elbow position-measuring-rotary-encoder and limit switches are also attached on the Shoulder segment. The up-down movement of the Shoulder is limited within 110° range.

2.4.4 Elbow Segment

The Elbow segment consists of following components:

1. Elbow segment (dimension; L = 3.8 cm, W = 3.8 cm and H = 43.2 cm)
2. Spur driven gear wheel
3. Pivot Shaft (dimension; Ø 1 **c**m × 11.6 cm)
4. Wrist cables support
5. Wrist segment holder.

The Elbow segment is attached on the terminal end of the Shoulder segment with the help of Elbow pivot shaft. The Elbow segment is manufactured from MS pipe (22 SWG). To make the Elbow segment lightweight, the upper and lower sides of the box pipe is carefully slotted. The slot cutting is made in such a way that the strength of pipe is not affected. Also, two extra pieces of 16 SWG gauge MS sheet of size (3.6 cm (L) × 5 cm (W)) are welded to reinforce the both ends of Elbow segments so that it can hold the weight and torque of Wrist segment payload. Wrist position-measuring rotary-encoder and limit switches are also attached on the Elbow segment. A Web Cam is also attached on the Elbow segment through a MS sheet clamp. The Web Cam assists the operator for handling the objects with the Gripper and to search for the obstacles during movements of mobile platform and for visual surveys of labs. The elbow segment up-down sweep is within 180° range.

2.4.5 Wrist Segment

The Wrist segment consists of following components:

1. Wrist segment (dimension; L = 2.54 cm, W = 2.54 cm and H = 21 cm)
2. 1st worm gear module (gear ratio = 1 : 22)
3. 2nd worm gear module (gear ratio = 1 : 100)
4. Gripper-Push-Pull (GPP) holder
5. Gripper cable support

The Wrist segment is divided into two parts, i.e. Wrist and the Gripper. The Wrist segment is attached to the upper portion of Elbow segment with the help of Wrist segment holder. The Wrist segment is also manufactured from MS box pipe (22 SWG) having above dimensions. The wrist has 210^0 rotational movement with the help of a double worm geared assembly (gear ratio = 1 : 2200). The double worm geared assembly is shown in Figs. 2.10 and 2.11. The double worm gear module operates through a car speedometer cord coupled with a 12 V DC motor. The speedometer cord drives the 1st worm gear module having gear ratio 1 : 22. The worm wheel of 1st module drives the worm gear of 2nd worm gear module (1 :100). This produces very precise and control movement of wrist. The other end of the speedometer cord is fixed with the shaft of a DC motor. The DC motor is fixed to the Waist segment as shown in Figs. 2.12 and 2.13.

The Wrist rotation is limited within 210^0 range. The Wrist segment terminates into a Gripper. The actuator of the Gripper is located at Wrist segment. Two scissor action levers pull-push the gripper pair to open and grip the object. The gripper action is conducted through a clutch wire whose one end is connected with the scissor action levers and the other end is fixed to the actuator sliding screw.

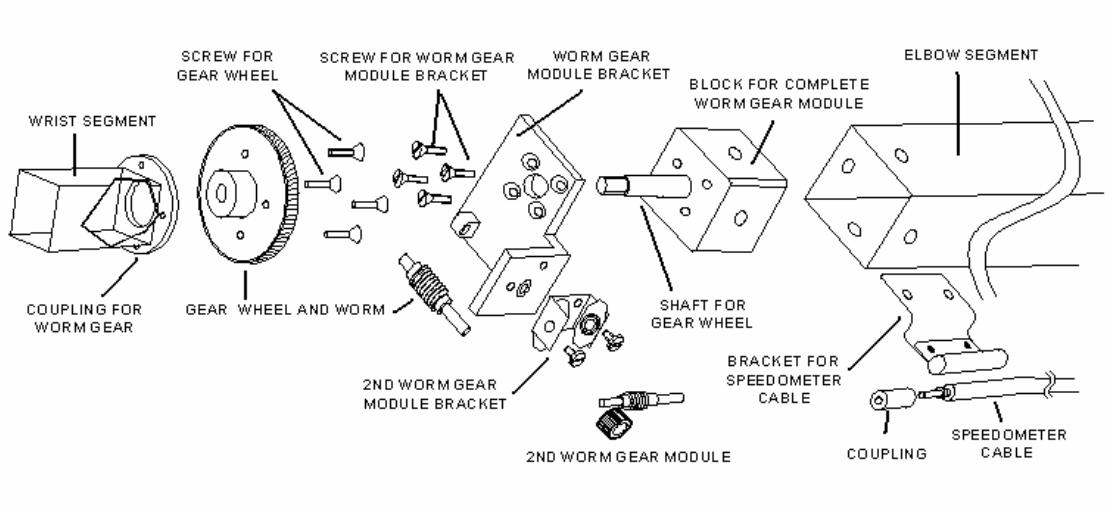

Fig. 2.10: Exploded view of Wrist rotation double worm geared assembly

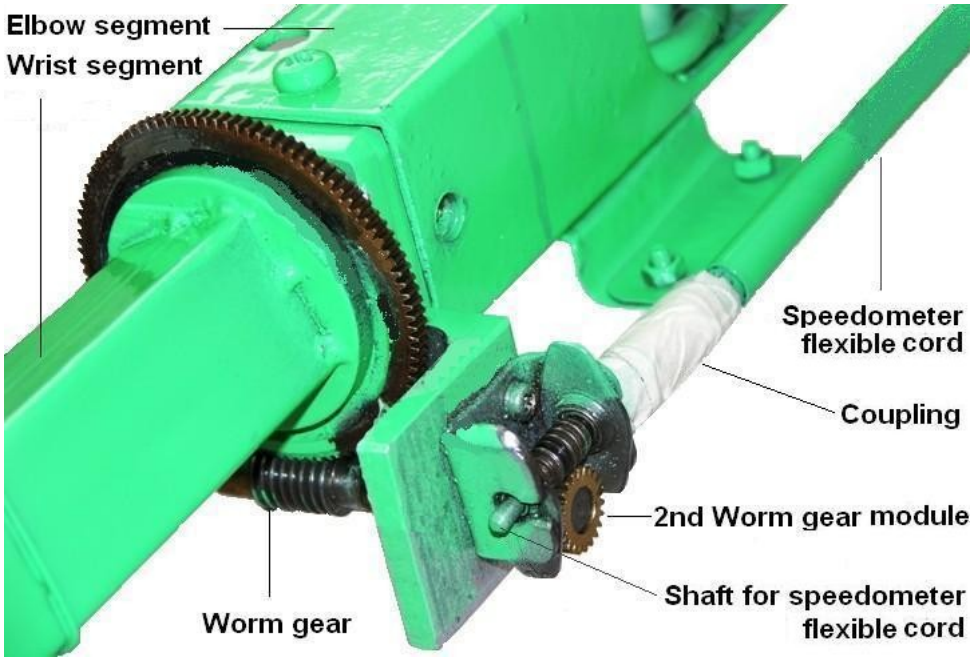

Fig. 2.11: Wrist rotation double worm geared assembly.

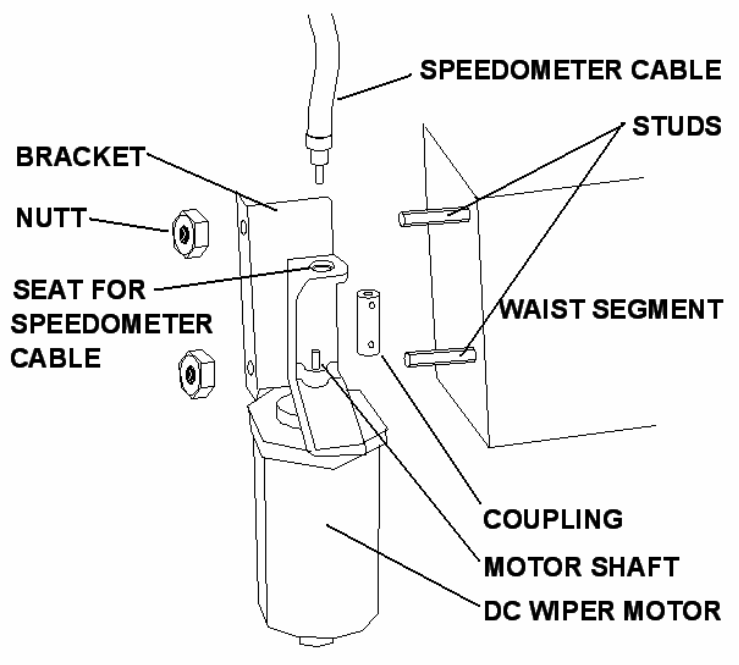

Fig. 2.12: Exploded view of Wrist rotation DC motor assembly.

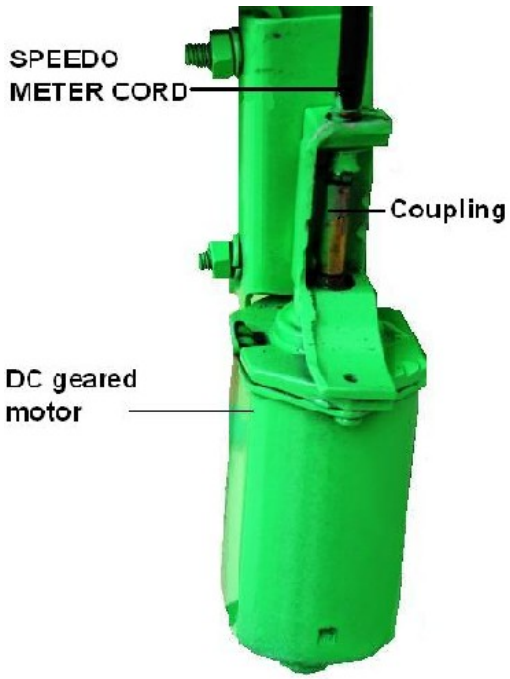

Fig. 2.13: Wrist rotation DC motor assembly.

2.4.6 Gripper Segment

The Gripper segment consists of following components:

1. Two Gripper pairs (dimension; L = 2.1 cm, W = 1.6 cm and H = 17 cm)
2. Two scissor action levers
3. Retrieving spring

The Gripper is located at the terminal end of the second half of Wrist segment. The Gripper pair is made of commercial aluminum. It is especially designed for a secure gripping of radioactive materials. The gripper is capable of carrying payload up to 2100 g and can grasp an object of 12 cm in diameter without disturbing the platform stability. The object may be cylindrical, flat or cubical in shape. The gripper is also capable of gripping about 0.35 mm thickness wire or a small object. This capability is very useful in picking an accidentally dropdown irradiated sample on the floor.

A special rubber lining is affixed to inner working side of the gripper to grip the object securely and safely. The lining material can easily be decontaminated or replaced if contaminated or damaged. The gripping action is generated through an actuator with a linear push-pull mechanism. This actuator is manufactured with a car power-window DC motor. A nut (8M) is fitted in the worm gear wheel. A 13 cm long stud (8M) is grinded longitudinally so that the threads of the stud disappears and can slides easily through a slip-fit keyhole having a dimension of 0.8 cm × 0.4 cm. One end of the sliding stud is provided with a 0.3 mm hole to hookup the clutch wire. A U-shaped MS strip bracket provided with keyhole is fixed on the gear box of the DC motor. The stud is passed through the keyhole and enters in the gear wheel nut. When gear wheel rotates, the stud moves linearly due to the keyhole. Hence the stud acts as a lead screw, which moves to and fro according to the direction of nut rotation. The Gripper assembly is shown in Figs. 2.14 and 2.15.

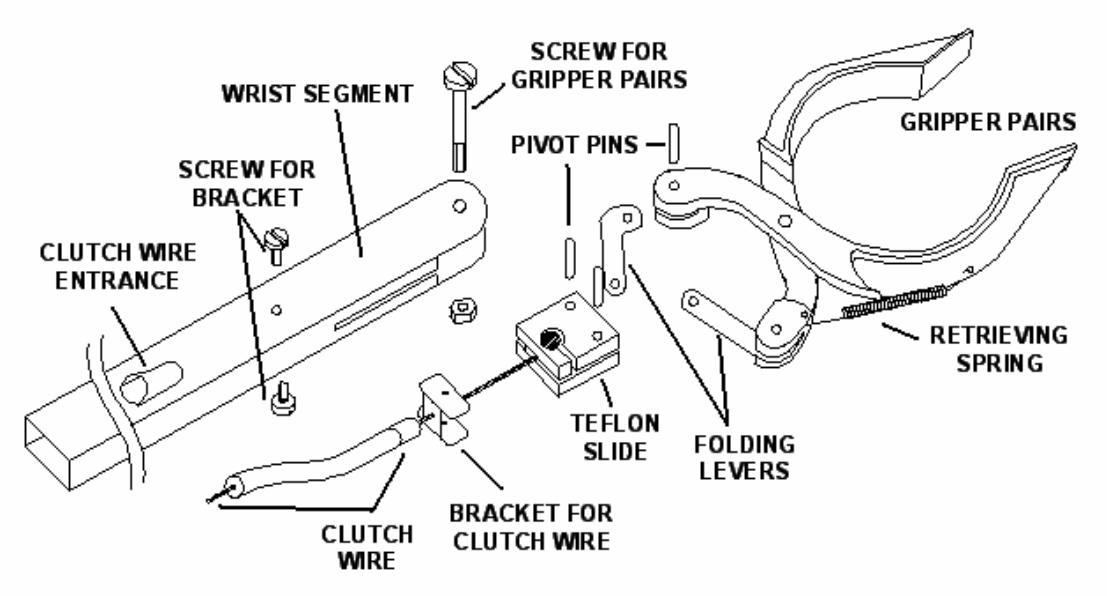

Fig. 2.14: Exploded view of RPAR Gripper assembly.

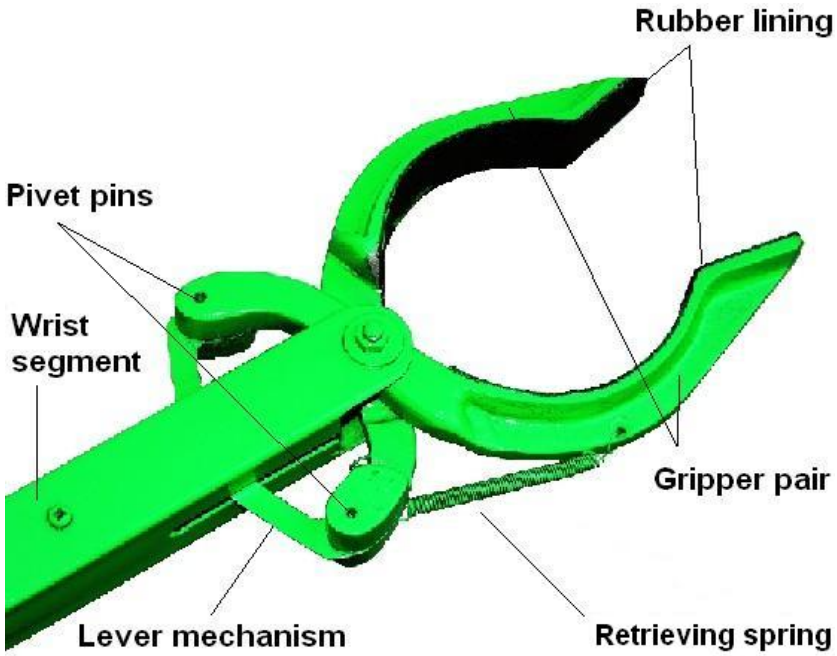

Fig. 2.15: RPAR Gripper assembly.

A motorcycle clutch wire is fixed to the gripper pair and the actuator lead-screw. When the actuator lead screw pulls the clutch wire, the gripping end gets closer to grasp the object, while push action is used to open the gripper to release the object.

The main idea for the use of car power window DC motor was that the worm gear wheel is provided with a built-in controllable torque clutch mechanism that is very helpful to adjust a desirable and safe gripping pressure of the gripper pair.

The clutch wire push-pull actuator assembly is derived from a 12 V DC, 1.2A geared motor. The complete actuator assembly is shown in Figs. 2.16 and 2.17.

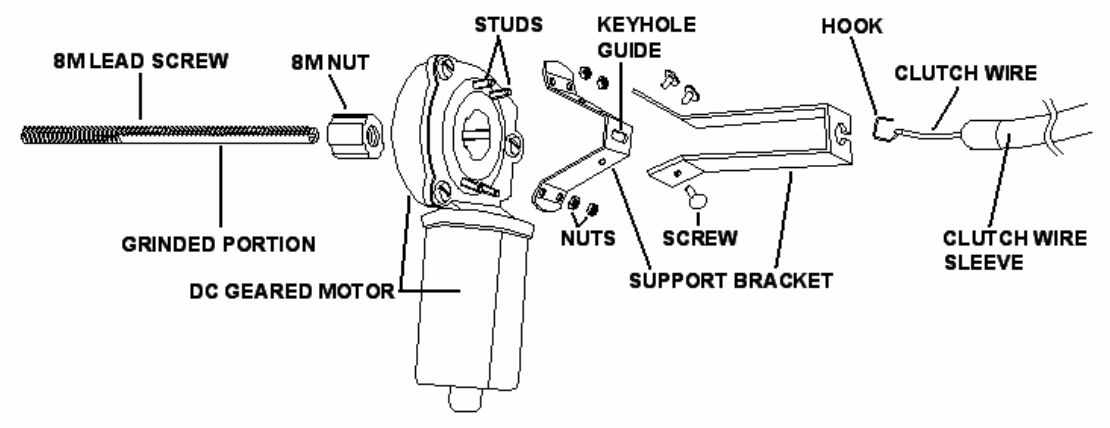

Fig. 2.16: Exploded view of actuator assembly for the Gripper mechanism.

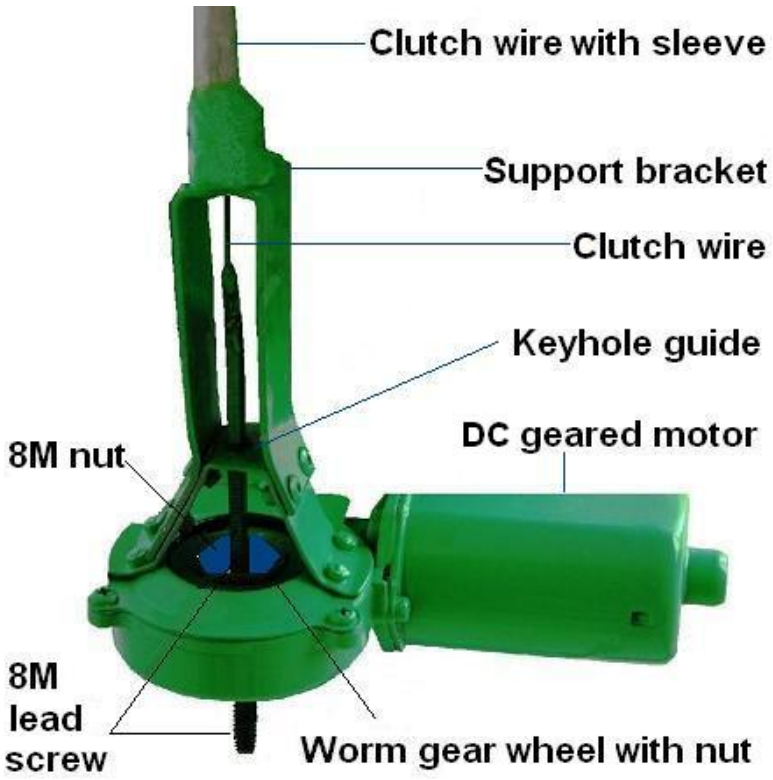

Fig. 2.17: Actuator Assembly for the Gripper mechanism.

2.5 CONCLUSION

This chapter has described the design and fabrication of different mechanical systems and mechanisms of Radiation Protection Assistant Robot (RPAR). The mechanical systems are cubical platform, differential wheel assembly, Waist, Shoulder, Elbow, Wrist, Gripper and their controlling and driving mechanisms. All these systems are locally designed and fabricated. These systems and their mechanisms were thoroughly tested and were found to work appropriately and satisfactorily in different tasks and assignments of RPAR.

CHAPTER

THREE

DESIGN AND DEVELOPMENT: ELECTRICAL AND ELECTRONICS COMPONENTS

3.1 INTRODUCTION

This chapter describes the hardware design consideration related to electrical and electronics components of Radiation Protection Assistant Robot (RPAR). Different types of modules, cards and circuits used to operate and control RPAR are also discussed.

The RPAR is powered with a 12 V DC, 17 AH rechargeable battery through which 12 V are directly supplied to all the driving modules of motors. Whereas the 5 V supply required for TTL digital logic circuits of interfacing and controller boards circuitry is generated through a DC-to-DC converter ICs (7805) that are capable to convert 12 V DC into 5 V DC. A battery-recharging unit is also incorporated in the robot to recharge when the battery required. The RPAR can perform its task continuously for 85 minutes when battery is fully charged. Two types of motor driver modules are designed and incorporated in RPAR. The Relay Logic Module (RLM) has a maximum of 10 A current ratings. Five

RLMs are used in RPAR. These modules are used to drive Gripper mechanism, Shoulder, Waist segment DC motors and two differential wheels DC motors. The relay in the RLM module has high current rating and greater radiation stability and hardening (Vandegriff 1990). The other module is H-bridge driver Module (HBM) with maximum current rating up to 4 A. Two HBMs are used in RPAR. One module drives the wrist rotational mechanism DC motor (12 V 2.5 A) while other HBM controls the Elbow DC motor (12 V 2.5 A). A pulse width modulation (PWM) circuit is used in the HBM. All the seven modules are controlled through parallel port of the onboard (slave) computer via an interfacing circuit. These interfacing circuits act as buffer between the robotic hardware and the onboard PC. The optocoupler ICs (4N25) are used for safe interfacing between the modules and the PC, to protect the PC from electric surge. The flow diagram of the object's integrated layout of RPAR is shown in Fig. 3.1.

An embedded controller card was also designed and developed to measure the real time positions of different segments of RPAR with the help of potentiometers acted as position sensors. The microcontroller on the card sends data to the onboard computer through serial port. The onboard (slave) computer and tele-computer (master) (Pentium IV, 3.2GHz, Intel Original LGA 775) are interconnected with the help of Wireless Ethernet by using a Wireless access point (D-link, DWL-2100AP, 802.11g), which communicates at 108Mbps data transfer rate. The electronics of this robot is well shielded by double walled lead jacket filled with mineral oil to protect it from the ionizing and scattering radiations.

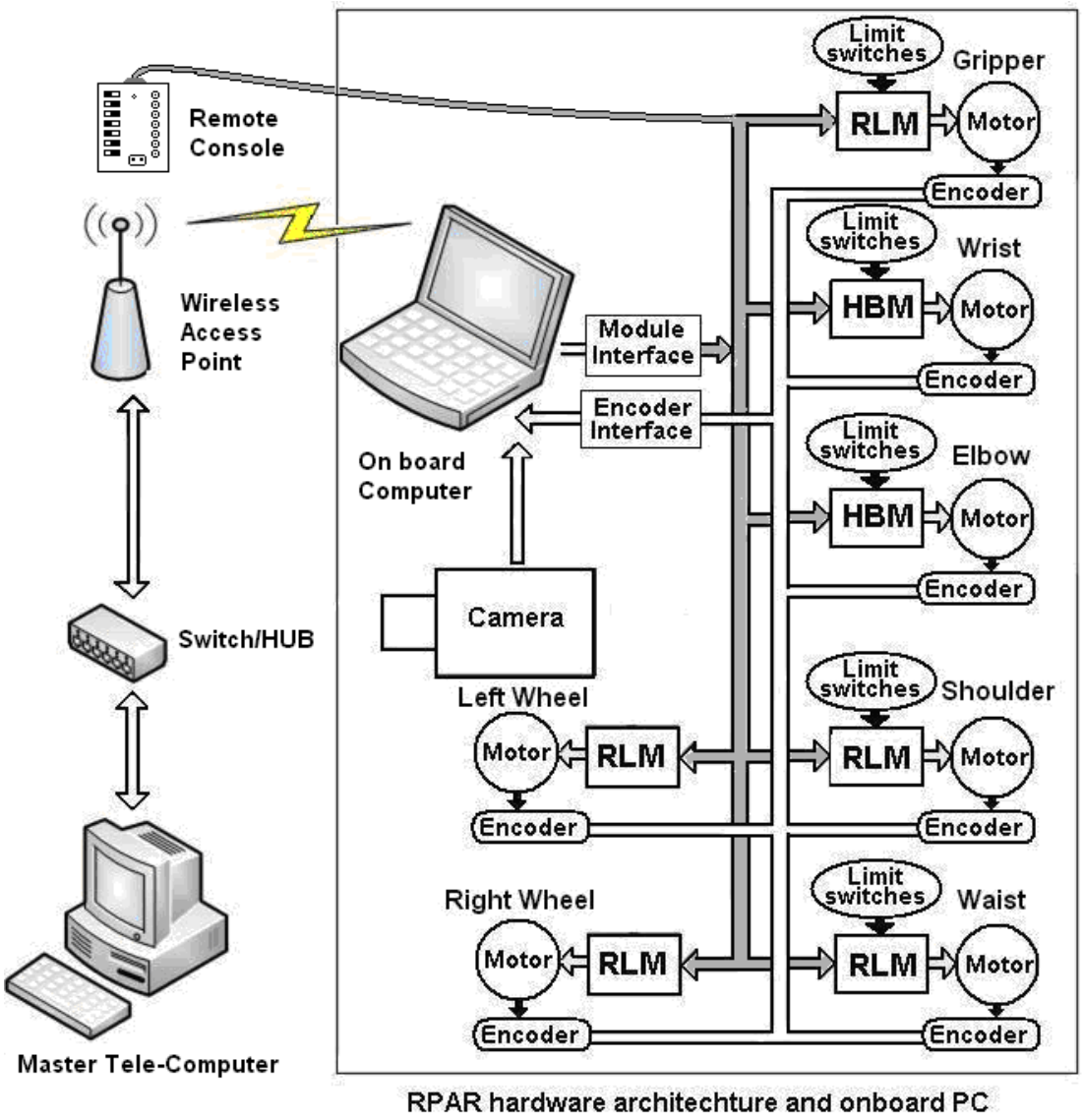

Fig. 3.1: Block diagram of interfacing and connections of RPAR.

3.2 RELAY LOGIC MODULE (RLM)

The Relay Logic Modules (RLM) are designed and developed to control five 12 V DC motors having current rating up to 10 A. This module comprises of four similar units. The specifications of components used for the construction of RLM are given in Table.

3.1. The circuit diagram of RLM is shown in Fig. 3.2. Two units are used to control one motor. One relay is used to select the direction and other relay is employed to start or stop the motor.

Table 3.1: Components list of RLM.

S. No.	Components	Quantity
1.	Relay (DC 12 V, 10 A, DPDT)	04
2.	FET (IRF 640)	04
3.	Optocoupler (4N25)	04
4.	Resistor 4.7 kΩ, ¼ W	04
5.	Resistor 10 kΩ, ¼ W	04
6.	Resistor 1 kΩ, ¼ W	08
7.	LED	04
8.	Connector 2 pins	02
9.	Connector 6 pins	01
10.	Diode IN4005	04

The RLM is designed to control two motors simultaneously. The connector J1 is a 6-pins connector for power and control signals. Pin 1 and Pin 2 of J1 connector are used to control 1st motor. Pin 1 is for the rotational direction bit of 1st motor. If set at "0" then the motor will rotates clockwise and if it is set at "1" then the motor rotates anticlockwise.

The Pin 2 of J1 connector is for start/enable or stop/disable of the 1st motor. When Pin 2 of J1 is set at "1" it will start/enable the 1st motor and vice versa. Pin 3 & 4 of J1 connector are for the 2nd motor controls. Here Pin 3 is direction selection bit and Pin 4 is for start/enable or stop/disable of 2nd motor. Pin 5 & 6 of J1 connector are power-supply pins of the module. Pin 5 is for 12 V DC and Pin 6 is ground pin. The 1st motor is connected to J2 connector while 2nd motor is connected to J3 connector.

The RLM has advantages over the HBM. It can be used for motors having current rating from 4-10 A. Two motors can be controlled simultaneously through one RLM. Heat sinks are not required to cool down any chip. Another advantage of RLM is that there is no voltage drop across the module. Where as 1.5 V drop was observed across the L298 in HBM, which causes less power to motor and lesser torque to arm or wheel.

The main disadvantage with RLM is that power is transmitted to motors of RPAR immediately, resulting in jerking behaviors of arms and mobile platform. Additional circuitry is required to deal with this problem. Also speed of the motor cannot be varied through this module.

Mainly five motors of RPAR are being operated with RLMs, including two differential gear motors of platform, waist & shoulder mechanism motors and gripper actuator motor.

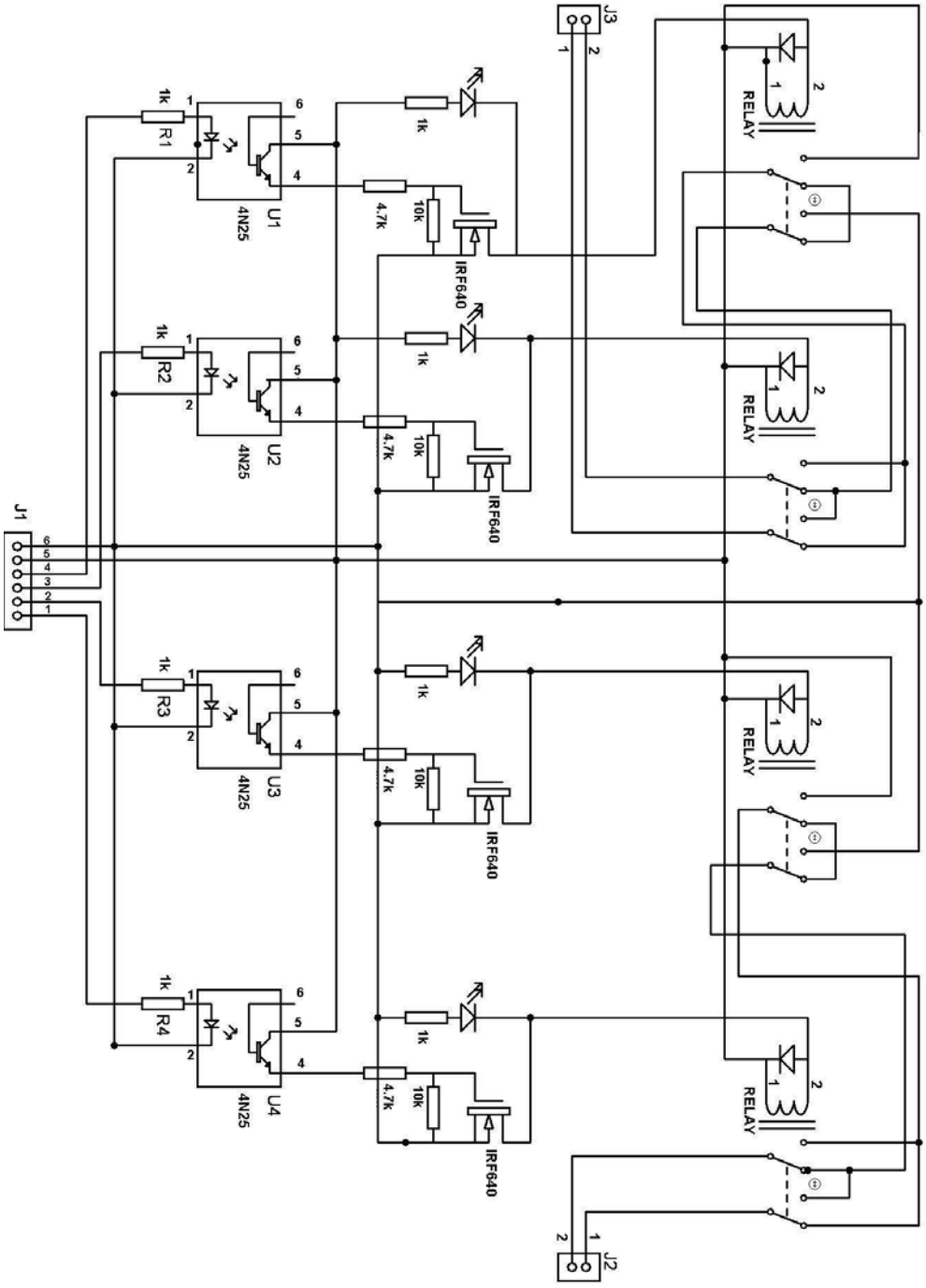

Fig. 3.2: Circuit diagram of Relay Logic Module.

3.3 H-BRIDGE MODULE (HBM)

The HBM is designed and developed to control one DC motor having current rating up to 4 A. This module is comprised of following components;

Table 3.2: Components list of HBM.

S. No.	Components	Quantity
1.	H Bridge IC L298	01
2.	IC T820M	01
3.	IC 74LS00	01
4.	Transistor NPN C1384	01
5.	Relay (DC 12 V, 5 A, SPDT)	01
6.	Resistor 68 Ω, ¼ W	01
7.	Resistor 22 Ω, ¼ W	02
8.	Resistor 1 kΩ, ¼ W	02
9.	Resistor 10 kΩ, ¼ W	01
10.	Potentiometer 10 kΩ,	01
11.	LED	01
12.	Diode IN4005 1.0 A 50-1000 V	05
13.	Capacitor 47 nF/50V	01
14.	Capacitor 100 nF/50V	03
15.	Capacitor 0.33 μF/50V	01
16.	Connector 2 pins	02
17.	Connector 6 pins	01
18.	L298 Cooling Fan	01

This module comprises of one H-Bridge IC (L298) attached with Pulse Width Modulation circuit (PWM). The L298 is an integrated monolithic circuit in a 15-lead Multiwatt and Power SO20 packages. It is a high voltage, high current dual full-bridge

driver designed to accept standard TTL logic levels and drives inductive loads such as relays, solenoids, DC and stepping motors. Two enable inputs are provided to enable or disable the device independently of the input signals. The emitters of the lower transistors of each bridge are connected together and the corresponding external terminal can be used for the connection of an external sensing resistor. An additional supply input is provided so that the logic can work at a lower voltage. The L298 chip is capable of controlling two motors independently along with the associated fly back and free wheeling diodes, bypass capacitors etc. In parallel configuration, the L298 can control one motor with repetitive peak current of more than 2 A but less than 4 A. The parallel configuration is used in the H-Bridge module.

A PWM signal is given to enable pins 5 and 11 of IC L298 for motor control. The PWM signal is generated from a IC T820M and associated components in the HBM. The waveform of the PWM or duty cycle of a period can be varied with the help of 10 k Ω potentiometer (RV1), which in used to adjust the desire speed of DC motor and torque of arm. The motor will move faster if the duty cycle is higher.

The J2 is a 6-pin connector. Pin 1 and Pin 2 of J2 connector are used to provide the voltage to the HBM. Pin 1 is provides 5 V DC while Pin 2 is a ground pin. Pin 3 is spare. Pin 4 provides 12 V DC to the module. Pin 5 is start/enable or stop/disable pin of HBM and eventually enables or disables the motor. When Pin 5 is set at "1", it activates HBM 's relay that provides power to the ICs and starts the motor and vice versa. The relay is used to provide voltage only when the motor is required to work otherwise continuous voltage will warm the L298 IC. Pin 6 of J2 connector is direction pin of the motor. If set at "0" the motor will rotate clockwise and if it is set at "1", counter clockwise rotation will be obtained. The 12 V DC motor is connected at J2.

The HBM has advantage over the RLM in motor speed controllability. Any required speed and torque can be obtained from this module. However, this module has a number of disadvantages. DC motors having current more than 4 A can't be controlled with this module. Only one motor can be controlled with this module. A heat sink and a cooling fan are required to cool down L298 chip. The main drawback is voltage drop across the L298 in this module, thus delivering less power to motor and in turn lesser torque to arm or wheel. So only low torque motors can be controlled through this module. A circuit diagram of HBM is shown in the Fig. 3.3.

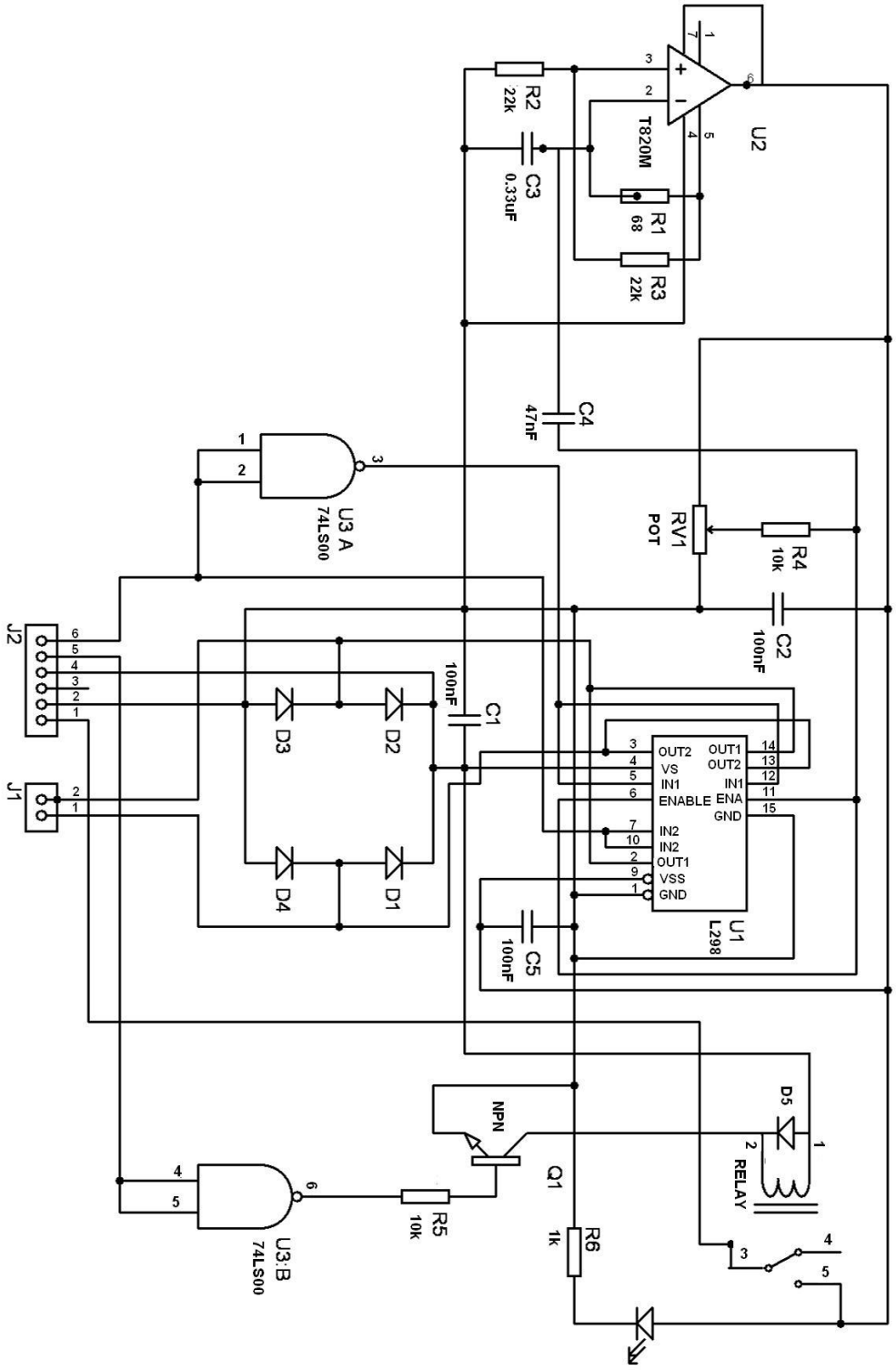

Fig. 3.3: Circuit diagram of H-Bridge Module.

3.4 PARALLEL PORT INTERFACE MODULE

RPAR can be controlled with a remote console or Tele-computer through a Parallel Port Interface Module (PPIM). The PPIM consists of two interfacing cards.

(i) Buffer Card

(ii) Demultiplexer Card

3.4.1 Buffer Card

The Buffer card is used to connect the robot electronics to the printer port of an on-board computer through the Demultiplexer card. The Buffer card consists of components mentioned in Table 3.3 with their specifications.

Table 3.3: Components list of Buffer Card.

S. No.	Components	Quantity
1.	IC 4N25	08
2.	IC 74LS245	01
3.	IC 7805	01
4.	Resistor 1 kΩ, ¼ W	17
5.	Resistor 10 kΩ, ¼ W	08
6.	Capacitor 0.1μF/50V	02
7.	LED	09
8.	Connector 25 pins D type female	01
9.	Connector 8 pins female	01

Eight optocoupler ICs were used to isolate the on-board computer from the RPAR electrical and electronic circuitry to save on-board PC from any high voltage surge produced during switching of the RPAR system.

The Pin 2 to Pin 9 of printer port is 8 bit data bus or data lines. These data lines are connected to the Buffer card through optocoupler ICs. Data from optocoupler are latched with the help of buffer/latched IC (74LS245). The latched data is transmitted to Demultiplexer card through an 8 bit data bus. The circuit diagram of the Buffer card is shown in Fig. 3.4.

3.4.2 Demultiplexer Card

Demultiplexer card consists of a Demux IC (74HC154) and four Hex buffer (74LS367) drivers ICs. The Demux receives four binary weighted input lines (1, 2, 4, 8)/(A, B, C and D) and provides sixteen outputs. If the device is enabled, these inputs determine which one of the 16 normally high outputs will go low, so only one output or Hex buffer IC can be switched "on" or enabled at a time. The first four of eight bit data outputs from the parallel port are provided to the Address pins (ABCD) of Demux IC through the optocoupler ICs and latched IC of Buffer card. In this way four-bit address bus can control sixteen hex buffer devices. A limitation of the Demux is that only one Hex buffer IC can be activated at a time. Therefore, only two motors can be controlled through one Demux IC. As mentioned earlier, two bits are required to control a DC motor (One bit to enable/disable the motor while other to select the direction (CW/CCW)), therefore two HBM or one RLM can be connected to one Hex buffer driver IC (74367). Remaining four bit data of 8-bit LPT data is provided to all the Hex buffer drivers. But the data is being transmitted from that Hex buffer driver that is

enabled by Demux IC through appropriate address data at its address pins i.e. A, B, C and D. Component list of Demultiplexer card is given in Table 3.4 and circuit diagram is shown in Fig. 3.5.

Table 3.4: Components list of Demultiplexer Card.

S. No.	Components	Quantity
1.	IC 74154	01
2.	IC 74LS367	04
3.	Resistor 1 kΩ, ¼ W	01
4.	LED	01
5.	Ribbon cable 8-bit	01
6.	Connector 2 pins for supply	01
7.	Connector 25 pins D type female	01
8.	Connector 8 pins female	01

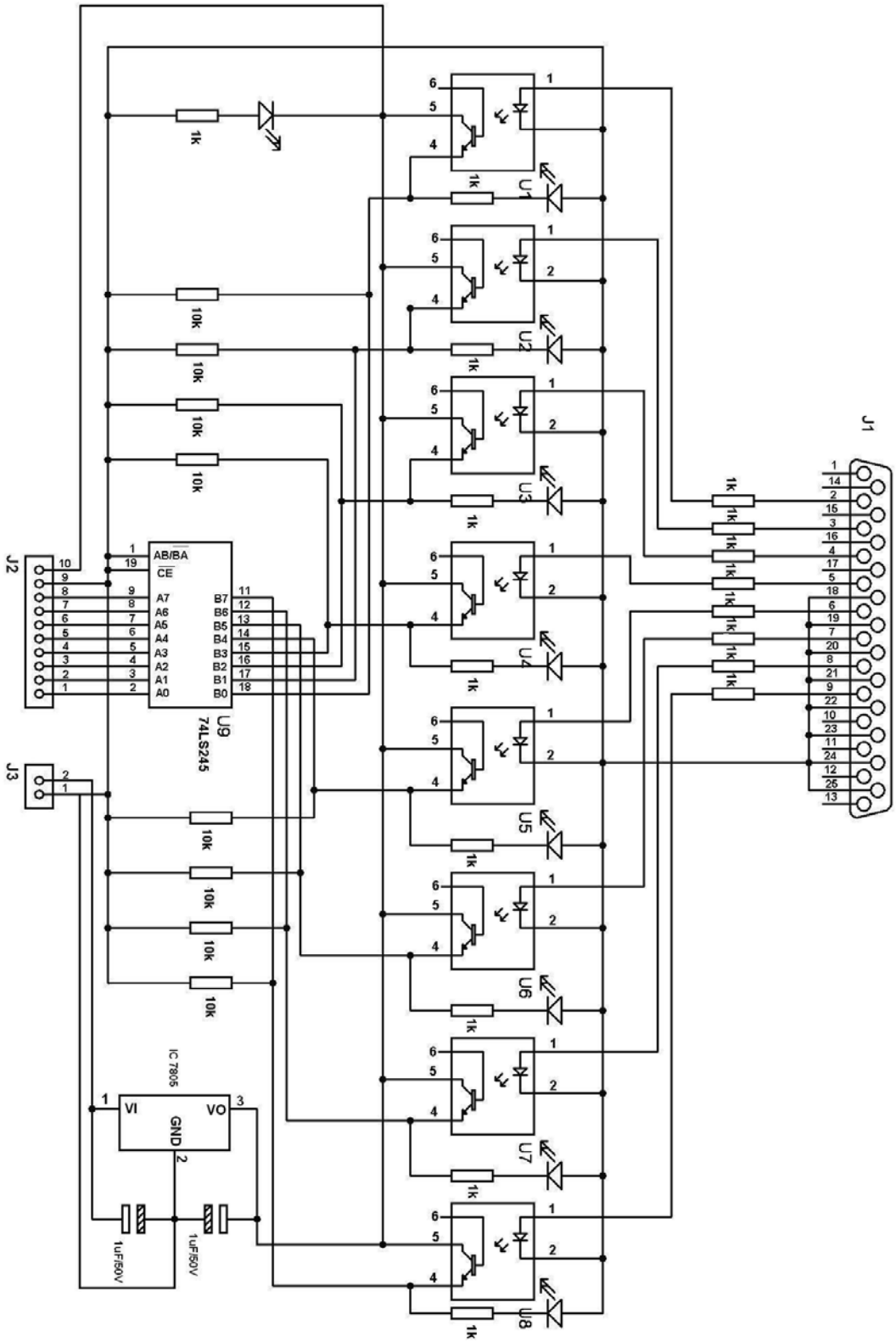

Fig. 3.4: Circuit diagram of Buffer card.

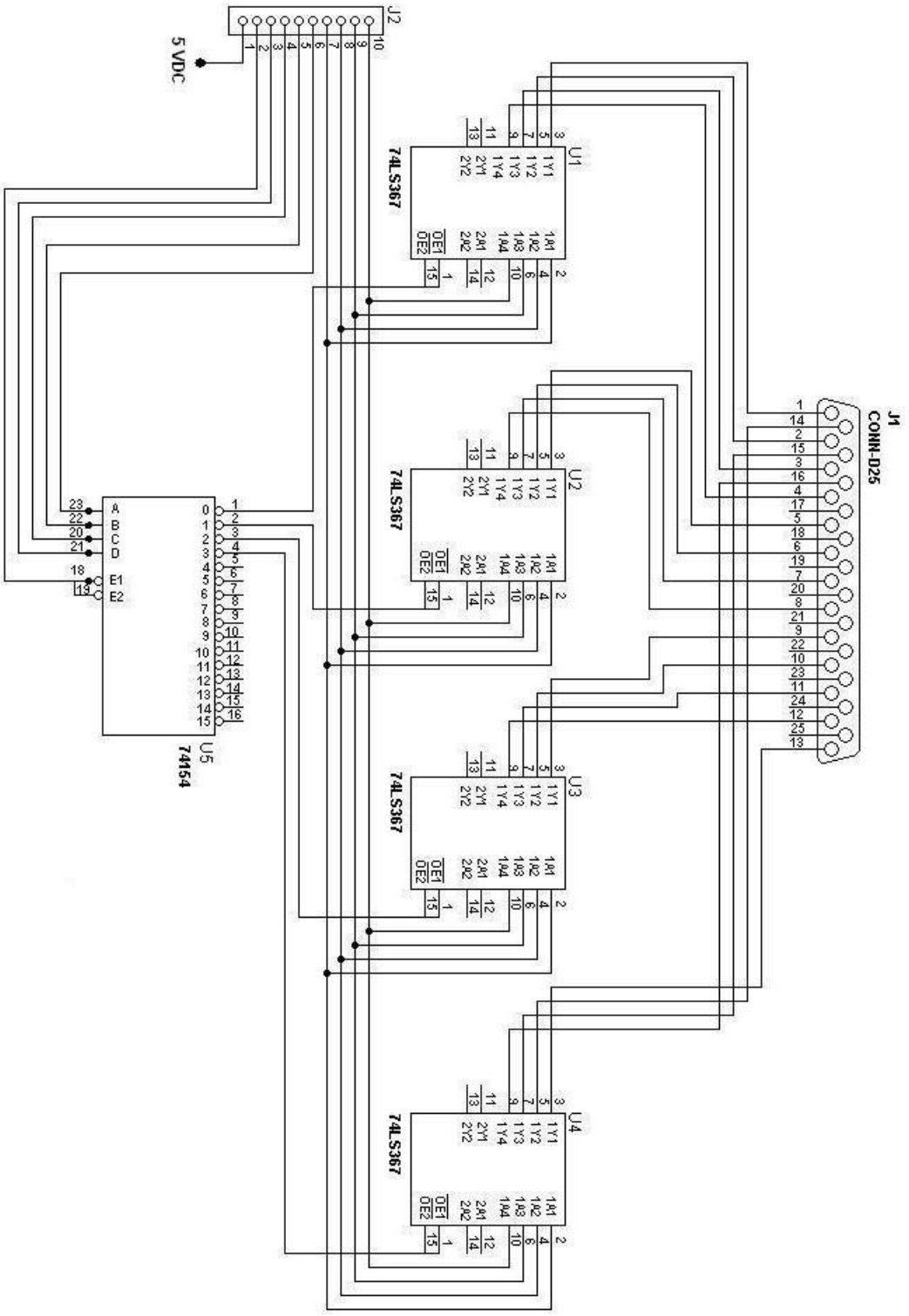

Fig. 3.5: Circuit diagram of Demultiplexer card

3.5 LIMIT SWITCHES MODULE (LSM)

Limit Switches Module (LSM) was also designed, fabricated and incorporated to restrict the movement of each RPAR articulate arm's segment in a desired range and to protect them from any mechanical damage by operator error or false signal etc. The LSM was a vital part of robot to fulfill Isaac Asimov's Laws of Robotics i.e. "A robot must protect its own existence" (Critchlow 1985).

The LSM comprises of five similar circuits. Each circuit is working independently. One circuit is used to restrict gripper open-close motion within a safe range. Second circuit is used to restrict wrist motion within safe 210^0 sweep. The third circuit enables the elbow to move up to secure 180^0. The fourth circuit allows shoulder to move only harmless 110^0. The fifth and final circuit of LSM permits the waist to rotate within 195^0 and secure the wires from over stretch and damage.

The LSM restricts the segments with the help of limit switches attached at each segment. One switch is used to set the upper limit and second to set the lower limit. Each circuit of LSM module consists of one AND gate (Triple 3-Input AND gate, IC 7411) and one Not gate (IC 7404). The specifications of the ICs and other components are given in Table. 3.5. The circuit diagram of the LSM circuit is shown in Fig. 3.6.

Table 3.5: Components list of Limit Switches Module.

S. No.	Components	Quantity
1.	IC 74LS11	02
2.	IC 74LS04	01
3.	Resistor 10 kΩ, ¼ W	10
4.	Resistor 1 kΩ, ¼ W	06
5.	LED	01
6.	Connector 20 pins	02
7.	Connector 2 pins	01

The LSM has two 20-pins connectors J1 and J2. The Pin 1 to 4 of J1 connector are connected to the limit switches (at COM and NO pins of the limit switch) of gripper. Pin 5 of J1 is Enable-1 or input bit of the circuit either from the remote console or onboard computer. Pin 6 of J1 is the direction bit of gripper and Pin 7 is Enable-2 or output of this limit circuit. This Enable-2 is connected to the Gripper's module to activate the Open-Close mechanism. Pin 8 of J1 is Not Connected (NC). Pin 9 to 12 of J1 are connected to the limit switches of Wrist assembly. Pin 13 of J1 is for Enable-1, Pin 14 is for direction bit and Pin 15 is Enable-2 of Wrist motion module. Pin 16 of J1 is NC. Pin 17 to 20 of J1 are connected to the limit switches of Elbow segment.

Pin 1 of J2 connector is for Enable-1, Pin 2 of J2 is for direction bit and Pin 3 of J2 is Enable-2 of Elbow movement motion. Pin 4 of J2 is NC. Pin 5 to 8 of J2 are connected to the limit switches of Shoulder segment. Pin 9 of J2 is for Enable-1, Pin 10 of J2 is for direction bit and Pin 11 is for Enable-2 of Shoulder motion module. Pin 12 of J2 is NC. Similarly, Pin 13 to 16 of J2 is connected to the limit switches of Waist segment. Pin 17 of J2 is for Enable-1, Pin18 of J2 is for direction bit and Pin 19 is for Enable-2 of waist motion module. Pin 20 of J2 connector is NC. J3 connector is providing +5 V and ground to the card.

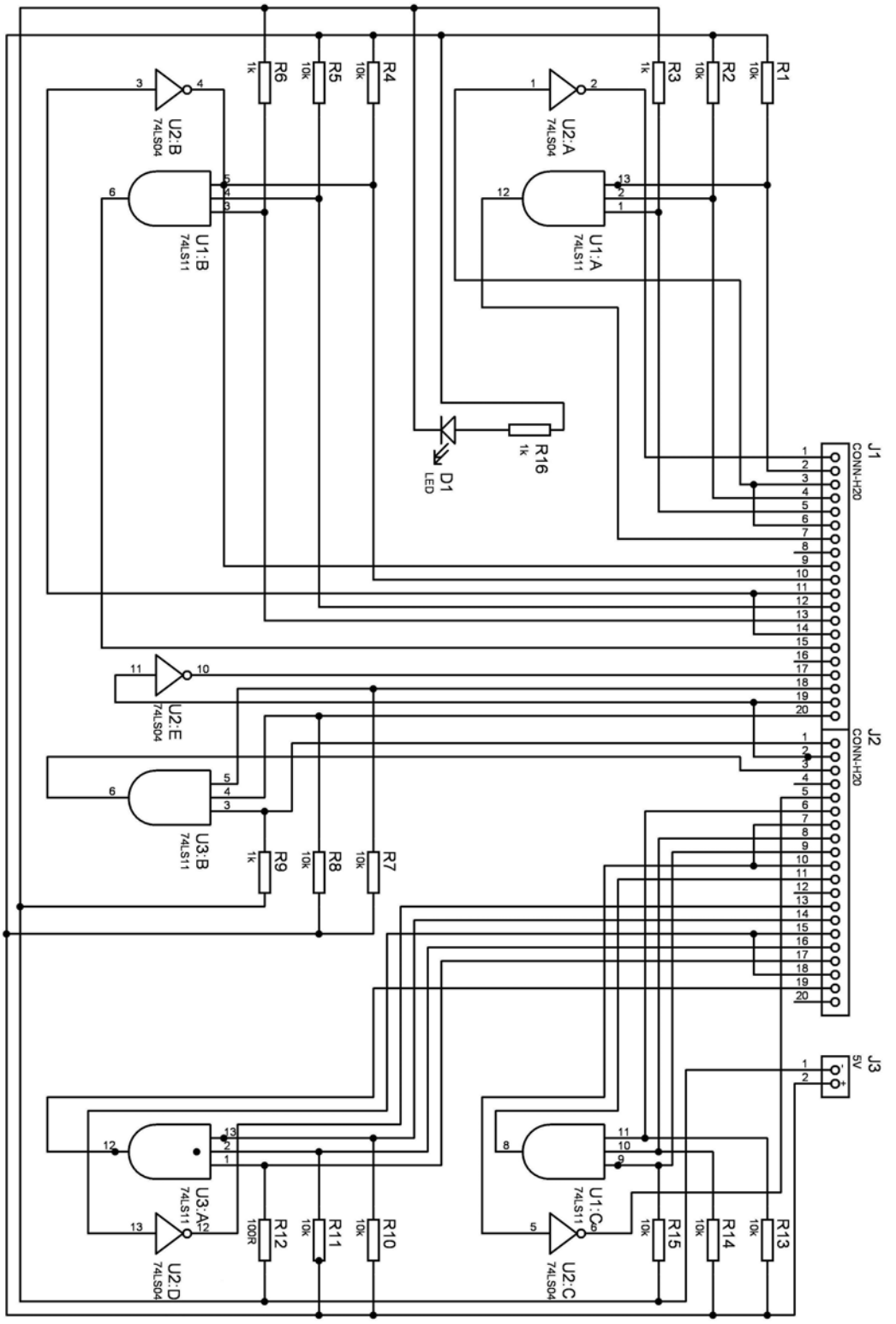

Fig. 3.6: Circuit diagram of Limit Switches Module

3.5.1 Working Logic of one LSM circuit

As mentioned earlier, LSM consists of five identical circuits. The working logic is similar in all. To explain the working logic, one of the circuits associated with Gripper movement module is being described in this section.

When the Pin 6 of J1 connector or direction bit is set at "1" through toggle switch and simultaneously the Gripper enable switch is pressed from the wired consol and the Enable-1 becomes "1". This action will turn the Enable-2 to "1" i.e. Pin 7 of J1 becomes "1", if both the limit switches are at normally open state (un-pressed) as shown in Fig. 3.7.

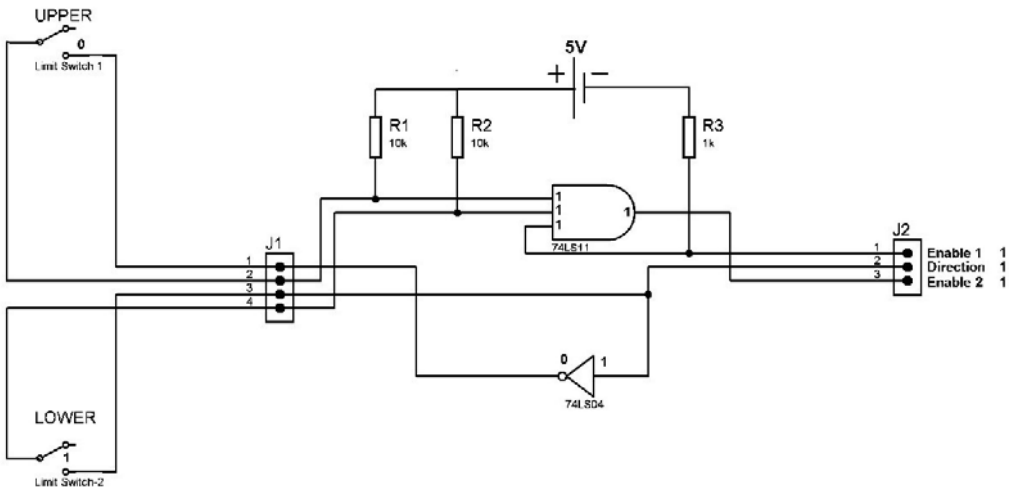

Fig. 3.7: Both switches are un-pressed and direction bit is "1".

The Enable-2's "1" state energizes the RLM and starts the motor to open the gripper pair. When this state remains at "1" the gripper motor continuously rotates till it presses the upper limit switch. As soon as the limit switch is pressed the corresponding input of AND gate becomes "0" and the Enable-2 becomes "0". This action de-energizes the RLM and stops the motor. The action is illustrated in Fig. 3.8.

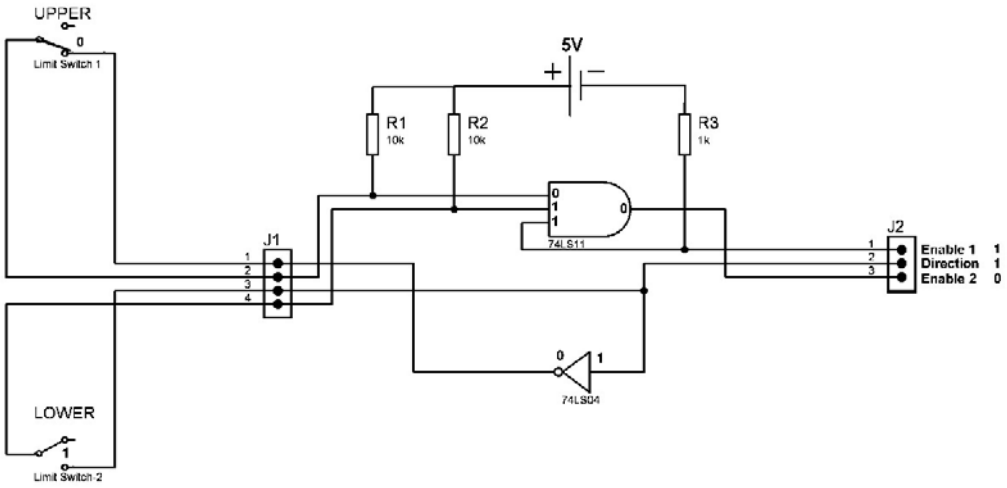

Fig. 3.8: Upper limit switch is pressed.

Now the Gripper actuator motor can rotates in inverse direction only, i.e. when the direction is set at "0" state. So, when direction bit is set at "0" it makes the Enable-2 at "1" state and gripper motor starts moving in opposite direction. The action is illustrated in Fig. 3.9.

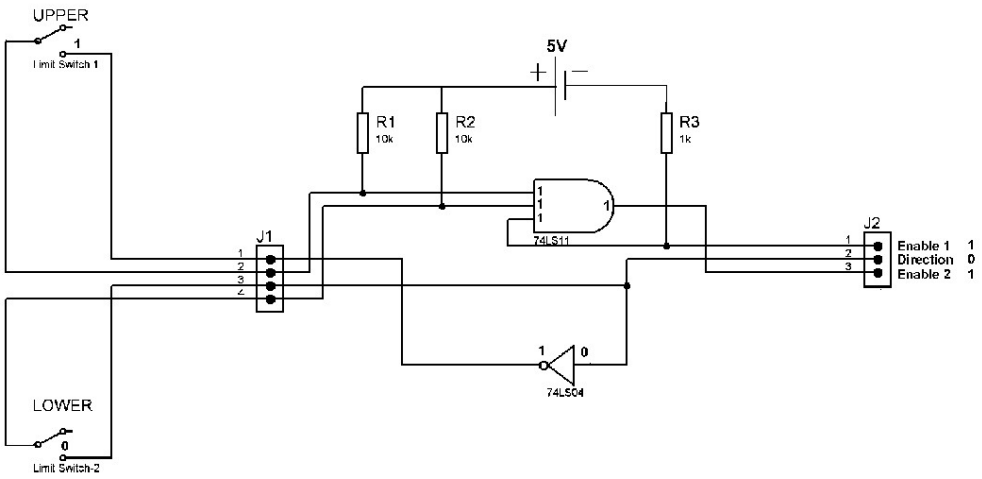

Fig. 3.9: Both switches are un-pressed and direction "0".

When the Gripper pair reaches its lower limit, the lower limit switch will be pressed and send "0" to the corresponding input of AND gate, which turns the Enable-2 "0" and stop the motor. This action is illustrated in Fig. 3.10. Now the gripper motor can move only in opposite direction when the direction bit is at "1" state. Similar logic is used in remaining four limit switch circuits of the LSM.

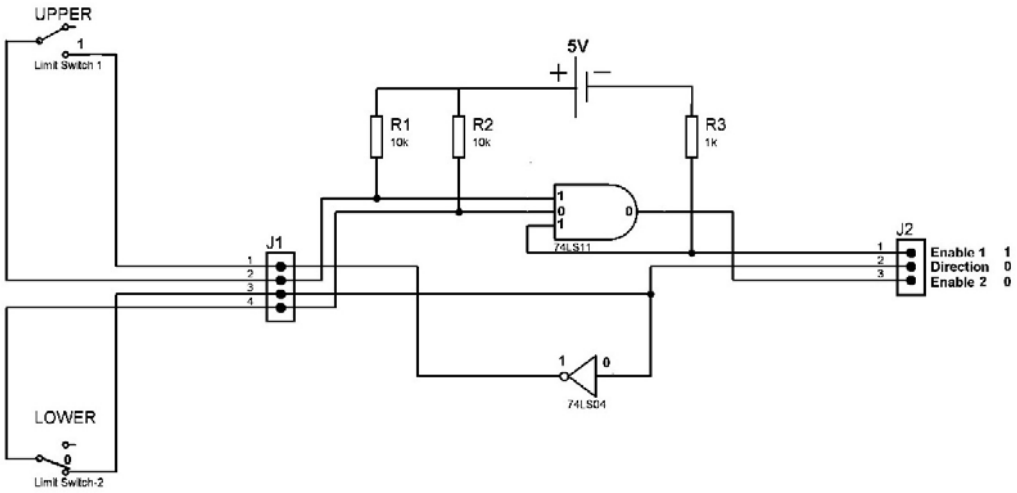

Fig. 3.10: Lower limit switch is pressed.

3.6 DESIGN DESCRIPTION OF CONTROL PANEL

A control panel for RPAR has been designed and fabricated to control and monitor the operation of RPAR platform and articulated robotic arm by voltage and current status of the battery etc. Components list of Control Panel is given in Table 3.6. The circuit diagram of control panel is shown in Fig. 3.11 and front panel in Fig.3.12.

Table 3.6: Components list of Control Panel.

S. No.	Components	Quantity
1.	Voltmeter 15 V	01
2.	Ammeter 20 A	01
3.	Automotive Ignition Switch.	01
4.	Toggle Switch (Current Direction Switch)	01
5.	Relay (DC 12 V, 10 A, DPDT)	01
6.	Resistor 1 kΩ, ¼ W	02
7.	Resistor 30 Ω, 10 W	01
8.	LED	02
9.	Bi-color LED (dimension; 3.0 × 5.3 mm) round shape	07
10.	Connector 2 pins	02
11.	Connector 15 pins	01
12.	Rechargeable battery 12 V, 17Ah sealed lead-acid type	01
13.	Fuse holder and fuse 10 A	01

Key-Switch is an automotive ignition switch. It has two modes, charging mode and power ON/OFF mode. So, when the key is at charging mode, 12V 17AH rechargeable battery starts charging. The RPAR will be "ON" when the key is at power "ON" mode. In "OFF" mode, the key of RPAR can be removed from the switch in order to secure it from authorization use.

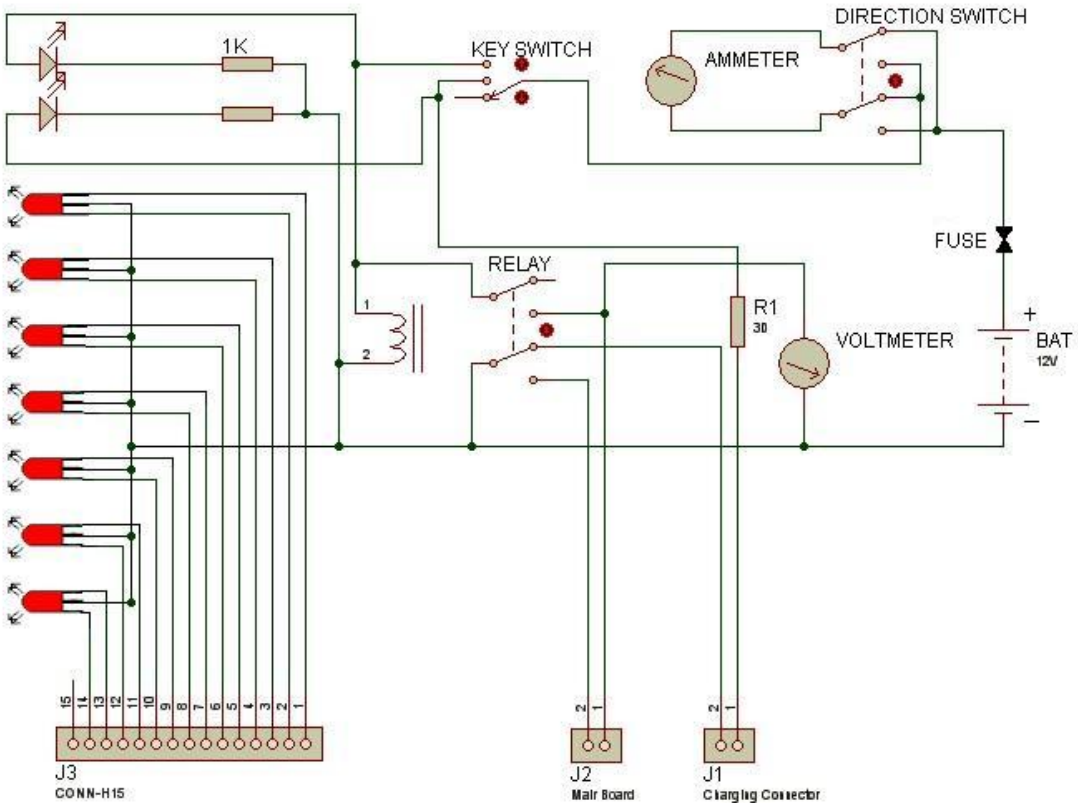

Fig. 3.11: Circuit diagram of Control Panel.

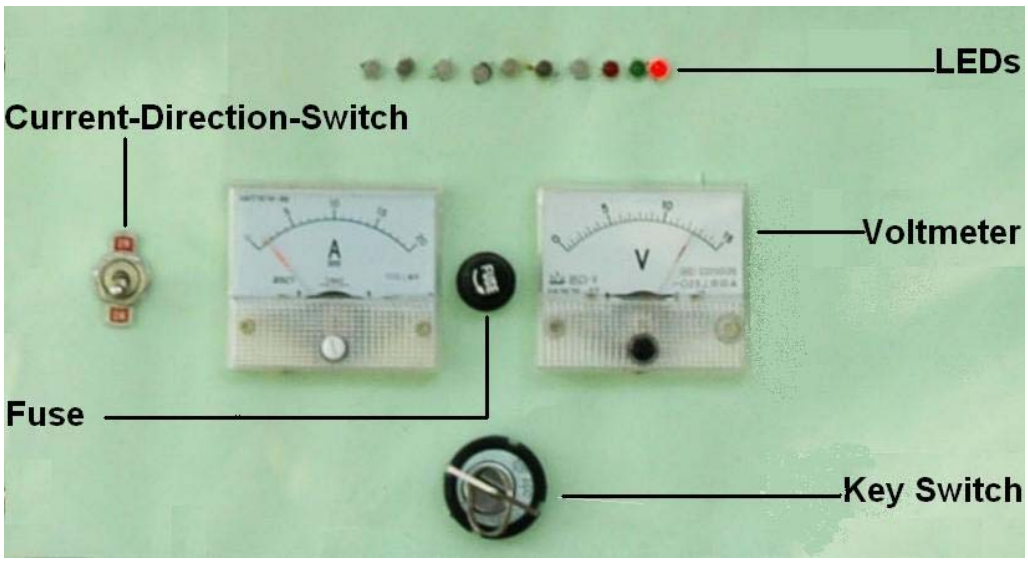

Fig. 3.12: Control Panel.

An ammeter is used to measure the battery charging and load current. The direction of charging current is opposite to the load current. So, the Current-Direction-Switch (CDS) is used to adjust the direction of current. When the CDS is upwards, the ammeter shows the charging current and vice versa. The battery charging is adjusted at 400 mA. The Voltmeter indicates the voltage status of battery in operation mode of RPAR only. Nine LED indicators have been incorporated on the control panel. Two LEDs are mono colored remaining seven are bi-colors one-package LEDs (with three leads/terminals). These LEDs show the status of various motors and activities of RPAR. The corresponding activities are given in Table 3.7.

Table 3.7: Color of LEDs representing the activities of different RPAR's segments.

LED NO.	Segment	Color	Activity
01	RPAR	Red	Battery charging
02	RPAR	Green	ON/Ready to use
03	Gripper	Green	Opining
		Red	Closing
04	Gripper	Green	Rotates CW
		Red	Rotates CCW
05	Elbow	Green	Moves Upward
		Red	Moves Downward
06	Shoulder	Red	Moves Upward
		Green	Moves Downward
07	Waist	Green	Rotates CW
		Red	Rotates CCW
08	RPAR	Red	Moves toward right/Forward
		Green	Moves toward left/Backward
09	RPAR	Red	Moves toward right/Forward
		Green	Moves toward left/Backward

The 8th and 9th BC-LEDs indicate the activities of the differential wheel motors. When the RPAR is moving rightward, the right wheel motor remains idle and the left motor becomes "ON", this situation is shown by the green light of 8th BC-LED, while green light of 9th BC-LED indicates leftward turning due to right wheel motor is "ON". Now, when both BC-LEDs (8th and 9th) turn green this indicate that the RPAR is moving forward while red light of both BC-LEDs indicates the RPAR moving backward.

The charging uni-direction four-pin D-type socket is located at the middle of the beam of the differential wheels. The RPAR is charged through this connector when the key is at charging mode. The battery charger is an external unit. It has current rating specification of 14.2 V DC up to 20 A current maximum.

3.7 REMOTE CONSOLE

The Remote Console has been designed and fabricated to control the RPAR. The remote consol is directly connected to the hardware of the RPAR for direct operation without the master and the on-board slave computers. List of the components used for the construction of remote console is given in Table 3.8.

Table 3.8: List of the Remote Console's Components.

S. No.	Components	Quantity
1.	IC 7805	01
2.	Push Switch, ST	07
3.	Push Switch, DT	01
4.	Two Way Switch	07
5.	Resistor 1 kΩ, ¼ W	01
6.	Capacitor 0.1μF/50V	02
7.	Connector 25 pins D type female	01
8.	Cable 8-pair	3.2 m

With remote console, the RPAR can be controlled up to a distance of 3.2 m as an electronic manipulator. The remote consol is also helpful to check different modules of RPAR. The operator console can also be used for quick and safe transportation of RPAR. The functions of different switches of remote console are given in Table. 3.9.

Table 3.9: Function of different switches of Remote Console.

S. No.	Switches	Segment	Function/Selection
1.	Push-Switch-A	Griper	ON/OFF
2.	Two-Way Switch-A	Griper	Open/Close
3.	Push-Switch-B	Wrist	ON/OFF
4.	Two-Way Switch-B	Wrist	CW/CCW
5.	Push-Switch-C	Elbow	ON/OFF
6.	Two-Way Switch-C	Elbow	Up/Down
7.	Push-Switch-D	Shoulder	ON/OFF
8.	Two-Way Switch-D	Shoulder	Up/Down
9.	Push-Switch-E	Waist	ON/OFF
10.	Two-Way Switch-E	Waist	CW/CCW
11.	Push-Switch-F	Left wheel	ON/OFF
12.	Two-Way Switch-F	Left wheel	Right/Forward
13.	Push-Switch-G	Right wheel	ON/OFF
14.	Two-Way Switch-G	Right wheel	Left/Backward
15.	Push-Switch, H	RPAR	ON/OFF

Push-Switches are used to "ON"/ Enable a segment and Two-Way switch is used to select the CW/CCW or Up/Down movement of the segment. Push-Switch-H is employed to move the RPAR forwards or backwards. The circuit diagram of the remote console is illustrated in Fig. 3.13 and Fig. 3.14.

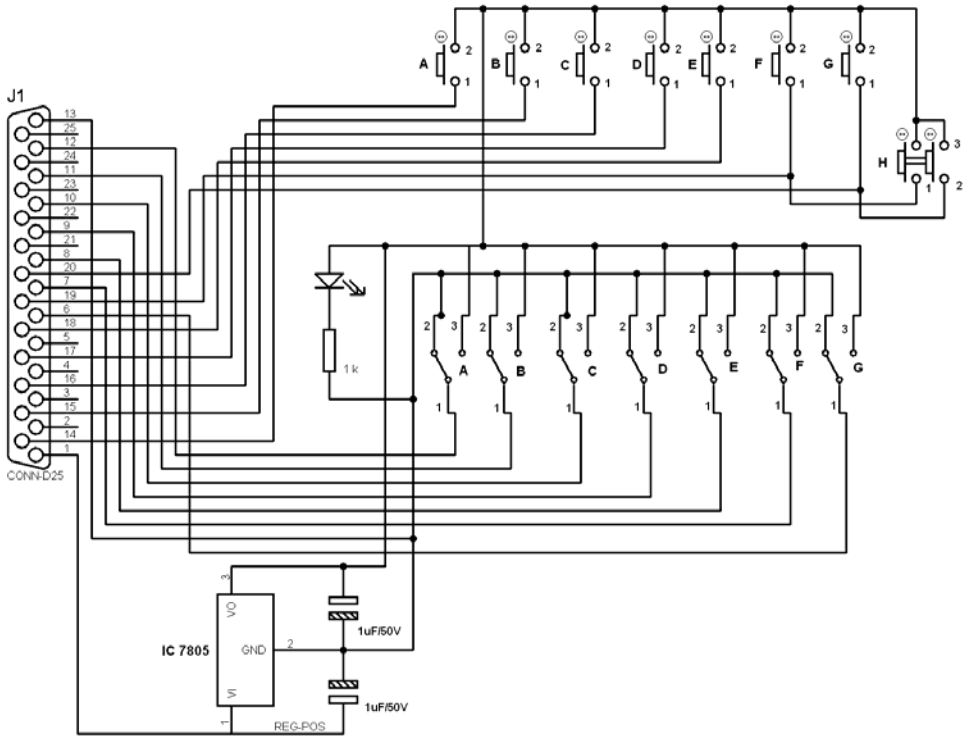

Fig. 3.13: Circuit Diagram of the Remote Consol.

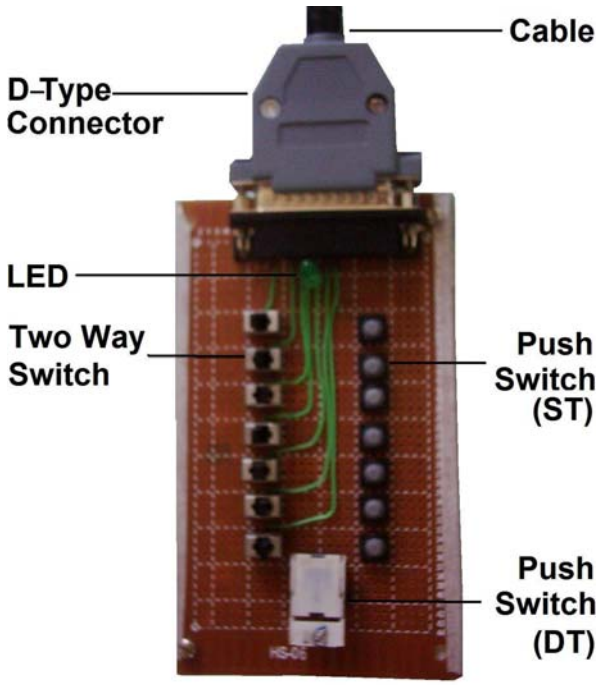

Fig. 3.14: Remote Consol.

3.8 EMBEDDED CONTROLLER CARD FOR QUAD SHAFTS

An embedded controller card was designed and developed to measure the real time position of different segments of RPAR with the help of potentiometers. The card reads the encoded data from the four potentiometers either in rotation or at any particular position of Wrist, Elbow, Shoulder and Waist segment. The microcontroller on the card decodes and sends data to the onboard computer through serial port. An interface and GUI based application software for quad channel encoder has also been developed. The potentiometers are connected to different shafts/segment with locally developed mechanical couplings. A spur gear is attached with the potentiometric encoder to read the Wrist's position as illustrated in Fig. 3.15. Elbow position is measured with the help of potentiometric encoder attached to the Elbow segment shaft as shown in Fig. 3.16. Where as, the Shoulder position is provided by the potentiometric encoder attached to the Shoulder segment shaft as revealed in Fig. 3.17.

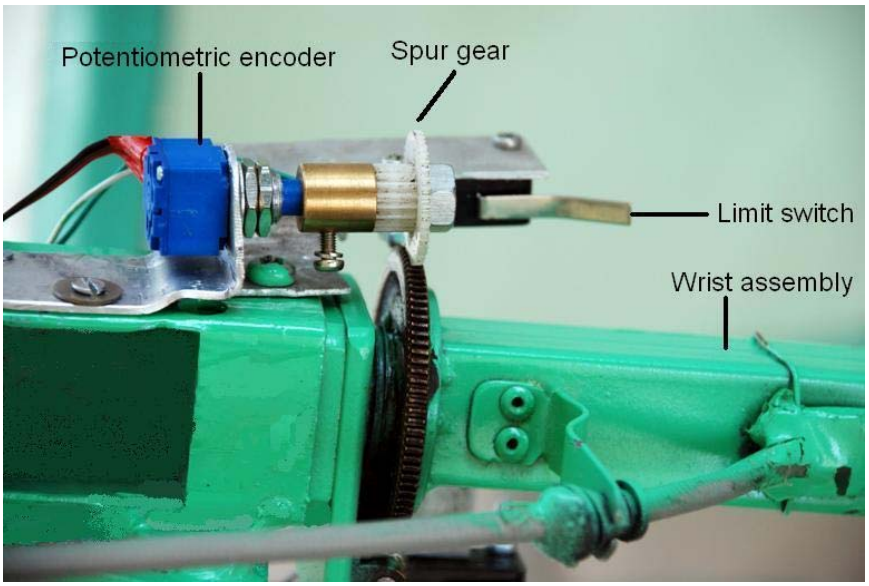

Fig. 3.15: Potentiometric encoder for the Wrist assembly.

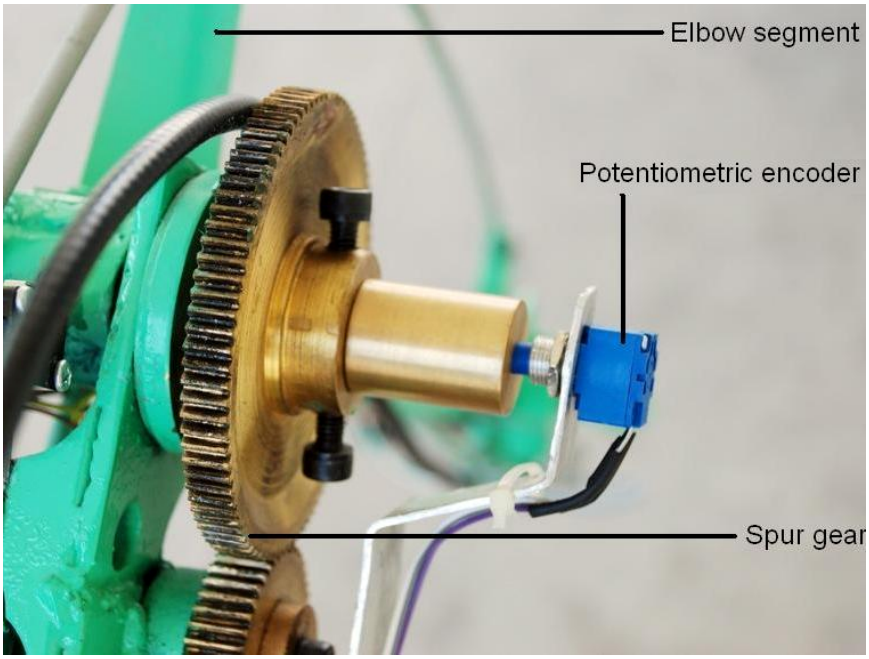

Fig. 3.16: Potentiometric encoder for the Elbow assembly.

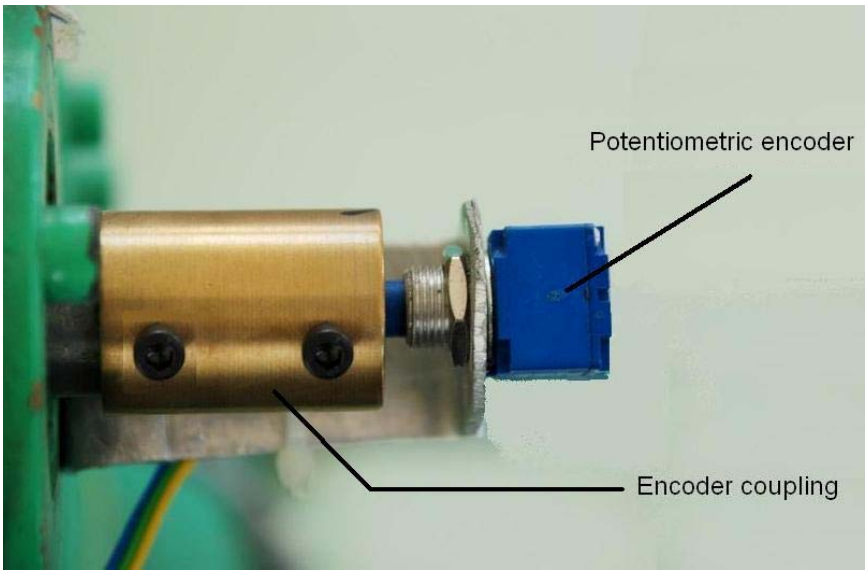

Fig. 3.17: Potentiometric encoder for the Shoulder assembly.

The Embedded Controller Card comprised of following features for synchronous data acquisition and asynchronous transmission.

- Power supply for controller card.
- Encoding and decoding scheme for quad shafts.
- Serial transmitter.
- Application software for displaying shaft orientation which is installed on the onboard computer and can also be assessed on an off board computer via remote desktop application through wireless Ethernet.

3.8.1 Specifications of Embedded Controller

1. Controller card requires +15V and -15V, so a module ($\pm$ 15 V/220 V) is used.
2. Inverter (12 V/220V) for providing 220V to the module.
3. Card supports Quad channels.
4. Card samples each channel after 200mSec.
5. Controller card serially transmit decoding values.
6. The baud rate of serial transmitter is 1200bps.
7. Application software contains a serial receiver and graphical interface.
8. Graphical interface regularly displays and plots the receiving data for each channel.
9. Controller card can detect an orientation of less then 1 degree.
10. Decoding error is negligible.

The component list of embedded controller card is given in Table 3.10.

Table 3.10: Components list of Embedded Controller Card.

S. No.	Components	Quantity
10.	IC 89C52	08
11.	IC AD574A	01
12.	IC HCC4529B	01
13.	IC 7407	01
14.	IC MC7805	01
15.	Resistor 330Ω, ¼ W	04
16.	Resistor 100Ω, ¼ W	01
17.	Resistor 1 kΩ, ¼ W	02
18.	Resistor 5 kΩ, ¼ W	02
19.	Resistor 4.7 kΩ, ¼ W	01
20.	Resistor 100 kΩ, ¼ W	01
21.	Variable Resistor 100Ω, ¼ W	02
22.	Variable Resistor 10 kΩ, ¼ W	04
23.	Capacitor 0.1μF/16V	01
24.	Capacitor 1μF/16V	06
25.	Capacitor 10μF/35V	01
26.	Capacitor 4.7μF/35V	02
27.	Capacitor 33pF/50V	02
28.	Capacitor 220nF/50V	01
29.	Capacitor 470nF/50V	01
30.	Crystal 12MHz	01
31.	Connector 3 pins Male	04
32.	Push button	01
33.	Voltage module 220V, 780 mA, +15 V 800 mA, and -15 V DC 800 mA.	01
34.	Inverter 12 V to 220 V AC, 500 VA	01

The block and circuit diagram is given Figs. 3.18 and 3.19.

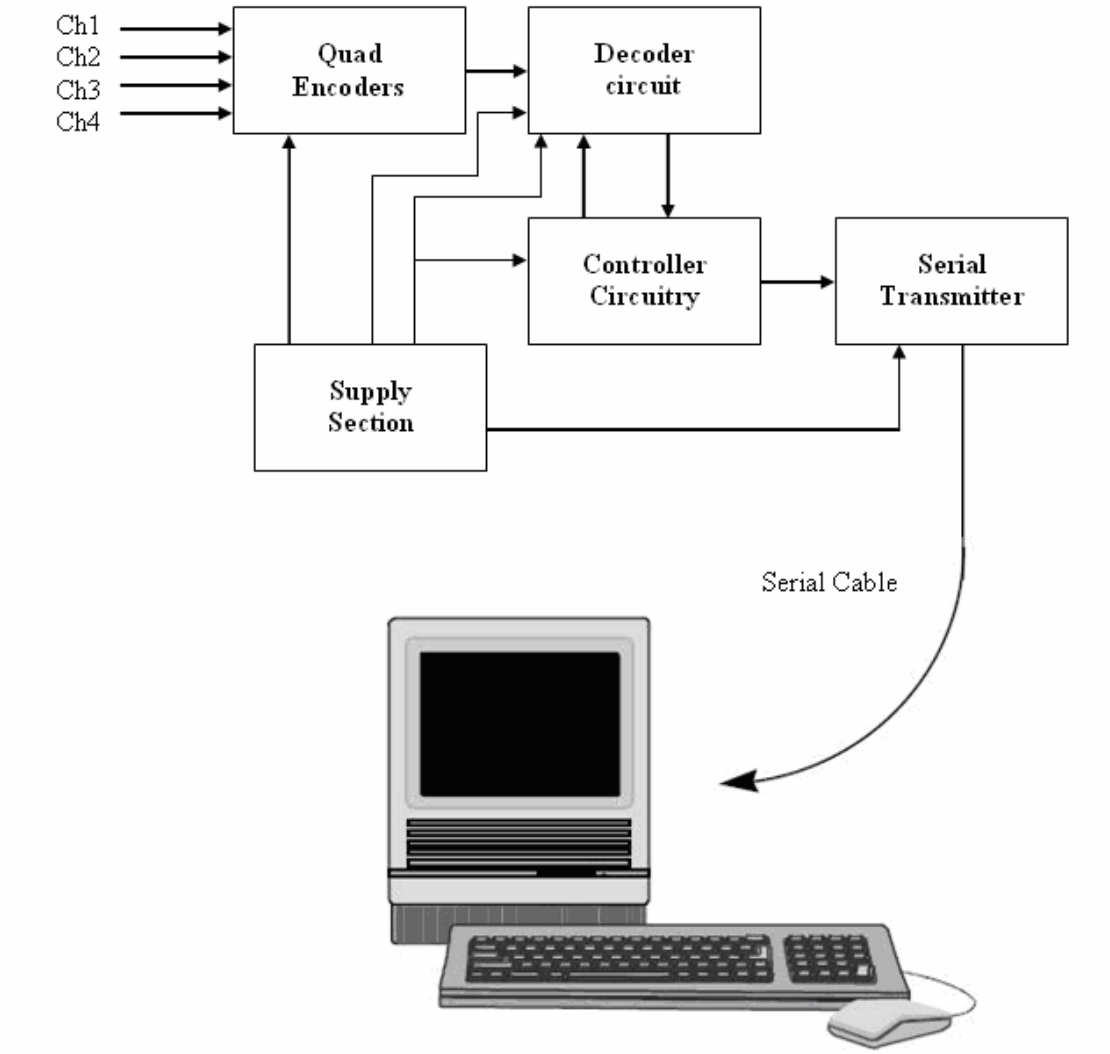

Fig. 3.18: Embedded Controller Card Block Diagram

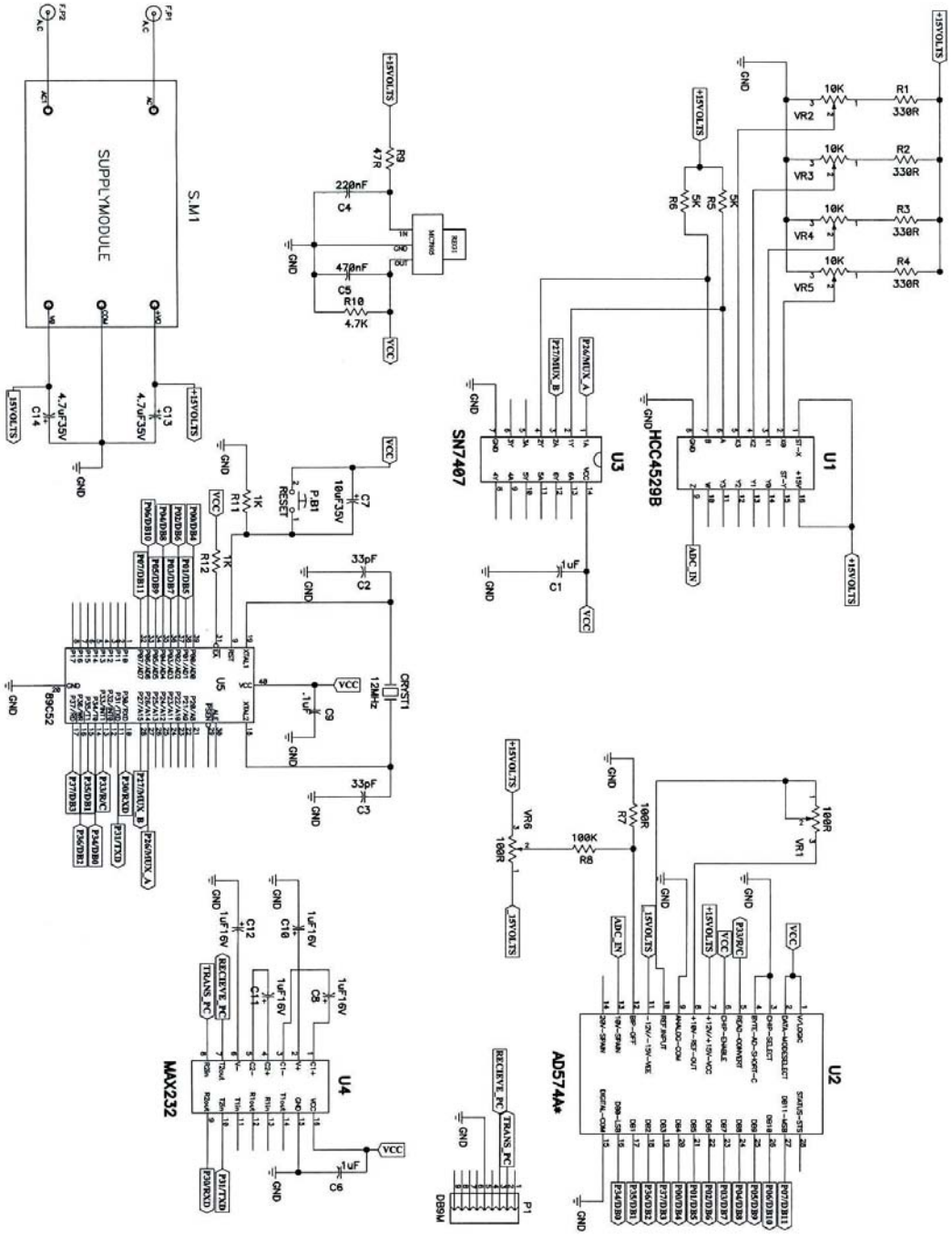

Fig 3.19: Circuit diagram of Embedded Controller Card

3.9 CONCLUSION

This chapter described the design and development of different hardware components of Radiation Protection Assistant Robot (RPAR). These diverse modules, cards and circuits were developed to operate different mechanical systems and mechanisms of RPAR. Also the working of Relay logic, H-Bridge, Limit Switch modules, Buffer and Demux card, Control panel and Embedded Controller Card were discussed. These modules and cards were tested and were found working satisfactorily in different tasks and assignments of RPAR.

CHAPTER

FOUR

DESIGN AND DEVELOPMENT: SOFTWARE

4.1 INTRODUCTION

This chapter describes the software design consideration of Radiation Protection Assistant Robot (RPAR) being developed in this work. High-level language (Visual Basic 6.0) was used to develop robotic interfacing and controlling program. All the inputs for the modules were controlled through parallel port. So far two softwares were developed to control the RPAR. These are named as RPAR SOFT and Demo soft. A Shaft Encoders Data Acquisition Software (SEDAS) was also developed to read the position of different links of RPAR with the help of an Embedded Controller Card, connected to the serial port of onboard computer.

4.2 DESCRIPTION OF SOFTWARE "RPAR SOFT"

This software is used to control different segments and to move the RPAR platform. Each segment of the robot is controlled through the keyboard. When a

particular key is being pressed the corresponding segment will start functioning, while when the key is released the segment will stop the function. The RPAR SOFT has a provision to change key assignment of any segment function of RPAR moving mechanism. All the RPAR functions and their corresponding keys are given in Table 4.1. The Graphic User Interface (GUI) of the RPAR SOFT is illustrated in Fig. 4.1.

Table 4.1: The corresponding key functions of Keyboard, their Decimal and Hex value and 8-bit data.

Segment	Key	Value		8 Bit Data	Function
		Decimal	Hex		
Gripper	Q	32	20	0010 0000	Close
	1	48	30	0011 0000	Open
Wrist	W	192	C0	1100 0000	CCW
	2	128	80	1000 0000	CW
Elbow	E	33	21	0010 0001	Down
	3	49	31	0011 0001	Up
Shoulder	4	129	81	1000 0001	Up
	R	193	C1	1100 0001	Down
Waist	5	34	22	0010 0010	CW
	T	50	32	0011 0010	CCW
RPAR	6	130	82	0010 0000	Moving Left
	Y	194	C2	1100 0010	Moving Right
RPAR	7	35	23	0010 0011	Forward
	U	51	33	0011 0011	Backward
RPAR	--	07	07	0000 0111 *	All OFF

* When all the above keys were released, this data sent to "OFF" the segment/RPAR.

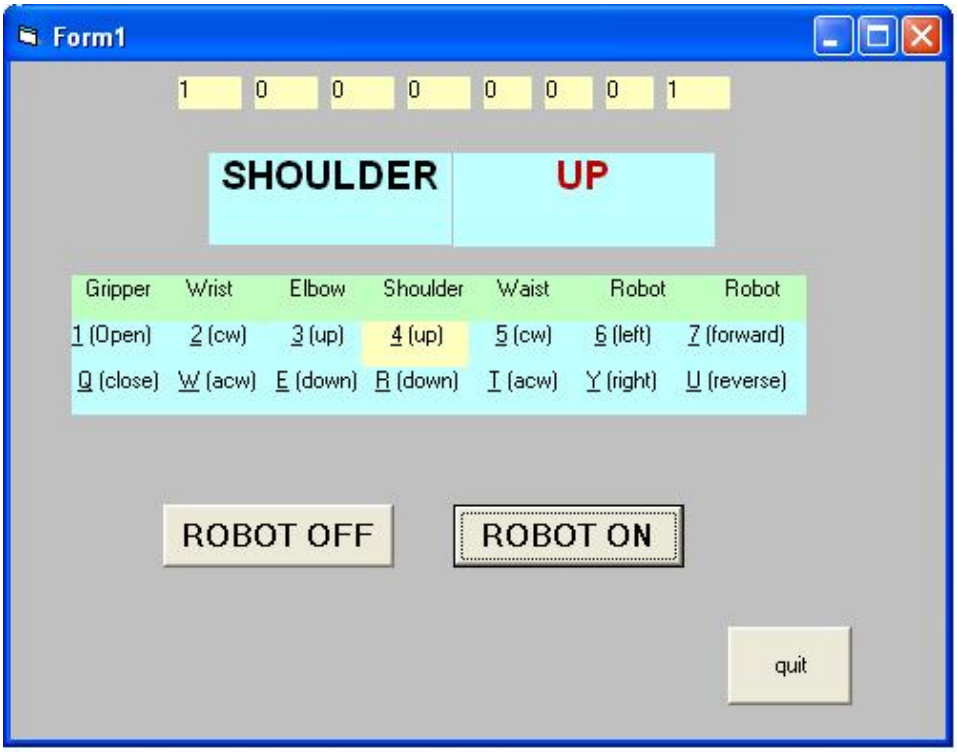

Fig. 4.1: RPARSOFT moving the shoulder up.

The Fig. 4.1 indicates the control of RPAR Shoulder segment, when the numeric key "4" is pressed and the shoulder segment is moving upward.

4.2.1 RPARSOFT Working Logic.

When a particular key is pressed, a predefined value in Hex sent its equivalent binary value to the parallel port at address 378H. The Hex value of the corresponding key contains 8-bits data which is further divided into 4-bits controlling data and 4-bits address information This 8-bit data is fed to Demultiplexer card after passing through the Buffer card. The 4-bit address information is given to demultiplexer (Demux) IC (74154) and 4-bit controlling data to Hex buffer driver ICs (74LS367). The Demux IC enables the desired Hex buffer driver IC which energizes the required module or RPAR/RPAR segment after passing through the Limit Switch Module. Flowchart of RPARSOFT is given in Fig. 4.2.

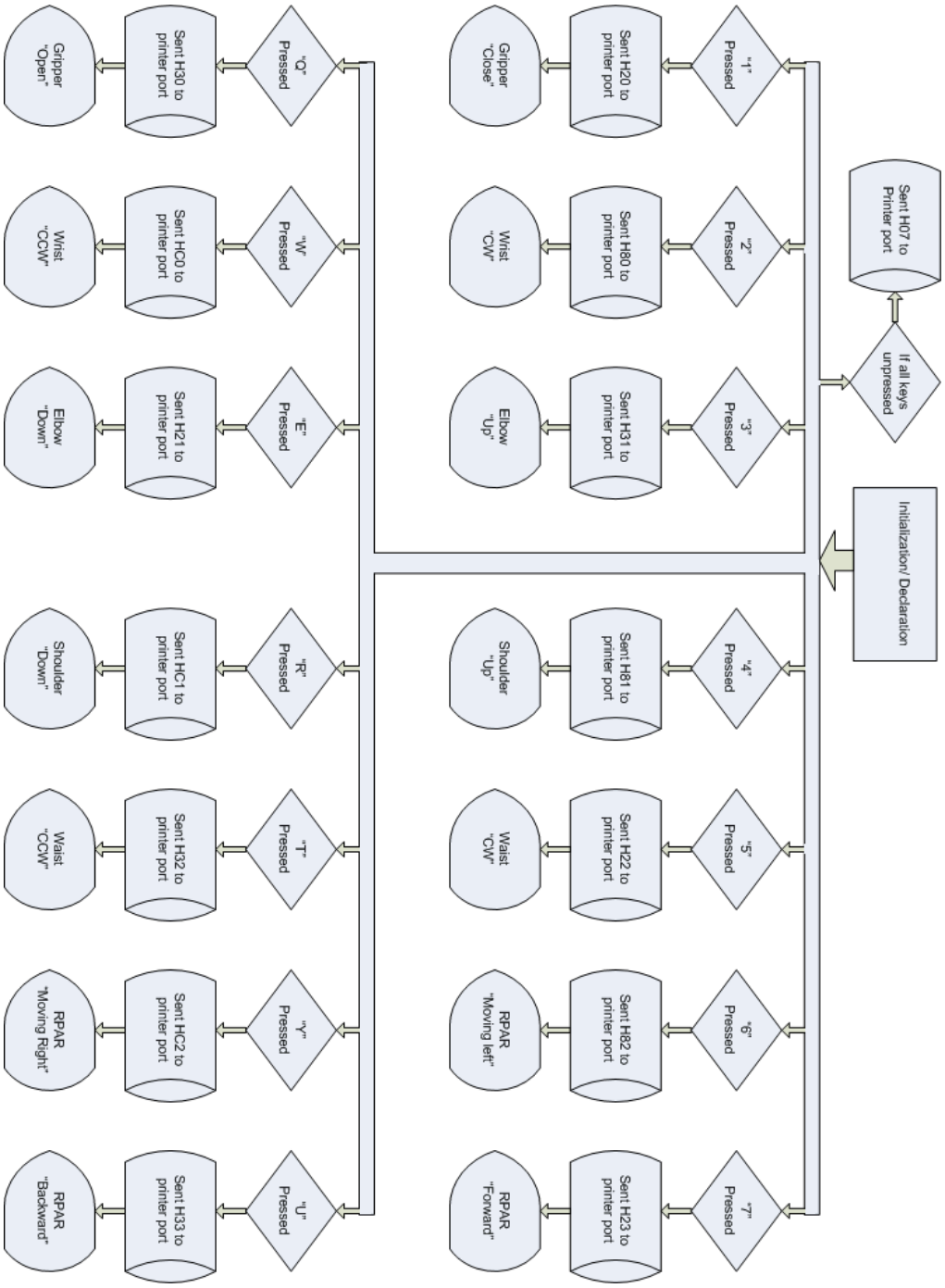

Fig. 4.2: Flowchart of RPARSOF.

4.3 DESCRIPTION OF SOFTARE "RPAR DEMO"

The RPAR DEMO is a demo program designed and developed to demonstrate the function of different segments/modules of RPAR. Each segment of RPAR moves in either direction i.e. clockwise/anticlockwise, upward/downward, left/right turns, forward/backwards movement and gripper opening/closing action. The demo program can also be used for initial checkup of the RPAR before an actual task. The demo program stepwise checks all the movement mechanisms of the RPAR. It first checks the opening and closing action of the gripper, then checks the wrist clockwise and anticlockwise rotations, then the elbow segment upwards and downwards movement. Then the Shoulder's up and down movements and finally, the Waist clockwise and anticlockwise sweeps. After self-checking of articulated robotic arm, the platform moves in right, left, forward and backward directions. In this way the demo program checks all the control electronics of modules and moving mechanisms of the RPAR.

While the demo program is operating, the keys and mouse remain ineffective and inactive for the operator. After the demo or self-checking program, the RPAR is in standby mode for performing any task. The background color of the performed action will change from cyan to yellow. The flowchart of RPAR DEMO is given in Fig. 4.3 and the main GUI screen of the Demo version program is shown in Fig. 4.4.

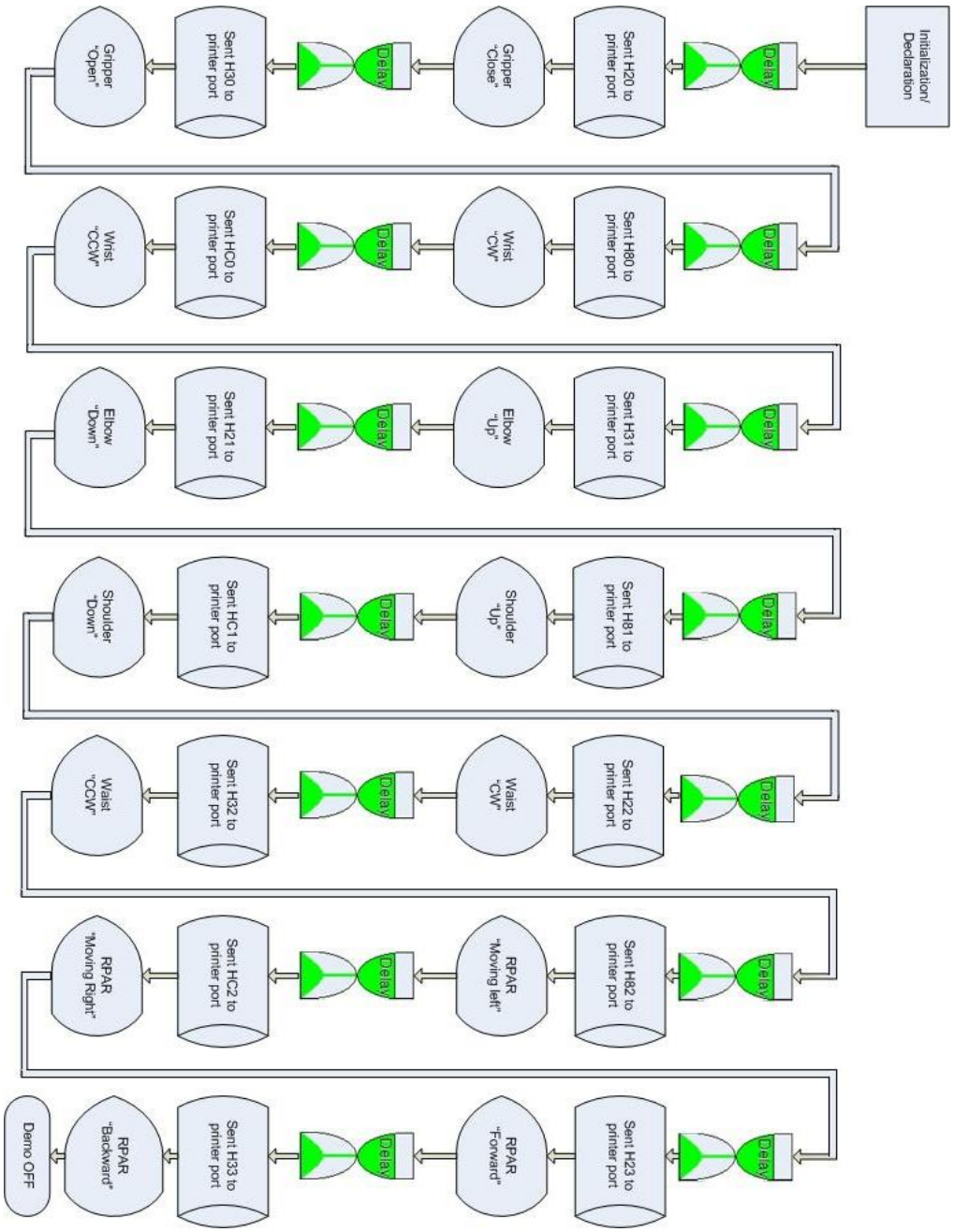

Fig. 4.3: Flowchart of RPAR DEMO.

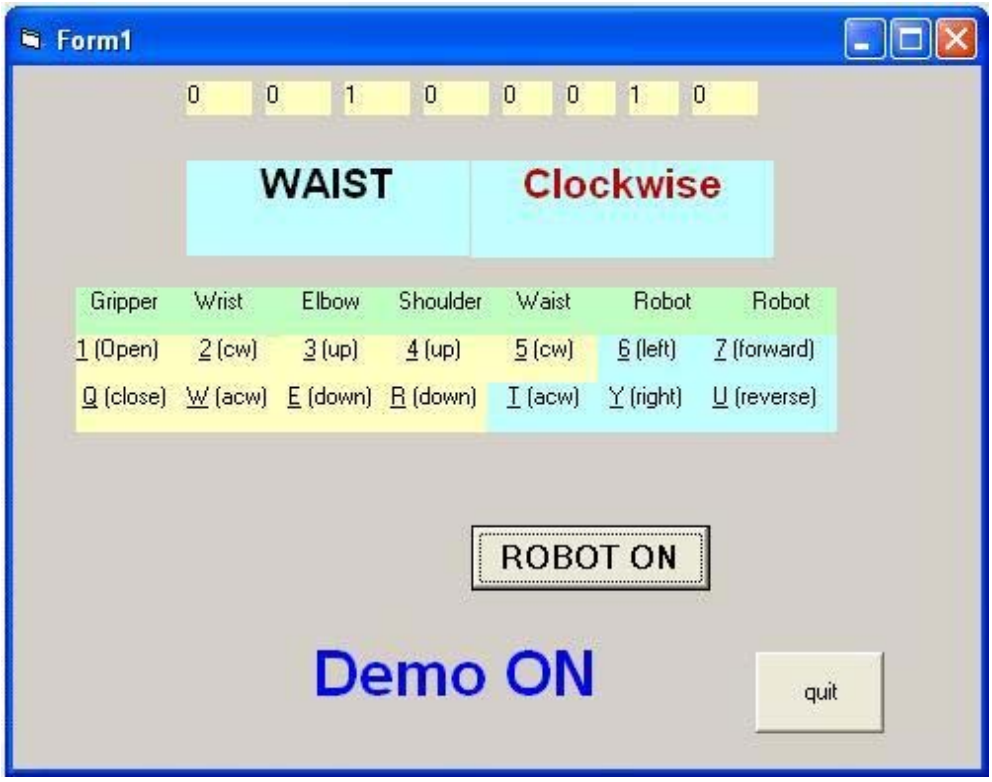

Fig. 4.4: RPAR Demo software moving the waist in clockwise direction.

4.4 SHAFT ENCODERS DATA ACQUISITION SOFTWARE

Shaft Encoders Data Acquisition Software (SEDAS) was developed to read and analysis the data from the Embedded Controller Card. The flowchart of SEDAS is given in Fig. 4.5. The software describes the orientation of shafts in user friendly environment by plotting angle as a function of time (Fig. 4.6). The software also keeps the soft copy of the positions at a particular time of all the encoders in a text format file.

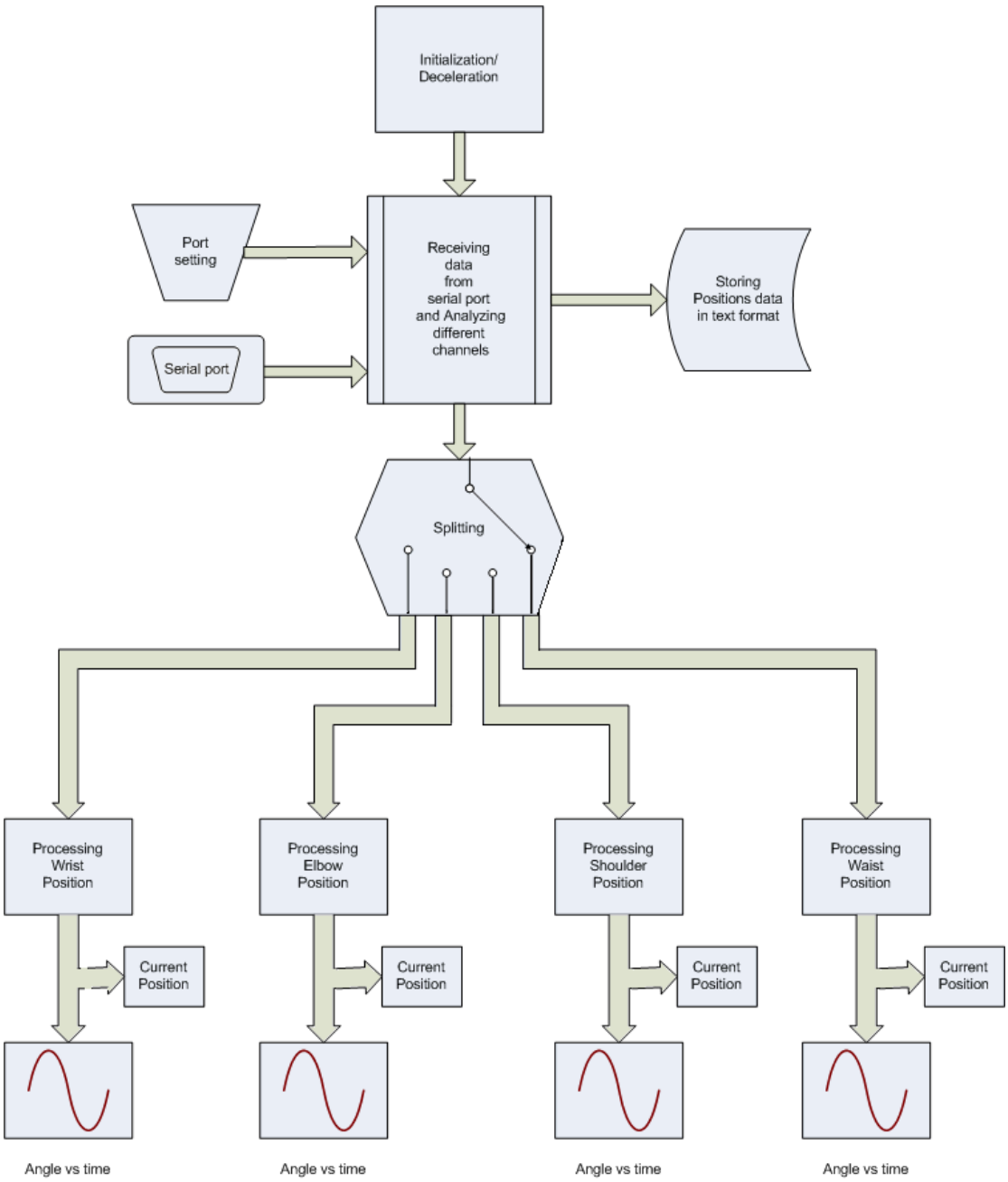

Fig. 4.5: Flowchart of SEDAS

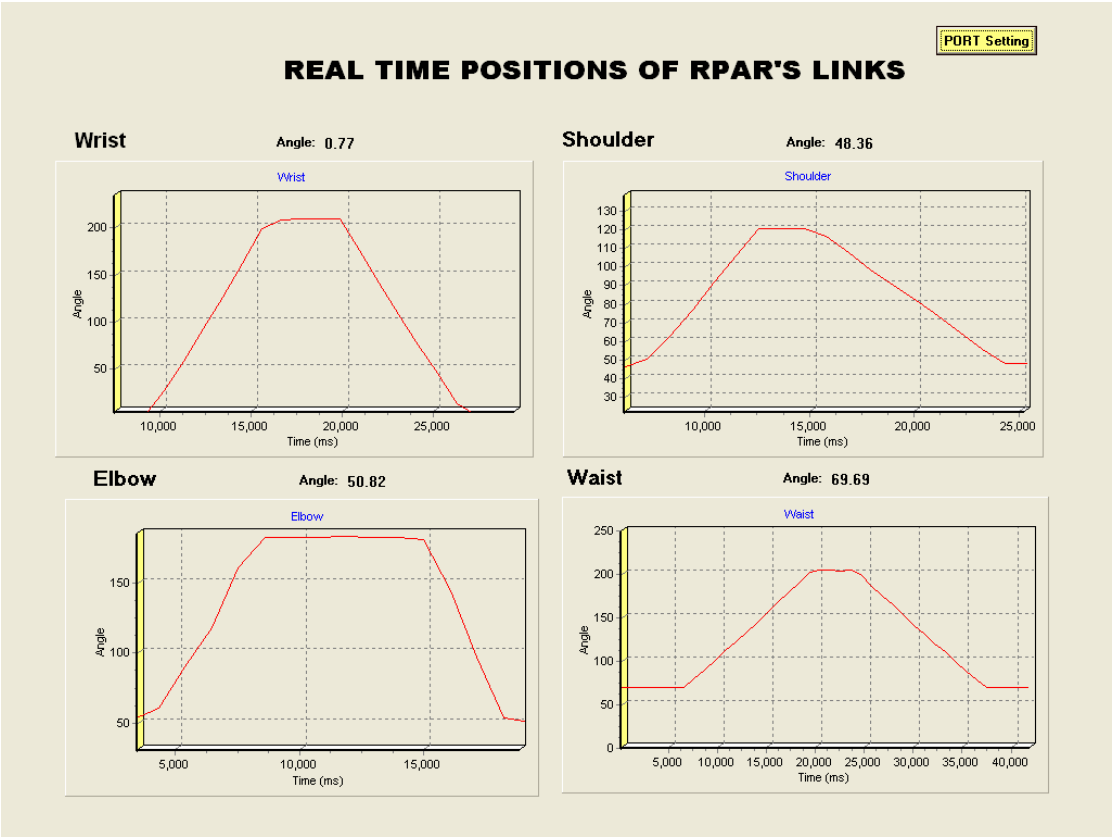

Fig. 4.6: Graphic User Interface of SEDAS

4.5 WIRELESS CONTROL OF RPAR

After loading the RPARSOFT in the onboard computer (Laptop), remote desktop control setting is made on the onboard and off board computers. The RPARSOFT is accessed on the off board computer after establishing the remote desktop connection through wireless Ethernet. As such, RPAR is wirelessly controlled through the keyboard of off board computer. The RPAR can be controlled wirelessly up to a maximum range of 100 m from the wireless LAN access point in an open area.

4.6 CONCLUSION

This chapter described the design and development of software (RPARSOFT, RPARDEMO and SEDAS) used to control, self checking and measuring the shaft's position of Radiation Protection Assistant Robot (RPAR). These software were found to control effectively different modules, circuits and cards of RPAR during various assignments and tasks. The wireless control of RPAR is also described in this chapter.

CHAPTER

FIVE

KINEMATICS STUDY

5.1 INTRODUCTION

To achieve better controllable and performance of robotic devices, the kinematics and workspace analysis is essential. The kinematics refers to the properties of geometrical movements with reference to the gripper-tip of fixed points in links regardless of their masses or the forces acting on them. The kinematics study is vital for the evaluation of the controllability and precise positioning of the robotic platform and articulated robotic arm's gripper-tip. Two modes of kinematics have been considered to evaluate the effective performance of the RPAR articulated robotic arm. These modes are discussed in this chapter.

5.2 FORWARD KINEMATICS

The forward kinematics of the articulated robotic arm of RPAR is concerned with the transformation of position or momentary orientation information in the joint-space to Cartesian-space (Xia and Wang; 2000). The forward kinematics is described by

$$r(t) = f(\theta(t)) \tag{1}$$

Where

$\theta(t)$ = m-vector of joints variables

$r(t)$ =n-vector of Cartesian variables

$f(\cdot)$ =Continuous non-linear function whose structure and parameters are known for a given manipulator.

By assigning the link-frames according to the Denavit-Hartenberg (D-H) Convention (Denavit and Hartenberg; 1955), the forward kinematics for RPAR articulated robotic arm are derived. In D-H convention notation, the d_i units is the translation or the offset along z_i from the x_{i-1}, θ_i degrees rotation about z_i of x_{i-1} into x_i in the right-hand sense, α_i degrees is a rotation or twist about axis x_{i-1} of z_{i-1} into z_i in the right-hand sense and b_i units is a displacement along x_{i-1} from z_{i-1} to z_i. The out-of-plane axis can be obtained by using the right-hand rule on each pair of link-axis. The coordinate transformation matrix T_{i-1}^{i}, relating link-frame i to link-frame j and can be derived from the following expression (Wolovich 1987);

$$T_{i-1}^{i} = \begin{bmatrix} \cos\theta_i & -\sin\theta_i & 0 & b_i \\ \cos\alpha_i \sin\theta_i & \cos\alpha_i \cos\theta_i & -\sin\alpha_i & -d_i \sin\alpha_i \\ \sin\alpha_i \sin\theta_i & \sin\alpha_i \cos\theta_i & \cos\alpha_i & d_i \cos\alpha_i \\ 0 & 0 & 0 & 1 \end{bmatrix} \quad (2)$$

The D-H parameters for RPAR articulated robotic arm have been determined according to the information available in the literature (Carignan and Howard; 2000) and are given in Table 5.1.

Table 5.1: D-H parameters for RPAR articulated robotic arm.

Link / DH Parameters	1	2	3	4
α_i	0^0	90^0	0^0	90^0
b_i	0	0	e	f
θ_i	θ_1	θ_2	θ_3	θ_4
d_i	h	0	0	0

e = 46.1, f = 76.4 and h =101.5 cm.

The schematic geometrical diagram of the articulated robotic arm is shown in Fig.5.1.

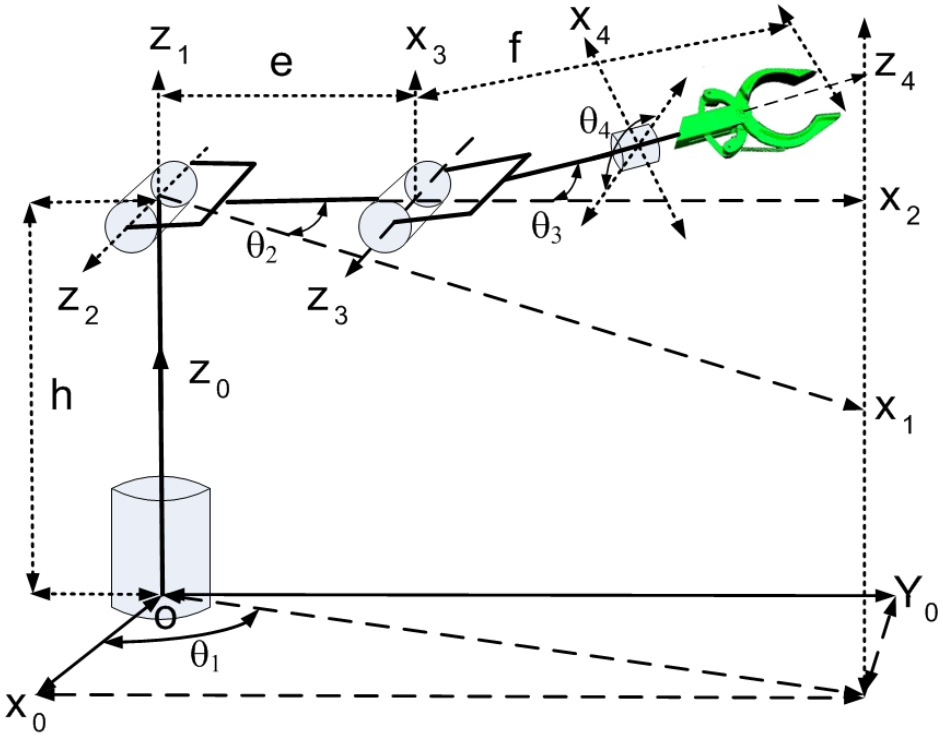

Fig. 5.1: Schematic geometry diagram of RPAR articulated robotic arm.

Direct substitution of the individual column elements of Table 5.1 into Eq. (2) provides the coordinate transformation matrix T_{i-1}^{i} of positions and orientation of each link and are given as in the following matrix;

$$T_0^1 = \begin{bmatrix} \cos\theta_1 & -\sin\theta_1 & 0 & 0 \\ \sin\theta_1 & \cos\theta_1 & 0 & 0 \\ 0 & 0 & 1 & h \\ 0 & 0 & 0 & 1 \end{bmatrix} \tag{3}$$

$$T_1^2 = \begin{bmatrix} \cos\theta_2 & -\sin\theta_2 & 0 & 0 \\ 0 & 0 & -1 & 0 \\ \sin\theta_2 & \cos\theta_2 & 0 & 0 \\ 0 & 0 & 0 & 1 \end{bmatrix} \tag{4}$$

$$T_2^3 = \begin{bmatrix} \cos\theta_3 & -\sin\theta_3 & 0 & e \\ \sin\theta_3 & \cos\theta_3 & 0 & 0 \\ 0 & 0 & 1 & 0 \\ 0 & 0 & 0 & 1 \end{bmatrix} \tag{5}$$

and

$$T_3^4 = \begin{bmatrix} \cos\theta_4 & -\sin\theta_4 & 0 & f \\ 0 & 0 & -1 & 0 \\ \sin\theta_4 & \cos\theta_4 & 0 & 0 \\ 0 & 0 & 0 & 1 \end{bmatrix} \tag{6}$$

The resulting expression for position orientation of the gripper tip with respect to the elbow, T_0^4 is calculated from (Corke 1996) and is given by Eq. (7)

$$T_0^4 = T_0^1 T_1^2 T_2^3 T_3^4 \tag{7}$$

$$T_0^4 = \begin{bmatrix} c_1c_4c_{23} + s_1s_4 & -c_1s_4c_{23} + s_1c_4 & c_1s_{23} & fc_1c_{23} + ec_1c_2 \\ s_1c_4c_{23} - c_1s_4 & -s_1s_4c_{23} - c_1c_4 & s_1s_{23} & fs_1c_{23} + es_1c_2 \\ c_4s_{23} & -s_4s_{23} & -c_{23} & fs_{23} + es_2 + h \\ 0 & 0 & 0 & 1 \end{bmatrix} \quad (8)$$

Where s_1 and c_1 represent $\sin\theta_1$ and $\cos\theta_1$ respectively. Further more $c_2c_3 - s_2s_3 = \cos(\theta_2 + \theta_3)$, which is abbreviated as c_{23}, and $s_2c_3 + s_3c_2 = \sin(\theta_2 + \theta_3)$, which is denoted as s_{23}.

The last column of matrix expressions in Eq. (8) yields the position equation of the gripper-tip and can be expressed as follows;

$$\begin{bmatrix} D_x \\ D_y \\ D_z \end{bmatrix} = \begin{bmatrix} fc_1c_{23} + ec_1c_2 \\ fs_1c_{23} + es_1c_2 \\ fs_{23} + es_2 + h \end{bmatrix} \quad (9)$$

5.3 INVERSE KINEMATICS

The inverse kinematics involves the existence and uniqueness of a solution and determines method for its effectiveness and efficiency. The inverse kinematics calculations are difficult and become more compounded due to requirement of real-time solutions of feedback information during robotic operations. However, in real-time solution, the procedure for calculations of inverse kinematics for redundant manipulators is very important in robotics and therefore was also employed for the inverse kinematics calculation for RPAR articulated robotic arm. Basically the inverse kinematics help to find the pivot-joint variables for desired position and orientations of the gripper tip by inverse mapping of the forward kinematics (D'Souza et al, 2001). The inverse kinematics equation is given by

$$\theta(t) = f^{-1}(r(t)) \tag{10}$$

The forward kinematics equations associated with both the position and orientation of RPAR is given by Eq. (8). As it is assumed that only three degrees of freedom, namely the rotation angles θ_1, θ_2 and θ_3, can be employed to alter its configuration, it follows that one can arbitrarily assign only three degree of freedom with respect to any desired configuration. The fourth degree of freedom, i.e. wrist motion does not alter the position of gripper or robot. Therefore, in regard to the inverse kinematics problem for the RPAR, the attention is restricted to the arbitrary specification of its final gripper origin position, $(p_x, p_y, p_z) = (D^4_{x0}, D^4_{y0}, D^4_{z0})$. Otherwise as stated earlier, in light of Eq. (8), following three equations will be solved:

$$p_x = f\cos\theta_1\cos\theta_{23} + e\cos\theta_1\cos\theta_2 = fc_1c_{23} + ec_1c_2 \tag{11}$$

$$p_y = f\sin\theta_1\cos\theta_{23} + e\sin\theta_1\cos\theta_2 = f\,\mathrm{s}_1\,\mathrm{c}_{23} + e\,\mathrm{s}_1\,\mathrm{c}_2 \tag{12}$$

and

$$p_z = f\sin\theta_{23} + e\sin\theta_2 + h = f\,\mathrm{s}_{23} + e\,\mathrm{s}_2 + h \tag{13}$$

for θ_1, θ_2 and θ_3, given any arbitrary, desired position (p_x, p_y, p_z), with e, f, and h the known and positive elbow length, shoulder distance, and height of the waist, respectively.

The positional equations will be determined for the RPAR in light of the explicit Eqs. (4) through (6) for the matrices, T_0^1, T_1^2, T_2^3, and T_3^4, which yield T_3^4 via the matrix composition of Eq. (8). More specifically, if $T_{34}{}^4$ and $T_{04}{}^4$ represent the final (fourth) or positional columns of T_3^4 and T_0^4, respectively, Eq. (8) directly implies that

$$T_0^1 T_1^2 T_2^3 T_{34}^4 = T_{04}^4 = \begin{bmatrix} c_1 c_2 e + c_1 c_{23} f \\ s_1 c_2 e + s_1 c_{23} f \\ h + e s_2 + f s_{23} \\ 1 \end{bmatrix} = \begin{bmatrix} p_x \\ p_y \\ p_z \\ 1 \end{bmatrix} \tag{14}$$

Now consider Eq. (3)

$$T_0^{\ 1} = \begin{bmatrix} c_1 & -s_1 & 0 & 0 \\ s_1 & c_1 & 0 & 0 \\ 0 & 0 & 1 & -h \\ 0 & 0 & 0 & 1 \end{bmatrix}$$

The premultiplication of Eq. (14) by

$$\left(T_0^{\ 1}\right)^{-1} = T_1^{\ 0} = \begin{bmatrix} c_1 & s_1 & 0 & 0 \\ -s_1 & c_1 & 0 & 0 \\ 0 & 0 & 1 & -h \\ 0 & 0 & 0 & 1 \end{bmatrix} \tag{15}$$

now implies that

$$T_1^0 T_0^1 T_1^2 T_2^3 T_{34}^4 = T_1^0 T_{04}^4 = T_{14}^{\ 4}$$

$$T_1^2 T_2^3 T_{34}^4 = T_{14}^4$$

so

$$\begin{bmatrix} c_1 & s_1 & 0 & 0 \\ -s_1 & c_1 & 0 & 0 \\ 0 & 0 & 1 & -h \\ 0 & 0 & 0 & 1 \end{bmatrix} \times \left\{ \begin{bmatrix} c_1 c_2 e + c_1 c_{23} f \\ s_1 c_2 e + s_1 c_{23} f \\ h + e s_2 + f s_{23} \\ 1 \end{bmatrix} = \begin{bmatrix} p_x \\ p_y \\ p_z \\ 1 \end{bmatrix} \right\}$$

$$\begin{bmatrix} c_1(c_1 c_2 e + c_1 c_{23} f) + s_1(s_1 c_2 e + s_1 c_{23} f) \\ -s_1(c_1 c_2 e + c_1 c_{23} f) + c_1(s_1 c_2 e + s_1 c_{23} f) \\ h + e s_2 + s_{23} f - h \\ 1 \end{bmatrix} = \begin{bmatrix} c_1 p_x + s_1 p_y \\ -s_1 p_x + c_1 p_y \\ p_z - h \\ 1 \end{bmatrix}$$

After simplifying,

$$\begin{bmatrix} c_2 e + c_{23} f \\ 0 \\ e s_2 + s_{23} f \\ 1 \end{bmatrix} = \begin{bmatrix} c_1 p_x + s_1 p_y \\ -s_1 p_x + c_1 p_y \\ p_z - h \\ 1 \end{bmatrix} \tag{16}$$

Now consider Eq. (4)

$$T_1^{\ 2} = \begin{bmatrix} c_2 & -s_2 & 0 & 0 \\ 0 & 0 & -1 & 0 \\ s_2 & c_2 & 0 & 0 \\ 0 & 0 & 0 & 1 \end{bmatrix}$$

Continue this procedure by next premultiplying Eq. (16) by

$$\left(T_1^{\ 2}\right)^{-1} = T_2^{\ 1} = \begin{bmatrix} c_2 & 0 & s_2 & 0 \\ -s_2 & 0 & c_2 & 0 \\ 0 & -1 & 0 & 0 \\ 0 & 0 & 0 & 1 \end{bmatrix} \tag{17}$$

now implies that

$$T_2^{\ 1} T_1^{\ 2} T_2^{\ 3} T_{34}^{4} = T_2^{\ 1} T_{14}^{4} = T_{24}^{4}$$

$$T_2^{\ 3} T_{34}^{4} = T_{24}^{4}$$

so,

$$\begin{bmatrix} c_2 & 0 & s_2 & 0 \\ -s_2 & 0 & c_2 & 0 \\ 0 & -1 & 0 & 0 \\ 0 & 0 & 0 & 1 \end{bmatrix} \times \left\{ \begin{bmatrix} c_2 e + c_{23} f \\ 0 \\ e s_2 + s_{23} f \\ 1 \end{bmatrix} = \begin{bmatrix} c_1 p_x + s_1 p_y \\ -s_1 p_x + c_1 p_y \\ p_z - h \\ 1 \end{bmatrix} \right\}$$

$$\begin{bmatrix} c_2(c_2 e + c_{23} f) + s_2(e s_2 + s_{23} f) \\ -s_2(c_2 e + c_{23} f) + c_2(e s_2 + s_{23} f) \\ 0 \\ 1 \end{bmatrix} = \begin{bmatrix} c_2(c_1 p_x + s_1 p_y) + s_2(p_Z - h) \\ -s_2(c_1 p_x + s_1 P_y) + c_2(p_Z - h) \\ s_1 p_x - c_1 p_y \\ 1 \end{bmatrix}$$

After salving,

$$\begin{bmatrix} e+c_3 f \\ s_3 f \\ 0 \\ 1 \end{bmatrix} = \begin{bmatrix} c_2(c_1 p_x + s_1 p_y) + s_2(p_Z - h) \\ -s_2(c_1 p_x + s_1 p_y) + c_2(p_Z - h) \\ s_1 p_x - c_1 p_y \\ 1 \end{bmatrix} \tag{18}$$

Now take the Eq (5)

$$T_2^{\ 3} = \begin{bmatrix} c_3 & -s_3 & 0 & e \\ s_3 & c_3 & 0 & 0 \\ 0 & 0 & 1 & 0 \\ 0 & 0 & 0 & 1 \end{bmatrix}$$

Finally premultiply Eq (18) by

$$\left(T_2^{\ 3}\right)^{-1} = T_3^{\ 2} = \begin{bmatrix} c_3 & s_3 & 0 & -ec_3 \\ -s_3 & c_3 & 0 & -es_3 \\ 0 & 0 & 1 & 0 \\ 0 & 0 & 0 & 1 \end{bmatrix} \tag{19}$$

now implies that

$$T_3^2 T_2^3 T_{34}^4 = T_3^2 T_{24}^4 = T_{34}^4$$

$$T_{34}^4 = T_{34}^4$$

so,

$$\begin{bmatrix} c_3 & s_3 & 0 & -ec_3 \\ -s_3 & c_3 & 0 & -es_3 \\ 0 & 0 & 1 & 0 \\ 0 & 0 & 0 & 1 \end{bmatrix} \times \left\{ \begin{bmatrix} e+c_3 f \\ s_3 f \\ 0 \\ 1 \end{bmatrix} = \begin{bmatrix} c_2(c_1 p_x + s_1 p_y) + s_2(p_Z - h) \\ -s_2(c_1 p_x + s_1 p_y) + c_2(p_Z - h) \\ s_1 p_x - c_1 p_y \\ 1 \end{bmatrix} \right\}$$

$$\begin{bmatrix} c_3(e+c_3 f) + s_3 s_3 f - ec_3 \\ -s_3(e+c_3 f) + c_3 s_3 f - es_3 \\ 0 \\ 1 \end{bmatrix} =$$

$$\begin{bmatrix} c_3c_2(c_1p_x + s_1p_y) + c_3s_2(p_Z - h) - s_3s_2(c_1p_x + s_1p_y) + s_3c_2(p_Z - h) - ec_3 \\ -s_3c_2(c_1p_x + s_1p_y) - s_3s_2(p_Z - h) - c_3s_2(c_1p_x + s_1p_y) + c_3c_2(p_Z - h) - es_3 \\ s_1p_x - c_1p_y \\ 1 \end{bmatrix}$$

the simplifying leads to

$$\begin{bmatrix} f \\ 0 \\ 0 \\ 1 \end{bmatrix} = \begin{bmatrix} c_{23}(c_1p_x + s_1p_y) + s_{23}(p_Z - h) - ec_3 \\ -s_{23}(c_1p_x + s_1p_y) + c_{23}(p_Z - h) - es_3 \\ s_1p_x - c_1p_y \\ 1 \end{bmatrix} \tag{20}$$

The positional equations for the RPAR are now defined as the nontrivial and unrepeated positional relations explicit in Eqs. (14), (16), (18) and (20), namely

$$c_1c_2e + c_1c_{23}f = p_x \tag{21}$$

$$s_1c_2e + s_1c_{23}f = p_y \tag{22}$$

$$h + es_2 + fs_{23} = p_z \tag{23}$$

$$c_2e + c_{23}f = c_1p_x + s_1p_y \tag{24}$$

$$-s_1p_x + c_1p_y = 0 \tag{25}$$

$$e + c_3f = c_2(c_1p_x + s_1p_y) + s_2(p_Z - h) \tag{26}$$

$$s_3f = -s_2(c_1p_x + s_1p_y) + c_2(p_Z - h) \tag{27}$$

$$f = c_{23}(c_1p_x + s_1p_y) + s_{23}(p_Z - h) - ec_3 \tag{28}$$

and

$$-s_{23}(c_1p_x + s_1p_y) + c_{23}(p_Z - h) - es_3 = 0 \tag{29}$$

These above positional equations are used to determined particular values of the waist rotation angle θ_1, the shoulder segment up-down movements θ_2 and the elbow segment up-down movements θ_3,

From Eq. (25)

$$-s_1 p_x + c_1 p_y = 0$$

$$\frac{s_1}{c_1} = \frac{p_y}{p_x}$$

$$\frac{\sin\theta_1}{\cos\theta_1} = \frac{p_y}{p_x} \tag{30}$$

$$\tan\theta_1 = \frac{p_y}{p_x}$$

$$\theta_1 = A\tan 2\left(\frac{p_y}{p_x}\right) \tag{31}$$

Where $A\tan 2$ is two-argument arc tangent function. It computes $A\tan^{-1}\left(\frac{p_y}{p_x}\right)$, but uses the signs of both p_y and p_x to determine the quadrant in which the resulting angle lies.

Now Eq. (30)

$$\frac{\sin\theta_1}{\cos\theta_1} = \frac{p_y}{p_x}$$

$$\frac{\sin^2\theta_1}{\cos^2\theta_1} = \frac{{p_y}^2}{p_x^{2x}}$$

This implies

$$p_x^2 - p_x^2\cos^2\theta_1 = {p_y}^2\cos^2\theta_1$$

or

$$\cos^2\theta_1 = \frac{p_x^2}{p_x^2 + {p_y}^2} \tag{32}$$

or

$$\cos\ \theta_1 = \frac{p_x}{\sqrt{p_x^2 + p_y^{\ 2}}} \tag{33}$$

Also from Eq. (32),

$$1 - \sin^2 \theta_1 = \frac{p_x^2}{p_x^2 + p_y^{\ 2}}$$

$$\sin\ \theta_1 = \frac{p_y}{\sqrt{p_x^2 + p_y^{\ 2}}} \tag{34}$$

Multiply Eq. (33) with p_x and Eq. (34) by p_y and after adding we will get;

$$p_Y s_1 + p_X c_1 = \sqrt{p_X^{\ 2} + p_Y^{\ 2}} \tag{35}$$

Now take Eq. (27)

$$s_3 f = -s_2(c_1 p_x + s_1 p_y) + c_2(p_Z - h)$$

Substituting $(c_1 p_x + s_1 p_y)$ from Eq. (35), we have,

$$s_3 f = -s_2\sqrt{p_X^{\ 2} + p_Y^{\ 2}} + c_2(p_Z - h)$$

Divided above expression by c_2 and simplifying, we have

$$c_2 = \frac{s_3 f}{-t_2\sqrt{p_X^{\ 2} + p_Y^{\ 2}} + (p_Z - h)} \tag{36}$$

Now take Eq. (26)

$$e + c_3 f = c_2(c_1 p_x + s_1 p_y) + s_2(p_Z - h)$$

After substituting $(c_1 p_x + s_1 p_y)$ from Eq. (35), it simplifies to;

$$e + c_3 f = c_2\sqrt{p^2{}_x + p_y^{\ 2}} + s_2(p_Z - h)$$

Divided above expression by c_2 implies;

$$\frac{e + c_3 f}{c_2} = \sqrt{{p_X}^2 + {p_Y}^2} + t_2(p_Z - h)$$

Where we have taken $t_2 = \frac{s_2}{c_2} = \tan\theta_2$

Further transformation of above expression obtained by using the value of c_2 from Eq. (36), gives

$$e + c_3 f = \frac{s_3 f}{-t_2\sqrt{{p_X}^2 + {p_Y}^2} + (p_Z - h)}(\sqrt{{p_X}^2 + {p_Y}^2} + t_2(p_Z - h))$$

or,

$$e + c_3 f = \frac{s_3 f(\sqrt{{p_X}^2 + {p_Y}^2} + t_2(p_Z - h)}{-t_2\sqrt{{p_X}^2 + {p_Y}^2} + (p_Z - h)}$$

and

$$e + c_3 f(-t_2\sqrt{{p_X}^2 + {p_Y}^2} + (p_Z - h)) = s_3 f(\sqrt{{p_X}^2 + {p_Y}^2} + t_2(p_Z - h)$$

After simplifying, we have

$$t_2 = \frac{(e + c_3 f)(p_Z - h) - s_3 f\sqrt{{p_X}^2 + {p_Y}^2}}{(e + c_3 f)(\sqrt{{p_X}^2 + {p_Y}^2}) + s_3 f(p_Z - h)}$$

or

$$\tan\theta_2 = \frac{(e + \cos\theta_3 f)(p_Z - h) - \sin\theta_3 f\sqrt{{p_X}^2 + {p_Y}^2}}{(e + \cos\theta_3 f)(\sqrt{{p_X}^2 + {p_Y}^2}) + \sin\theta_3 f(p_Z - h)} \tag{37}$$

So,

$$\theta_2 = A\tan 2\left(\frac{(e + \cos\theta_3 f)(p_Z - h) - \sin\theta_3 f\sqrt{{p_X}^2 + {p_Y}^2}}{(e + \cos\theta_3 f)(\sqrt{{p_X}^2 + {p_Y}^2}) + \sin\theta_3 f(p_Z - h)}\right) \tag{38}$$

Eq. (37) can be write as

$$\frac{s_2}{c_2} = \frac{(p_Z - h)(e + c_3 f) - f s_3 \sqrt{p_X{}^2 + p_Y{}^2}}{(p_Z - h) f s_3 + (e + c_3 f)\sqrt{p_X{}^2 + p_Y{}^2}}$$

Above eq. can be split as;

$$s_2 = \frac{(p_Z - h)(e + c_3 f) - f s_3 \sqrt{p_X{}^2 + p_Y{}^2}}{(p_Z - h)^2 + p_X{}^2 + p_Y{}^2}$$

Squaring both side the above Eq.

$$(s_2)^2 = \frac{((p_Z - h)(e + c_3 f))^2 + \left(f s_3 \sqrt{p_X{}^2 + p_Y{}^2} \right)^2 - 2 f s_3 \sqrt{p_X{}^2 + p_Y{}^2} (p_Z - h)(e + c_3 f)}{\left((p_Z - h)^2 + p_X{}^2 + p_Y{}^2\right)^2} \quad (39)$$

Similarly

$$c_2 = \frac{(p_Z - h) f s_3 + (e + c_3 f)\sqrt{p_X{}^2 + p_Y{}^2}}{(p_Z - h)^2 + p_X{}^2 + p_Y{}^2}$$

Squaring both side the above Eq.

$$(c_2)^2 = \frac{((p_Z - h) f s_3)^2 + \left((e + c_3 f)\sqrt{p_X{}^2 + p_Y{}^2} \right)^2 + 2 f s_3 \sqrt{p_X{}^2 + p_Y{}^2} (p_Z - h)(e + c_3 f)}{\left((p_Z - h)^2 + p_X{}^2 + p_Y{}^2\right)^2} \quad (40)$$

Adding Eq. (39) and Eq. (40) will give us;

$$1 = \frac{((p_Z - h)(e + c_3 f))^2 + \left(f s_3 \sqrt{p_X{}^2 + p_Y{}^2} \right)^2 + ((p_Z - h) f s_3)^2 + \left((e + c_3 f)\sqrt{p_X{}^2 + p_Y{}^2} \right)^2}{\left((p_Z - h)^2 + p_X{}^2 + p_Y{}^2\right)^2}$$

A little bit of algebraic manipulations yields

$$c_3 = \frac{(p_Z - h)^2 + p_X{}^2 + p_Y{}^2 - e^2 - f^2}{2ef} \quad (41)$$

That is,

$$\cos\theta_3 = \frac{(p_Z - h)^2 + p_X{}^2 + p_Y{}^2 - e^2 - f^2}{2ef}$$

Squaring both side Eq. (41)

$$(c_3)^2 = \left(\frac{(p_Z - h)^2 + {p_X}^2 + {p_Y}^2 - e^2 - f^2}{2ef} \right)^2$$

Above Eq. can be written as;

$$1 - {s^2}_3 = \frac{\left((p_Z - h)^2 + {p_X}^2 + {p_Y}^2 - e^2 - f^2\right)^2}{4e^2 f^2}$$

or

$${s^2}_3 = \frac{4e^2 f^2 - \left((p_Z - h)^2 + {p_X}^2 + {p_Y}^2 - e^2 - f^2\right)^2}{4e^2 f^2}$$

and

$$\sin\theta_3 = \frac{\pm\sqrt{4e^2 f^2 - \left((p_Z - h)^2 + {p_X}^2 + {p_Y}^2 - e^2 - f^2\right)^2}}{2ef} \tag{42}$$

From Eq. (41) and (42) we can get;

$$\frac{\sin\theta_3}{\cos\theta_3} = \frac{\pm\sqrt{4e^2 f^2 - \left((p_Z - h)^2 + {p_X}^2 + {p_Y}^2 - e^2 - f^2\right)^2}}{(p_Z - h)^2 + {p_X}^2 + {p_Y}^2 - e^2 - f^2}$$

or

$$\tan\theta_3 = \frac{\pm\sqrt{4e^2 f^2 - \left((p_Z - h)^2 + {p_X}^2 + {p_Y}^2 - e^2 - f^2\right)^2}}{(p_Z - h)^2 + {p_X}^2 + {p_Y}^2 - e^2 - f^2} \tag{43}$$

and therefore,

$$\theta_3 = A\tan 2\frac{\pm\sqrt{4e^2 f^2 - \left((p_Z - h)^2 + {p_X}^2 + {p_Y}^2 - e^2 - f^2\right)^2}}{(p_Z - h)^2 + {p_X}^2 + {p_Y}^2 - e^2 - f^2} \tag{44}$$

The value of *e, f* and *h* for RPAR are 46.10, 76.40 and 101.50 cm respectively. Now substitution of these values in Eqs. (31), (38) and (44);

$$\theta_1 = A\tan^{-1}\left(\frac{p_y}{p_x}\right)$$

$$\theta_2 = A\tan 2\left(\frac{(46.10 + 76.40\cos\theta_3)(P_Z - 101.5) - 76.40\sin\theta_3\sqrt{{P_X}^2 + {P_Y}^2}}{(46.10 + 76.40\cos\theta_3)(\sqrt{{P_X}^2 + {P_Y}^2}) + 76.40\sin\theta_3(P_Z - 101.5)} \right) \tag{45}$$

and

$$\theta_3 = A\tan 2\frac{\pm\sqrt{4(46.1)^2(76.4)^2-\left((P_Z-101.5)^2+P_X{}^2+P_Y{}^2-(46.1)^2-(76.4)^2\right)^2}}{(P_Z-101.5)^2+P_X{}^2+P_Y{}^2-(46.1)^2-(76.4)^2}$$

So

$$\theta_3 = A\tan 2\frac{\pm\sqrt{49619063.05-\left((P_Z-101.5)^2+P_X{}^2+P_Y{}^2-7962.17\right)^2}}{(P_Z-101.5)^2+P_X{}^2+P_Y{}^2-7962.17} \qquad (46)$$

So for any arbitrary values of p_x, p_y, p_z we can easily find the corresponding values of θ_1, θ_2 and θ_3. As an example we evaluate the sets of link angle values for which $p_x = 3$, $p_y = -1$ and $p_z = 4.5$.

$$\theta_3 = A\tan 2\frac{\pm\sqrt{49619063.05-\left((P_Z-101.5)^2+P_X{}^2+P_Y{}^2-7962.17\right)^2}}{(P_Z-101.5)^2+P_X{}^2+P_Y{}^2-7962.17}$$

$$\theta_3 = A\tan 2\frac{\pm\sqrt{49619063.05-\left((4.5-101.5)^2+(3)^2+(-1)^2-7962.17\right)^2}}{(4.5-101.5)^2+(3)^2+(-1)-7962.17}$$

After simplifying, we have

$$\theta_3 = \pm 78.06^o$$

For $\theta_3 = +78.06$

$$\theta_2 = A\tan 2\left(\frac{(46.1+76.4\cos\theta_3)(4.5-101.5)-76.4\sin\theta_3\sqrt{(3)^2+(-1)^2}}{(46.1+76.4\cos\theta_3)(\sqrt{(3)^2+(-1)^2})+76.4\sin\theta_3(4.5-10.5)}\right)$$

$$\theta_2 = A\tan 2(0.8847)$$

or

$$\theta_2 = 41.50^o$$

Similarly for $\theta_3 = -78.06$

$$\theta_2 = A\tan 2\left(\frac{5768.55}{7446.22}\right)$$

$$\theta_2 = 37.76^o$$

θ_1 is a dual-valued function and explicitly given by

$$\theta_1 = A\tan 2\left(\frac{p_y}{p_x}\right) \text{ and } \theta_1 = A\tan 2\left(\frac{-p_y}{-p_x}\right)$$

So for

$$\theta_1 = A\tan^{-1}\left(\frac{p_y}{p_x}\right)$$

$$\theta_1 = A\tan^{-1}\left(\frac{-1}{3}\right)$$

$$\theta_1 = -18.43$$

and for

$$\theta_1 = A\tan^{-1}\left(\frac{-p_y}{-p_x}\right)$$

$$\theta_1 = A\tan^{-1}\left(\frac{1}{-3}\right)$$

$$\theta_1 = 161.57$$

In summary following four sets of link angle values solve the inverse kinematic problem for the RPAR when $e = 46.1,\ f = 76.4,\ h = 101.5,\ p_x = 3,\ p_y = -1$ and $p_z = 4.5$.

θ_1 = -18.43 θ_2 = 41.50 θ_3 = 78.06 (47)

θ_1 = -18.43 θ_2 = 37.76 θ_3 = -78.06 (48)

θ_1 = 161.57 θ_2 = 41.50 θ_3 = 78.06 (49)

θ_1 = 161.57 θ_2 = 37.76 θ_3 = -78.06 (50)

There are four different mathematical solutions to the inverse kinematic problem when $p_x = 3,\ p_y = -1$ and $p_z = 4.5$ as given by Eqs. (47) through (50), only certain of

these may represent physical solutions. More specifically, for RPAR the physical link value limits for waist rotation (θ_1), shoulder rotation (θ_2) and elbow rotation (θ_3) are physically limited to angular values from -97.5° to +97.5°, -20° to +90° and -90° to +90°, respectively. Therefore, in the light of these rotational limitations, only two of the four mathematical solutions given by Eqs. (47) through (50) namely Eqs. (47) and (48), can be physically attained, i.e., Eqs. (47) and (48) represents the physical solutions to the inverse kinematic problem in the present case.

5.4 VALIDATION OF FORWARD KINEMATICS

Calculated forward kinematics was verified by substituting different values of θ_1, θ_2 & θ_3 and measuring the resultant RPAR's Gripper position, as given below;

CASE-I

$\theta_1 = 90°$, $\theta_2 = 0°$ and $\theta_3 = 0°$

Putting these values of θ_1, θ_2 and θ_3 in Eqs. (11) through (13) gives the following Gripper positions. These are illustrated in Fig. 5.2.

$$p_x = 0$$
$$p_y = e + f = 122.5 \ cm$$
$$p_z = h = 101.5 \ cm$$

The measured (true) value of p_x, p_z varies from -0.08 to 0.08 and 100.6 to 102.4 cm, respectively, whereas p_y is 122.50 cm. The root mean square (RMS) error in position is 1.04 cm.

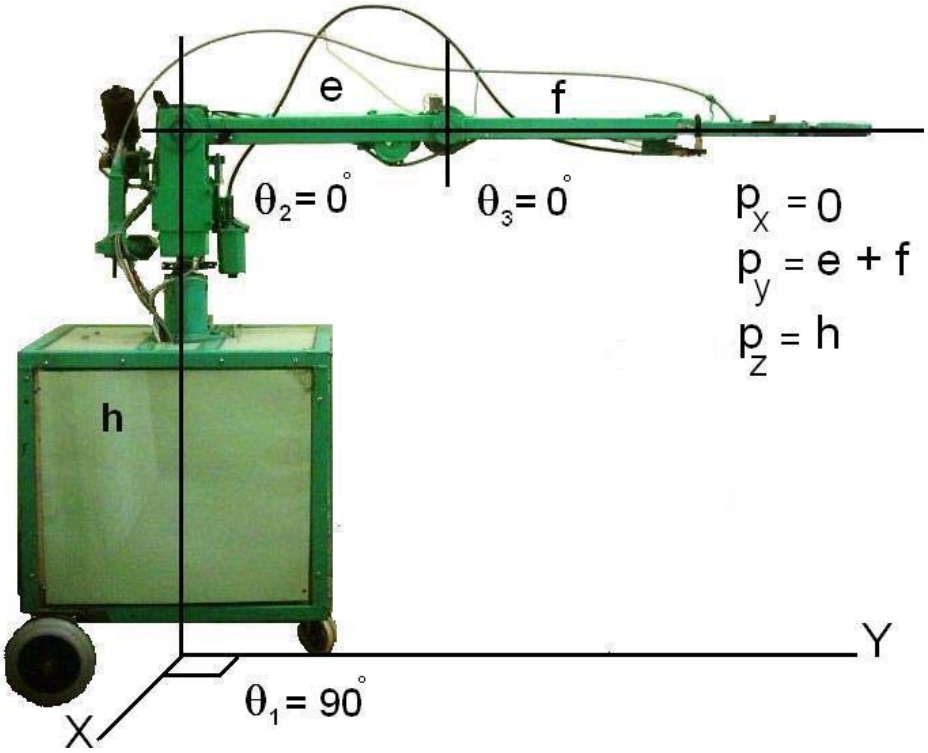

Fig. 5.2: RPAR for $\theta_1 = 90°$, $\theta_2 = 0°$ and $\theta_3 = 0°$

CASE-II

$\theta_1 = 0°$, $\theta_2 = 90°$and $\theta_3 = 0°$

The procedure described earlier yields the following Gripper positions. This is shown in Fig. 5.3.

$$p_x = 0$$
$$p_y = 0$$
$$p_z = h + e + f = 224 \ cm$$

The measured value of p_x, p_y varies from -0.08 to 0.08 and -0.09 to 0.09 cm respectively, whereas p_z is 224 cm. The RMS error in position in this case is 0.14 cm.

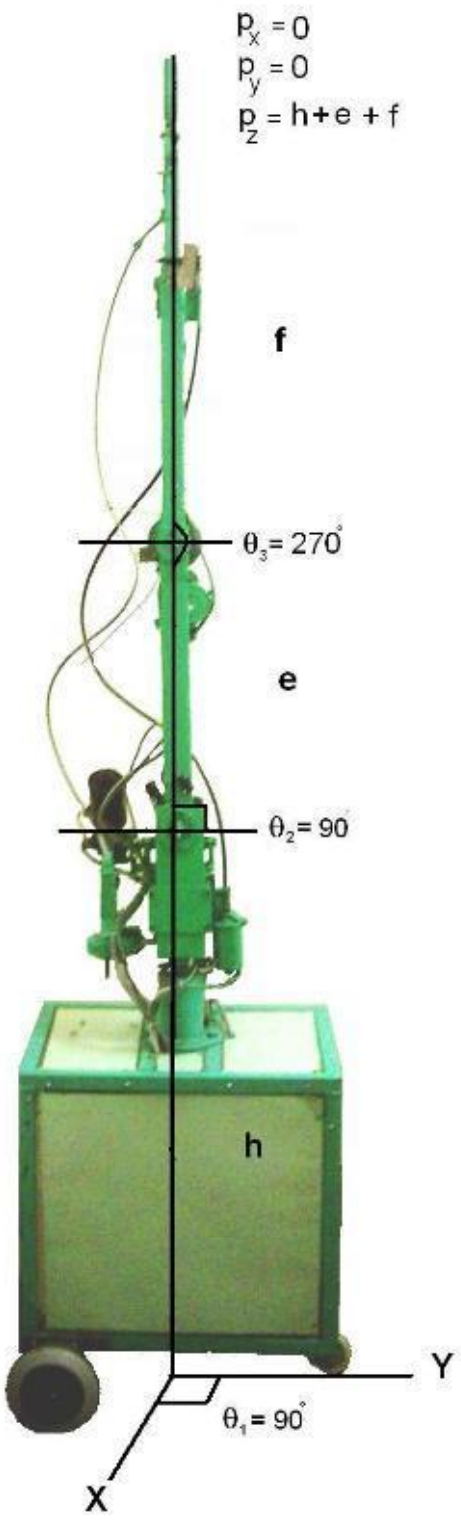

Fig. 5.3: RPAR for $\theta_1 = 0°$, $\theta_2 = 90°$ and $\theta_3 = 0°$

CASE-III

$\theta_1 = 90°$ $\theta_2 = 90°$ and $\theta_3 = 270°$,

We get the following Gripper positions as depicted in Fig. 5.4.

$p_x = 0$

$p_y = f = 76.4 \ cm$

$p_z = e + h = 147.6 \ cm$

The measured value of p_x, p_z varies from -0.08 to 0.08 and 146.7 to 148.4 cm respectively, whereas p_y is 76.4 cm. The RMS error in position is 0.98 cm.

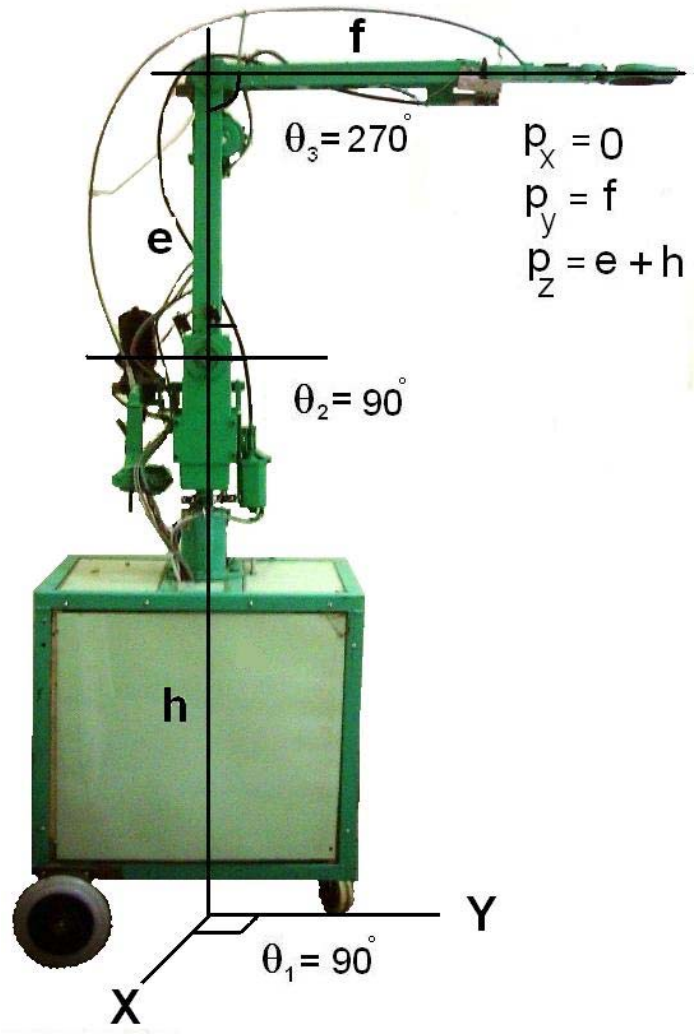

Fig. 5.4: RPAR for $\theta_1 = 90°$, $\theta_2 = 90°$ and $\theta_3 = 270°$

CASE-IV

$\theta_1 = 0°, \theta_2 = 0°$ and $\theta_3 = 0°$,

The resulting Gripper positions are:

$p_x = e + f = 122.5 \ cm$

$p_y = 0$

$p_z = h = 101.5 \ cm$

The measured value of p_y, p_z varies from -0.08 to 0.08 and 100.6 to 102.4 cm, respectively whereas p_x is 122.5. The RMS error in position is 1.04 cm and is illustrated in Fig. 5.5.

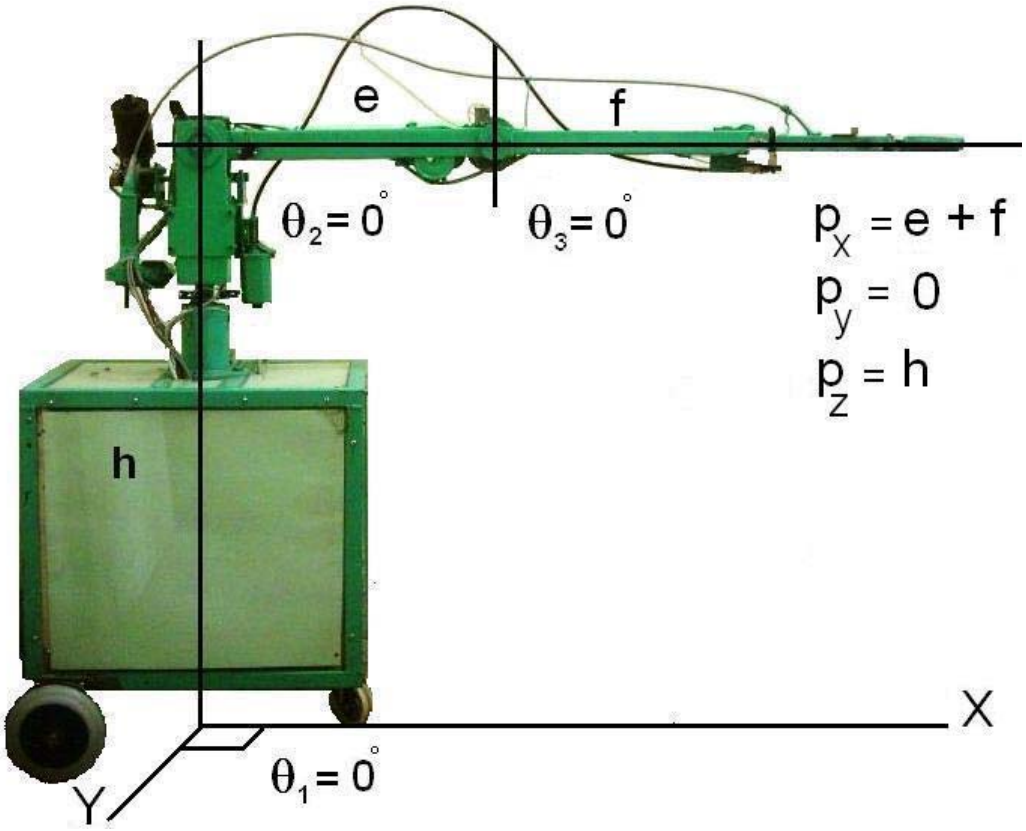

Fig. 5.5: RPAR for $\theta_1 = 0°, \theta_2 = 0°$ and $\theta_3 = 0°$

5.5 VALIDATION OF INVERSE KINEMATICS

Calculations of inverse kinematics are also verified by substituting various values of p_x, p_y & p_z and measuring the resultant RPAR's articulated arm's position i.e. θ_1, θ_2 and θ_3.

CASE-I

$$p_x = 0, p_y = e + f, p_z = h$$

Substituting these values of p_x, p_y & p_z in Eqs. (31), (38) and (44), the position of articulated arm as illustrated in Fig. 5.2, is

$\theta_1 = 90°$

$\theta_2 = 0°$

$\theta_3 = 0^o$

The measured value of θ_1, θ_2 & θ_3 are 90.38°, 0.21° and 0.34°, respectively. The RMS angular error is 0.32°.

CASE-II

$$p_x = 0, p_y = 0, p_z = h + e + f$$

The articulated arm's positions is as follow, also see Fig. 5.3.

$\theta_1 = 0°$

$\theta_2 = 90°$

$\theta_3 = 0°$

The measured value of θ_1, θ_2 & θ_3 are 0.28°, 90.36° and 0.34°, respectively. The RMS angular error is 0.33°.

CASE-III

$$p_x = 0, p_y = f, p_z = e + f$$

We get the following articulated arm's position.

$\theta_1 = 90°$

$\theta_2 = 90°$

$\theta_3 = 270°$

The measured value of θ_1, θ_2 & θ_3 are 90.38°, 90.36° and 270.54°, respectively. The RMS angular error is 0.43° and is also depicted in Fig. 5.4.

CASE-IV

$$p_x = e + f, p_y = 0, p_z = h,$$

Resulting articulated arm's positions comes to be ;

$\theta_1 = 0°$

$\theta_2 = 0°$

$\theta_3 = 0°$

The measured value of θ_1, θ_2 & θ_3 are 0.28°, 0.21° and 0.34°, respectively. The RMS angular error is 0.28° and is illustrated in Fig. 5.5. This error is mainly due to physical error sources such as geometric, mechanical system errors (machining and assembly tolerances) and errors in the robot joints. The joints errors include bearing run-out in rotating joints and backlash in manipulator joints and actuator transmissions. Elastic deformation or joint flexibility due to payload and gravity can also result in large end-effector errors in the long range manipulator systems. Measurement, actuator and control errors resulting from the control system also reflected in end-effector positioning error

(Mavroidis et al; 1997 and Meggiolaro et al; 2005). The physically errors are usually small and depend upon the robot arm structure. Its value increases at the end-effector with the increasing length of the links.

The main purpose of RPAR is to provide assistance to radiation protection worker in radiation/contamination surveys, radioactive material handling etc. Since these jobs do not demand highly precise movements, the errors in the end-effector position are acceptable.

5.6 MANIPULATOR JACOBIAN

The performance of the articulated robotic arm segments (manipulator's segments) depends on their controllability and pivot limitations. These can be evaluated by manipulator Jacobian Matrix. This matrix represents infinitesimal change in position relationship between the joint displacements and the gripper tip location at newly acquired position and the arm segment configuration (Asada and Slotine; 1986).

Jacobian matrix is a matrix which has its first three rows as the positional Jacobian and the remaining three rows as the orientation Jacobian. The first three rows of J (the positional Jacobian) can be obtained by direct differentiation of a manipulator's positional equation. i.e., differentiate D_x for the RPAR, as given by Eq. (9) i.e.,

$$\begin{bmatrix} D_x \\ D_y \\ D_z \end{bmatrix} = \begin{bmatrix} f\cos\theta_1\cos\theta_{23} + e\cos\theta_1\cos\theta_2 \\ f\sin\theta_1\cos\theta_{23} + e\sin\theta_1\cos\theta_2 \\ f\sin\theta_{23} + e\sin\theta_2 + h \end{bmatrix}$$

$$D_x = f\cos\theta_1\cos\theta_{23} + e\cos\theta_1\cos\theta_2$$

It can be written as

$$D_x = fc_1c_{23} + ec_1c_2$$

After differentiating

$$\dot{D}_x = (-es_1c_2 - fs_1c_{23})\dot{\theta}_1 + (-ec_1s_2 - fc_1s_{23})\dot{\theta}_2 - (fc_1s_{23})\dot{\theta}_3$$
$$\dot{D}_x = -s_1(ec_2 + f\,c_{23})\dot{\theta}_1 - c_1(es_2 + f\,s_{23})\dot{\theta}_2 - (fc_1s_{23})\dot{\theta}_3 \quad (51)$$

Now D_Y from Eq. (9) and after differentiation gives

$$\dot{D}_y = c_1(ec_2 + fc_{23})\dot{\theta}_1 - s_1(es_2 + fs_{23})\dot{\theta}_2 - (fs_1s_{23})\dot{\theta}_3 \quad (52)$$

Similarly,

$$\dot{D}_z = (fc_{23} + ec_2)\dot{\theta}_2 + fc_{23}\dot{\theta}_3 \quad (53)$$

The three rows of Oriental Jacobian can be obtained by using the vector relations; i.e.,

$$\begin{bmatrix} \dot{\phi}_x \\ \dot{\phi}_y \\ \dot{\phi}_z \end{bmatrix} = \begin{bmatrix} w_x \\ w_y \\ w_z \end{bmatrix} = \begin{bmatrix} s_1(\dot{\theta}_2 + \dot{\theta}_3) \\ -c_1(\dot{\theta}_2 + \dot{\theta}_3) \\ \dot{\theta}_1 \end{bmatrix} \quad (54)$$

Where w_x, w_y and w_z denote the angular velocities of the tool frame (or any object carried by the end effector or gripper) relative to the base axes, namely x_0, y_0 and z_0, respectively.

The Jacobian matrix of 4-DOF manipulator by using the Eqs. (51) through (54) is given as;

$$J = \begin{bmatrix} -s_1(ec_2 + fc_{23}) & -c_1(es_2 + fs_{23}) & -fc_1s_{23} \\ c_1(ec_2 + fc_{23}) & -s_1(es_2 + fs_{23}) & -fs_1s_{23} \\ 0 & fc_{23} + c_2e & fc_{23} \\ 0 & s_1 & s_1 \\ 0 & -c_1 & -c_1 \\ 1 & 0 & 0 \end{bmatrix} \quad (55)$$

As the elements of the Jacobian are functions of joint displacements, therefore, varies with the arm's links configuration. For instant three joints of RPAR articulated robotic arm move at joint-velocities $\dot{\theta} = \left[\dot{\theta}_1, \dot{\theta}_2, \dot{\theta}_3\right]^T$, $v = \left[\dot{x}, \dot{y}, \dot{z}\right]^T$ will be the resulting gripper-tip velocity vector. So, By taking derivative of $\begin{bmatrix} D_x \\ D_y \\ D_z \end{bmatrix}$ with respect to t, Eq. (9) becomes;

$$\frac{dDx}{dt} = j\frac{d\theta}{dt}$$

that is,

$$V = J\dot{\theta} \tag{56}$$

Thus the manipulator Jacobian determines the velocity relationship between the joints and the gripper-tip. J_1, J_2 and J_3, are three 3×1 vectors for the first, second and third columns of the Jacobian matrix, respectively. Eq. (56) can be written as;

$$V = J_1\dot{\theta}_1 + J_2\dot{\theta}_2 + J_3\dot{\theta}_3 \tag{57}$$

Each column of the Jacobian matrix represents the gripper-tip velocity vector generated by the corresponding joint motion at unit velocity while all other joints are immobilized. The resultant gripper-tip velocity is given by summing the three vectors.

5.7 REAL TIME POSITIONS MEASUREMENT

Real time positions of different links of RPAR is measured with the help of embedded controller card, dedicated software and four potentiometers working as shaft

encoders. The real time positions of Wrist, Elbow, Shoulder and Waist are illustrated in Figs. 5.6 to 5.9.

Fig. 5.6 shows the real time position of Wrist segment. The rising curve shows the clockwise movement of Wrist at a rate of 18.94 deg.s^{-1}. After reaching its maximum position of 210°, it keeps its position for a few seconds and then starts moving counter clock wise at a rate of 17.43 deg.s^{-1}.

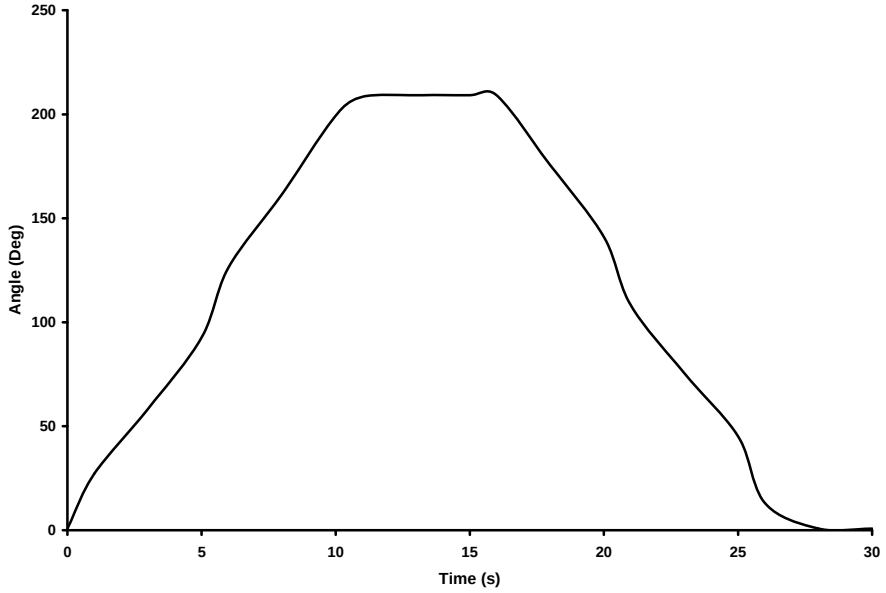

Fig. 5.6: Real time position of Wrist segment

Fig. 5.7 illustrates the real time position of Elbow link. The rising curve shows the upwards movement of Elbow at a rate of 11.61 deg.s^{-1}. After reaching its maximum position of 180°, it keeps its position for a few seconds and then starts moving downwards at a rate of 17.65 deg.s^{-1}. The downwards speed is greater than upwards because of gravity pull.

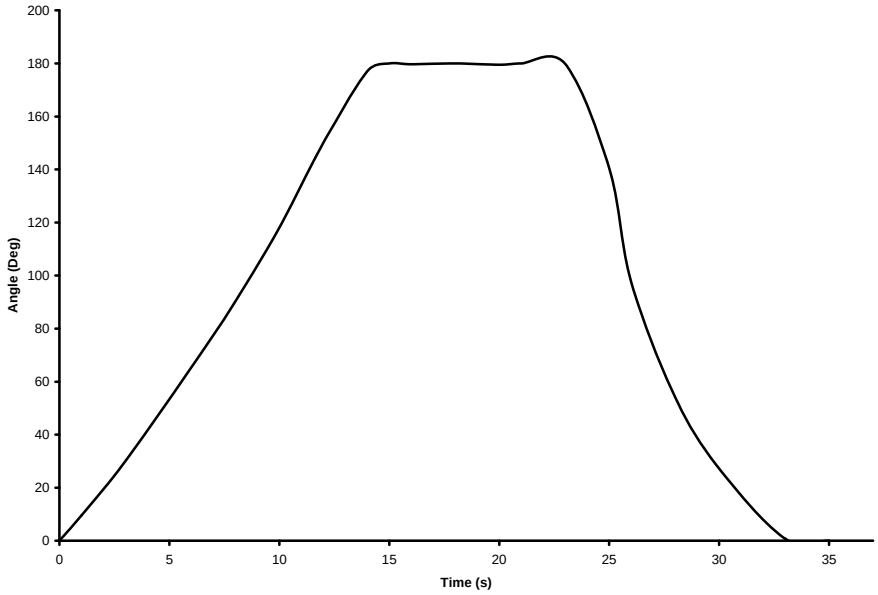

Fig. 5.7: Real time position of Elbow Link

Fig. 5.8 shows the real time position of Shoulder link. The rising curve shows the upwards movement of Shoulder at a rate of 4.32 deg.s^{-1}. After reaching its maximum position of 110°, it keeps its position for a few seconds and then starts moving downwards at a rate of 6.11 deg.s^{-1}. The downwards speed is greater than upwards because of gravity pull.

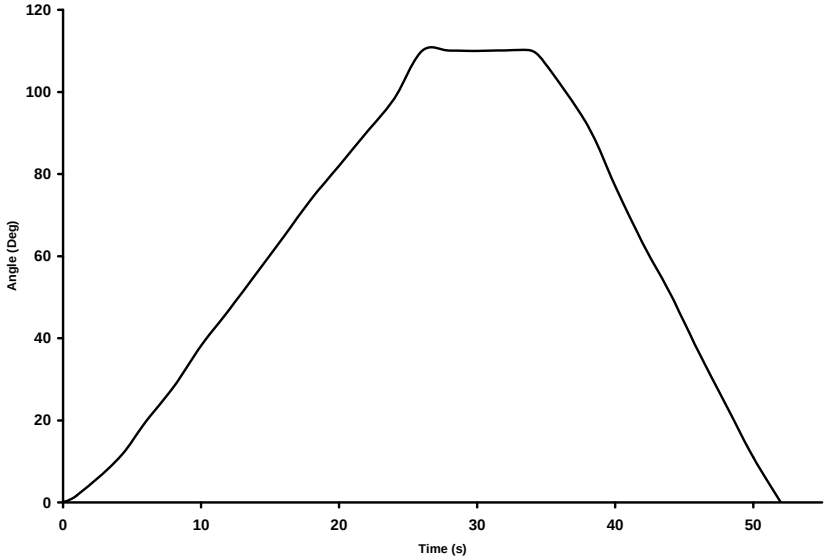

Fig. 5.8: Real time position of Shoulder Link

Fig. 5.9 explains the real time position of Waist segment. The rising curve shows the clockwise moment of Waist at a rate of 5.42 deg.s^{-1}. After reaching its maximum position of 195°, it keeps its position for a few seconds and then starts moving counter clock wise at a rate 6.09 deg.s^{-1}. There is no significant change on CW and CCW rates because effect of gravity on both movements is same.

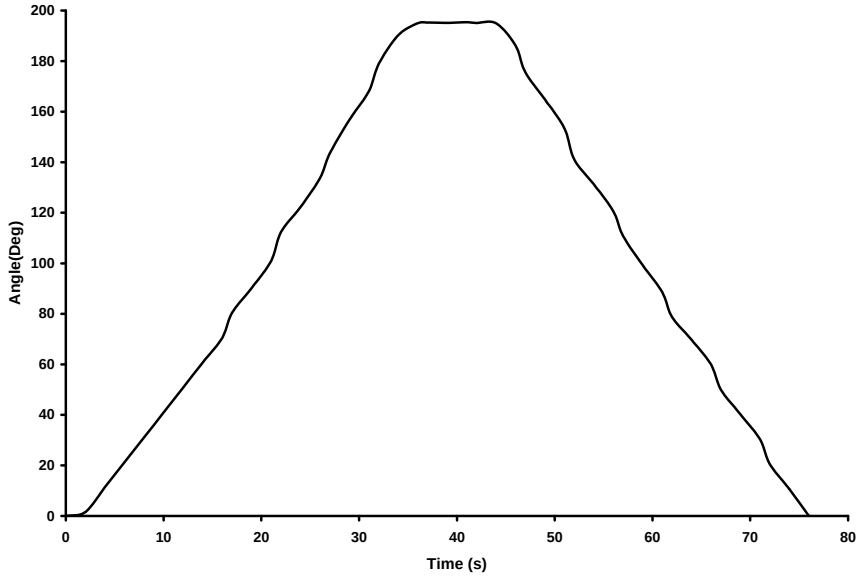

Fig. 5.9: Real time position of Waist segment

5.8 WORKSPACE ANALYSIS

The workspace of a manipulator is defined as the volume of space in which the manipulator is able to locate its end-effector or gripper. The workspace gets specified by the existence or nonexistence of solutions to the inverse problem. The region that can be reached by the origin of the end-effector frame with at least one orientation is called the Reachable Work Space (RWS). If a point in workspace can be reached only in one orientation, the manipulatability of the end-effector is very poor and it is not possible to do

any practical work satisfactorily with one fixed orientation. It is therefore, necessary to look for the points in workspace, which can be reached in more than one orientation. Some points within the RWS can be reached in more than one orientation. The space where the end-effector or gripper can reach every point from all orientations is called Dexterous Workspace (DWS). It is obvious that the DWS is either smaller (subset) or same as the RWS (Mittal and Nagrath; 2006).

The reachable space for RPAR articulated robotic arm is depicted in Fig. 5.10. This is a two dimensional geometrical view in which waist segment is stationary. The arc **a′b** has maximum accessible space thickness of about 14.26 cm. The arc **aa′** has tapered workspace which is gradually increased up to point **a′**, while arc **bb′** has a sharp upward decrease in workspace area. The shaded area in Fig. 5.10 is dexterous workspace.

Maximum and minimum edge boundaries of gripper-tip work envelope have been evaluated by putting certain limitation of θ_1 , θ_2 and θ_3 in the following sections.

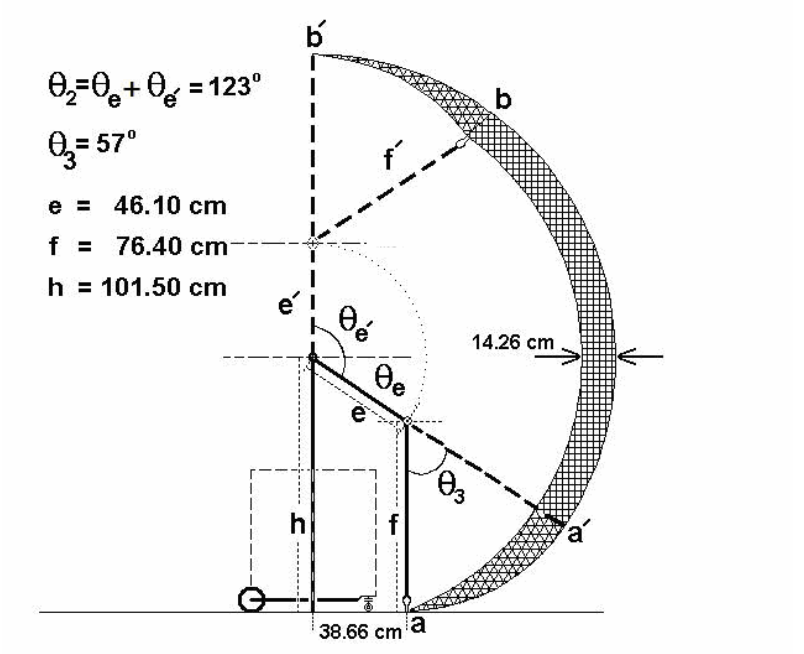

Fig. 5.10: A 2-Dimensional workspace of maximum and minimum edge boundary of RPAR articulated robotic arm.

CASE-I

The maximum reach of RPAR is generated by applying the "Algorthim-I" in which θ_1 is varied from 0° to 340°, θ_2 is varied from -20° to 90° and $\theta_3 = 0°$ (i.e. elbow is linear to shoulder) as shown in Fig. 5.11. The values of *e*, *f* and *h* are determined earlier as shown in Fig. 5.10.

Algorithm-I: Maximum reach of RPAR ($\Delta\theta_1$, $\Delta\theta_2$, $\theta_3 = 0°$)

Input: $\theta_3 = 0°, \Delta\theta_1, \Delta\theta_2$ (grid steps of angles θ_1, θ_2)

Output: X, Y, Z (3D Plot)

for $\theta_1 = 0$ **to** 340 **step** $\Delta\theta_1$

for $\theta_2 = -20$ to 90 **step** $\Delta\theta_2$

$$X(\theta_1, \theta_2, \theta_3) = f \cos\theta_1 \cos\theta_{23} + e \cos\theta_1 \cos\theta_2$$

$$Y(\theta_1, \theta_2, \theta_3) = f \sin\theta_1 \cos\theta_{23} + e \sin\theta_1 \cos\theta_2$$

$$Z(\theta_1, \theta_2, \theta_3) = f \sin\theta_{23} + e \sin\theta_2 + h$$

next θ_2

next θ_1

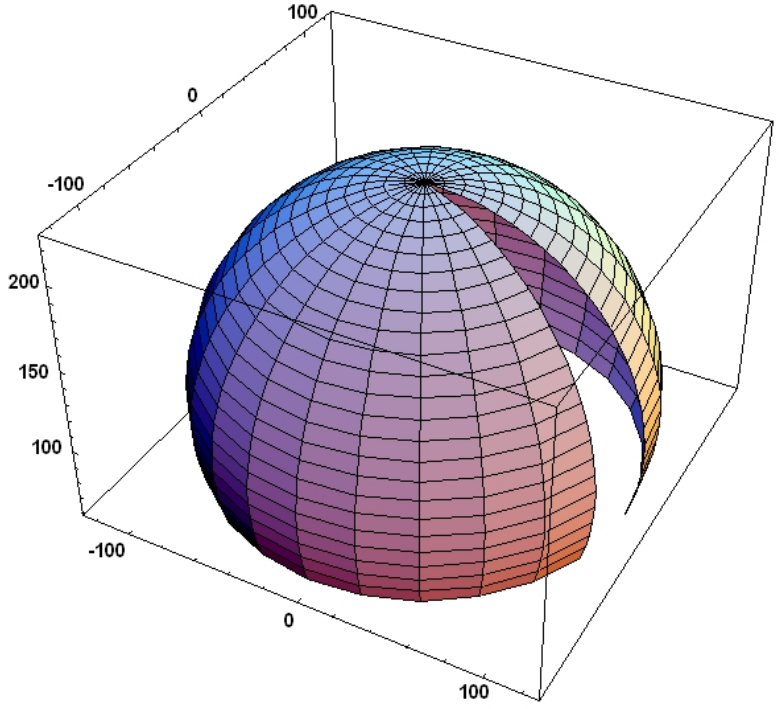

Fig. 5.11: Maximum reach of RPAR

CASE-II

Maximum reach of RPAR can also be generated by applying the "Algorthim-II" in which θ_1 is varied from 0° to 195°, θ_2 is varied from -20° to 90° and $\theta_3 = 0°$ (i.e. elbow is linear to shoulder) as shown in Fig. 5.12.

Algorithm-II: Maximum reach of RPAR after limitations ($\Delta\theta_1$, $\Delta\theta_2$, $\theta_3 = 0°$)

Input: $\theta_3 = 0°, \Delta\theta_1, \Delta\theta_2$ (grid steps of angles θ_1, θ_2)

Output: X, Y, Z (3D Plot)

for $\theta_1 = 0$ **to** 195 **step** $\Delta\theta_1$

for $\theta_2 = -20$ **to** 90 **step** $\Delta\theta_2$

$$X(\theta_1,\theta_2,\theta_3) = f\cos\theta_1\cos\theta_{23} + e\cos\theta_1\cos\theta_2$$
$$Y(\theta_1,\theta_2,\theta_3) = f\sin\theta_1\cos\theta_{23} + e\sin\theta_1\cos\theta_2$$
$$Z(\theta_1,\theta_2,\theta_3) = f\sin\theta_{23} + e\sin\theta_2 + h$$

next θ_2

next θ_1

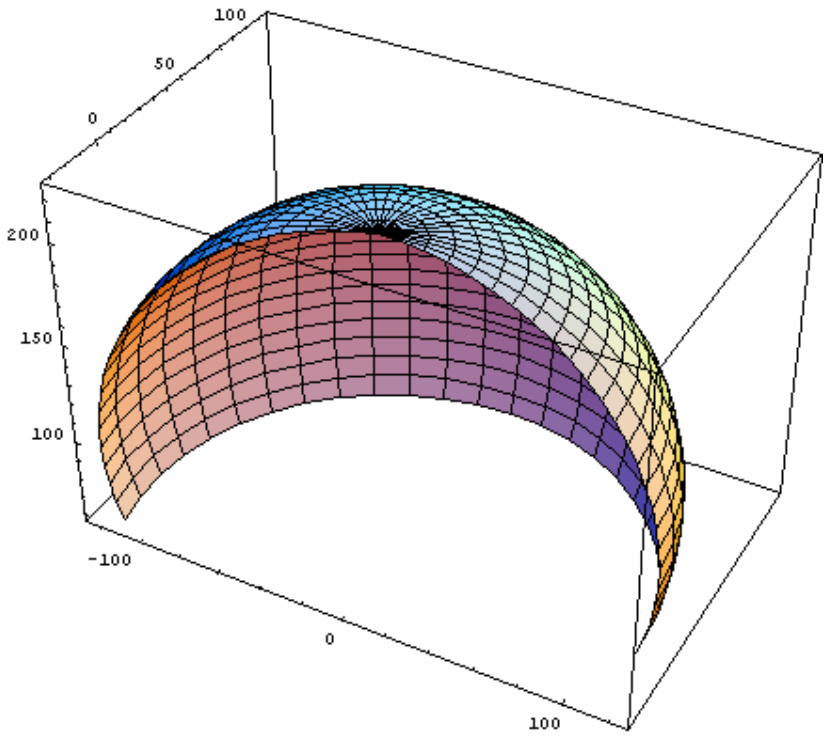

Fig. 5.12: Maximum reach of RPAR after limitations

CASE-III

Minimum reach of RPAR is generated by applying the "Algorthim-III" in which θ_1 is varied from $0°$ to $340°$, θ_2 is varied from $-20°$ to $90°$ and θ_3 is fixed at $57°$ as shown in Fig. 5.13.

Algorithm-III: Minimum reach of RPAR ($\Delta\theta_1$, $\Delta\theta_2$, $\theta_3 = 57°$)

Input: $\theta_3 = 57°$, $\Delta\theta_1, \Delta\theta_2$ (grid steps of angles θ_1, θ_2)

Output: X, Y, Z (3D Plot)

for $\theta_1 = 0$ **to** 340 **step** $\Delta\theta_1$

for $\theta_2 = -20$ to 90 **step** $\Delta\theta_2$

$$X(\theta_1,\theta_2,\theta_3) = f\cos\theta_1\cos\theta_{23} + e\cos\theta_1\cos\theta_2$$
$$Y(\theta_1,\theta_2,\theta_3) = f\sin\theta_1\cos\theta_{23} + e\sin\theta_1\cos\theta_2$$
$$Z(\theta_1,\theta_2,\theta_3) = f\sin\theta_{23} + e\sin\theta_2 + h$$

next θ_2

next θ_1

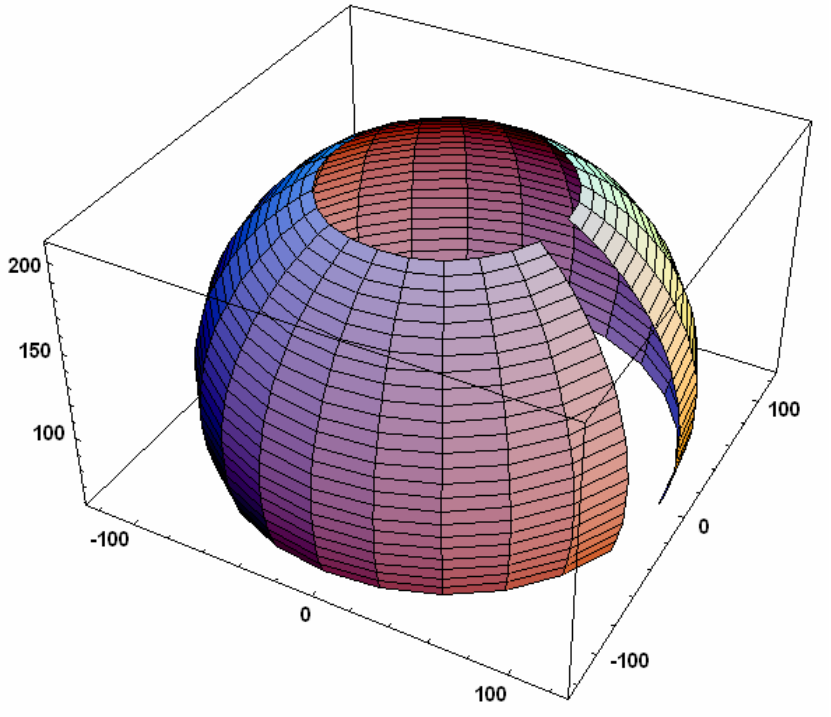

Fig. 5.13: Minimum reach of RPAR

CASE-IV

Minimum reach of RPAR can also be generated by applying the "Algorthim-IV" in which θ_1 is varied from $0°$ to $195°$, θ_2 is varied from $-20°$ to $90°$ and θ_3 is fixed at $57°$ as shown in Fig. 5.14. The assessable three dimensional workspace surfaces for gripper-tip, therefore, can be generated by applying different conditional algorithms.

Algorithm-IV: Minimum reach of RPAR after limitations ($\Delta\theta_1$, $\Delta\theta_2$, $\theta_3 = 57°$)

Input: $\theta_3 = 57°$, $\Delta\theta_1, \Delta\theta_2$ (grid steps of angles θ_1, θ_2)

Output: X, Y, Z (3D Plot)

for $\theta_1 = 0$ **to** 195 **step** $\Delta\theta_1$

for $\theta_2 = -20$ **to** 90 **step** $\Delta\theta_2$

$$X(\theta_1,\theta_2,\theta_3) = f\cos\theta_1\cos\theta_{23} + e\cos\theta_1\cos\theta_2$$
$$Y(\theta_1,\theta_2,\theta_3) = f\sin\theta_1\cos\theta_{23} + e\sin\theta_1\cos\theta_2$$
$$Z(\theta_1,\theta_2,\theta_3) = f\sin\theta_{23} + e\sin\theta_2 + h$$

next θ_2

next θ_1

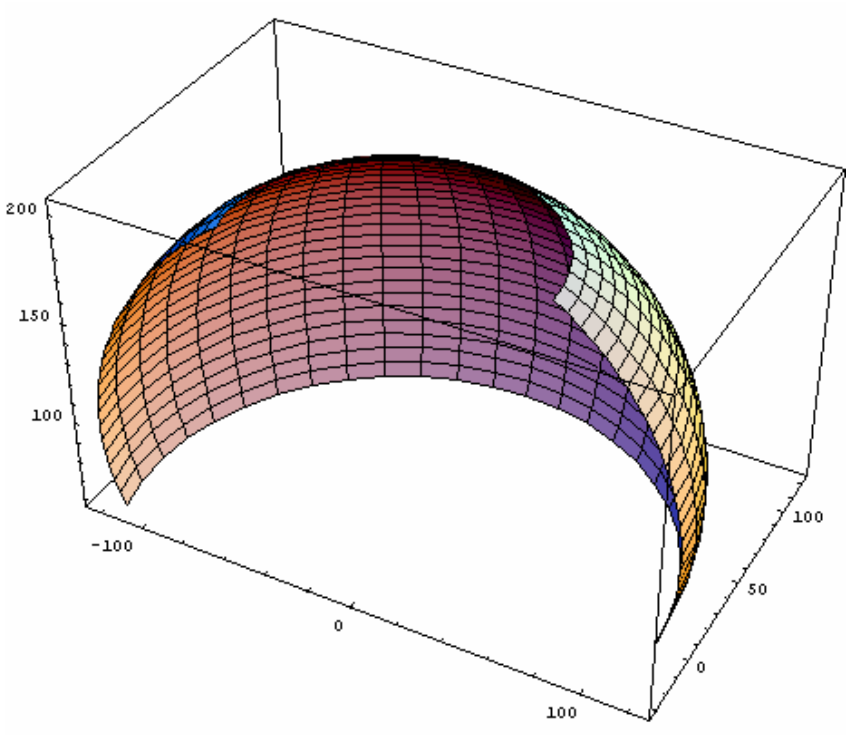

Fig. 5.14: Minimum reach of RPAR after limitations

5.9 REPEATABILITY RANGE OF RPAR

The repeatability tests of RPAR were performed by programming a specific cycle routine. In this routine, the Griper along with Waist, Shoulder and Elbow is moved from a testing point to another point and was brought back to the testing point. The change in the position of the Gripper was measured by using a digital dial indicator. This procedure was repeated for fifty times and repeatability of up to $\pm$0.9 mm was measured.

5.10 CONCLUSION

This chapter presented the forward and inverse kinematics studies of articulated robotic arm of Radiation Protection Assistant Robot (RPAR). The manipulator Jacobian and workspace analysis of this arm is also anticipated. Kinematics study and manipulator Jacobian analysis are essentially required for effective and efficient performance of a robotic arm. Repeatability of RPAR is studied by validation of forward and inverse kinematics. The workspace analysis can be used for maximum utilization of an articulated serial type robotic arm either with fixed or mobile platform. The calculated and measured values were found in good agreement.

CHAPTER

SIX

DYNAMICS ANALYSIS OF RPAR

6.1 INTRODUCTION

Dynamics deals with the forces and/or torques required to cause the motion of a system of bodies. Inertia forces are one of the major concerns for the dynamics studies. For the dynamics of a robot manipulator, the end effector is to be guided through a given path with certain prescribed motion characteristics. A set of torque and/or force functions must be applied at the actuated joints in order to produce a required motion. These actuation torque and/or force functions depend not only on the spatial and temporal attributes of the given path but also on the mass proportions of the links, the payload and the externally applied forces.

A recursive Newton-Euler formulation is used for the dynamical analysis of RPAR. Only 2-DOF of RPAR (Shoulder and Elbow link) is considered for this analysis. The Newton-Euler formulation incorporates all the forces acting on the individual links

of RPAR. Hence the resulting dynamical equations include all the forces of constraint between two adjacent links (Shoulder and Elbow).

The dynamical analysis of RPAR is made by the method given in the literature (Tsai, Lung-Wen, 1991). This method consists of a forward computation of the velocities and accelerations of each link, followed by a backward computation of the force and moments in each joints. The forces and moments acting on a typical link *i* of a serial manipulator are shown in Fig. 6.1

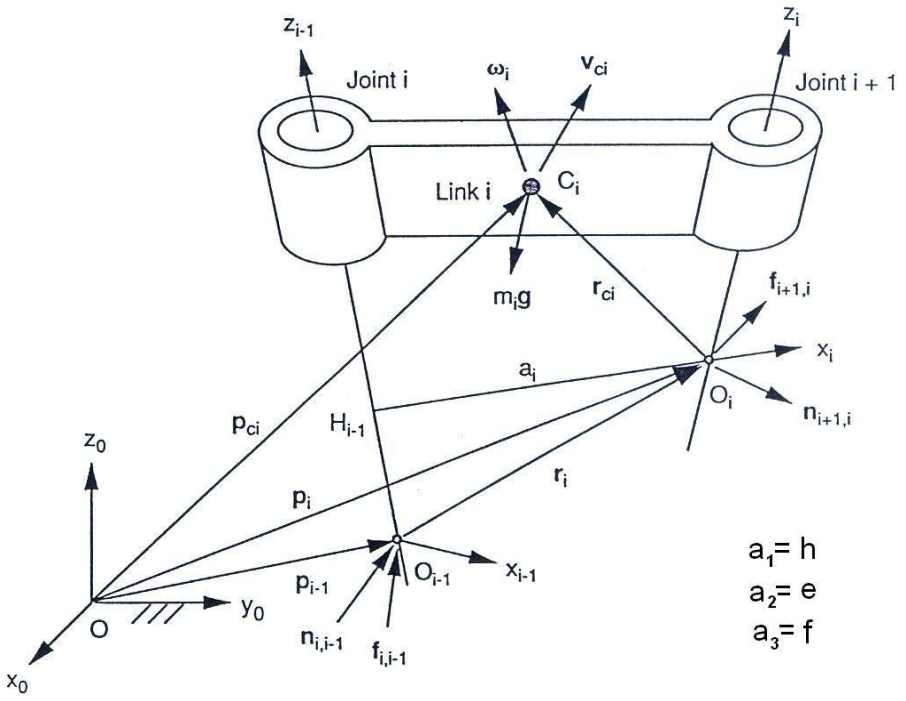

Fig. 6.1: Forces and moments exerted on link i.

6.2 FORWARD COMPUTATION

The angular velocity, angular acceleration, linear velocity and linear acceleration of each link are computed in terms of its preceding link. These velocities are computed in

a recursive manner, starting at the first moving link (Shoulder) and ending at the end-effector link (Gripper) for the dynamical analysis. The initial conditions for the base link are

$$v_1 = \dot{v}_1 = \omega_i = \dot{\omega}_i = 0.$$

6.2.1 Angular Velocity Propagation

Due to the serial construction of RPAR manipulator, the angular velocity of link i related to link $i-1$ is equal to $z_{i-1}\dot{\theta}_i$ or

$$\omega_i = \omega_{i-1} + z_{i-1}\dot{\theta}_i \tag{58}$$

Expressing Eq. (58) in the *i*th link frame, we obtain

$${}^{i}\omega_i = {}^{i}R_{i-1}\left({}^{i-1}\omega_{i-1} + {}^{i-1}z_{i-1}\dot{\theta}_i \right) \tag{59}$$

where

$${}^{i}R_{i-1} = \begin{bmatrix} c\theta_i & s\theta_i & 0 \\ -c\alpha_i s\theta_i & c\alpha_i c\theta_i & s\alpha_i \\ s\alpha_i s\theta_i & -s_i\alpha_i c\theta_i & c\alpha_i \end{bmatrix} \tag{60}$$

and ${}^{i-1}z_{i-1} = [0,0,1]^T$ is a unit vector pointing along the *i*th joint axis and expressed in the (*i-1*)th link coordinate system.

For the case of Shoulder and Elbow links of RPAR, $i = 2$ and 3 for considering only 2-DOF of RPAR for the dynamical analysis: as shown in Fig. 6.2.

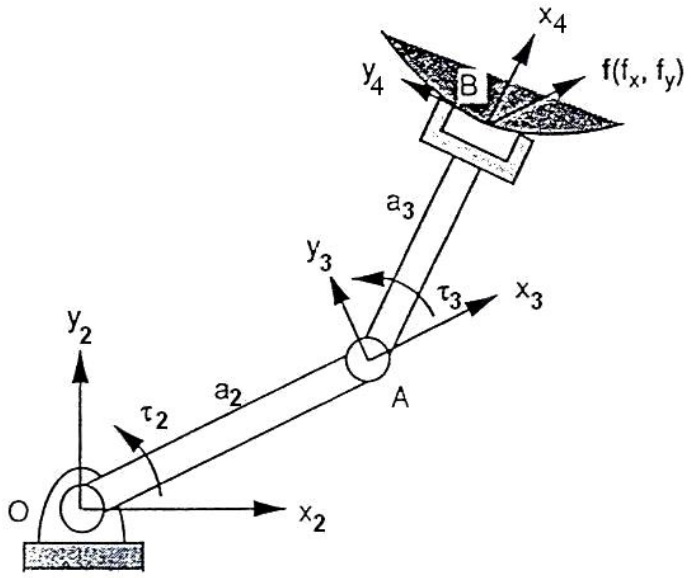

Fig. 6.2: Shoulder and Elbow links of RPAR

So,

$$ {}^{2}R_{1} = \begin{bmatrix} c\theta_2 & -s\theta_2 & 0 \\ s\theta_2 & c\theta_2 & 0 \\ 0 & 0 & 1 \end{bmatrix} \tag{61} $$

and

$$ {}^{3}R_{2} = \begin{bmatrix} c\theta_3 & -s\theta_3 & 0 \\ s\theta_3 & c\theta_3 & 0 \\ 0 & 0 & 1 \end{bmatrix} \tag{62} $$

So angular velocity of Shoulder is:

$$ {}^{2}\omega_{2} = {}^{2}R_{1}\left({}^{1}\omega_{1} + {}^{1}z_{1}\dot{\theta}_{2} \right) $$

Substituting the value of ${}^{1}\omega = 0_{1}$ in the above equation we get:

$$ {}^{2}\omega_{2} = \begin{bmatrix} 0 \\ 0 \\ \dot{\theta}_2 \end{bmatrix} \tag{63} $$

6.2.2 Angular Acceleration Propagation

The angular acceleration of link i is obtained by differentiating Eq. (58) with respect to time:

$$\dot{\omega}_i = \dot{\omega}_{i-1} + z_{i-1}\ddot{\theta}_i + \omega_{i-1} \times z_{i-1}\dot{\theta}_i \tag{64}$$

Expressing Eq. (64) in the ith link frame, we get

$${}^i\dot{\omega}_i = {}^iR_{i-1}\left({}^{i-1}\dot{\omega}_{i-1} + {}^{i-1}z_{i-1}\ddot{\theta}_i + {}^{i-1}\omega_{i-1} \times {}^{i-1}z_{i-1}\dot{\theta}_i \right) \tag{65}$$

Eq. (65) provides a recursive formula for computing the angular acceleration of link i in terms of link $i-1$.

So the angular acceleration for Shoulder is:

$${}^2\dot{\omega}_2 = {}^2R_1\left({}^1\dot{\omega}_1 + {}^1z_1\ddot{\theta}_2 + {}^1\omega_1 \times {}^1z_1\dot{\theta}_2 \right) \tag{66}$$

Putting the value of ${}^1\dot{\omega}_1 = 0$ and ${}^1\omega_1 = 0$ in the above equation we get:

$${}^2\dot{\omega}_2 = \begin{bmatrix} 0 \\ 0 \\ \ddot{\theta}_2 \end{bmatrix} \tag{67}$$

6.2.3 Linear Velocity Propagation

Referring to Fig. 6.1, the velocity of the origin O_i can be written in terms of O_{i-1} as follows:

$$v_i = v_{i-1} + \omega_i \times r_i \tag{68}$$

and Eq. (68) in the ith link frame as

$${}^iv_i = {}^iR_{i-1}v_{i-1} + {}^i\omega_i \times {}^ir_i \tag{69}$$

where

${}^{i}r_i = \begin{bmatrix} a_i \\ d_i s\alpha_i \\ d_i c\alpha_i \end{bmatrix}$ is a constant vector and for the RPAR this vector is:

$${}^{2}r_2 = \begin{bmatrix} e \\ 0 \\ 0 \end{bmatrix} \tag{70}$$

and

$${}^{3}r_3 = \begin{bmatrix} f \\ 0 \\ 0 \end{bmatrix} \tag{71}$$

6.2.4 Linear Acceleration Propagation

Linear acceleration of the origin O_i of frame i can be obtained by differentiating Eq. (71) with respect to time:

$$\dot{v}_i = \dot{v}_{i-1} + \dot{\omega}_i \times r_i + \omega_i \times (\omega_i \times r_i) \tag{72}$$

and Eq. (72) in the ith link frame as

$${}^{i}\dot{v}_i = {}^{i}R_{i-1}\,{}^{i-1}\dot{v}_{i-1} + {}^{i}\dot{\omega}_i \times {}^{i}r_i + {}^{i}\omega_i \times ({}^{i}\omega_i \times {}^{i}r_i) \tag{73}$$

Eq. (73) is a recursive formula for computing the linear acceleration of link i in terms of link $i-1$.

So, linear acceleration for Shoulder is:

$${}^{2}\dot{v}_2 = {}^{2}R_1\,{}^{1}\dot{v}_1 + {}^{2}\dot{\omega}_2 \times {}^{2}r_2 + {}^{2}\omega_2 \times ({}^{2}\omega_2 \times {}^{2}r_2) \tag{74}$$

Substituting the value of ${}^{1}\dot{v}_1, {}^{2}\dot{\omega}_2, {}^{2}r_2, and\ {}^{2}\omega_2$

$$ {}^{2}\dot{v}_2 = 0 + \begin{bmatrix} 0 \\ 0 \\ \ddot{\theta}_2 \end{bmatrix} \times \begin{bmatrix} e \\ 0 \\ 0 \end{bmatrix} + \begin{bmatrix} 0 \\ 0 \\ \dot{\theta}_2 \end{bmatrix} \times \left(\begin{bmatrix} 0 \\ 0 \\ \dot{\theta}_2 \end{bmatrix} \times \begin{bmatrix} e \\ 0 \\ 0 \end{bmatrix} \right) $$

or

$$ {}^{2}\dot{v}_2 = e \begin{bmatrix} -\dot{\theta}_2^3 \\ \ddot{\theta}_2 \\ 0 \end{bmatrix} \tag{75} $$

6.2.5 Linear Acceleration of the Center of Mass

The linear acceleration of the center of mass is computed by:

$$ {}^{i}\dot{v}_{ci} = {}^{i}\dot{v}_i + {}^{i}\dot{\omega}_i \times {}^{i}r_{ci} + {}^{i}\omega_i \times \left({}^{i}\omega_i \times {}^{i}r_{ci} \right) \tag{76} $$

and the linear acceleration of the center of mass of the Shoulder link is:

$$ {}^{2}\dot{v}_{c2} = {}^{2}\dot{v}_2 + {}^{2}\dot{\omega}_2 \times {}^{2}r_{c2} + {}^{2}\omega_2 \times \left({}^{2}\omega_2 \times {}^{2}r_{c2} \right) \tag{77} $$

Putting the values of ${}^{2}\dot{v}_2, {}^{2}\dot{\omega}_2, {}^{2}\omega_2$ and ${}^{2}r_{c2} = \begin{bmatrix} -e_c \\ 0 \\ 0 \end{bmatrix}$ in Eq. (77) gives

$$ {}^{2}\dot{v}_{c2} = e_c \begin{bmatrix} -\dot{\theta}_2^3 \\ \ddot{\theta}_2 \\ 0 \end{bmatrix} $$

where e_c is the position vector of the center of mass of Shoulder link and its value is 0.325 m. So;

$$ {}^{2}\dot{v}_{c2} = 0.325 \begin{bmatrix} -\dot{\theta}_2^3 \\ \ddot{\theta}_2 \\ 0 \end{bmatrix} \tag{78} $$

6.2.6 Acceleration of Gravity

Finally, the acceleration of gravity is transformed from the (*i-1*) link frame to the *i*th link frame is as follows:

$$ {}^{i}g = {}^{i}R_{i-1}\,{}^{i-1}g \tag{79} $$

And the acceleration of gravity expressed in the Shoulder frame is

$$ {}^{2}g = {}^{2}R_{1}\,{}^{1}g = \begin{bmatrix} -g_c s\theta_2 & -g_c c\theta_2 & 0 \end{bmatrix}^T \tag{80} $$

Similarly, for computing the velocities and accelerations of Elbow of RPAR, substituting the velocities and accelerations of Shoulder link into Eqs. (59), (65), (73) and (76), we obtain

$$ {}^{3}\omega_3 = \begin{bmatrix} 0 \\ 0 \\ \dot{\theta}_2 + \dot{\theta}_3 \end{bmatrix} \tag{81} $$

$$ {}^{3}\dot{\omega}_3 = \begin{bmatrix} 0 \\ 0 \\ \ddot{\theta}_2 + \ddot{\theta}_3 \end{bmatrix} \tag{82} $$

$$ {}^{3}\dot{v}_3 = \begin{bmatrix} e(\ddot{\theta}_2 s\theta_3 - \dot{\theta}_2^3 c\theta_3) - f(\dot{\theta}_2 + \dot{\theta}_3)^2 \\ e(\ddot{\theta}_2 c\theta_3 + \dot{\theta}_2^3 s\theta_3) + f(\ddot{\theta}_2 + \ddot{\theta}_3) \\ 0 \end{bmatrix} $$

or

$$ {}^{3}\dot{v}_3 = \begin{bmatrix} 0.46(\ddot{\theta}_2 s\theta_3 - \dot{\theta}_2^3 c\theta_3) - 0.764(\dot{\theta}_2 + \dot{\theta}_3)^2 \\ 0.46(\ddot{\theta}_2 c\theta_3 + \dot{\theta}_2^3 s\theta_3) + 0.764(\ddot{\theta}_2 + \ddot{\theta}_3) \\ 0 \end{bmatrix} \tag{83} $$

and

$$ {}^{3}\dot{v}_3^c = \begin{bmatrix} e(\ddot{\theta}_2 s\theta_3 - \dot{\theta}_2^3 c\theta_3) - f_C(\dot{\theta}_2 + \dot{\theta}_3)^2 \\ e(\ddot{\theta}_2 c\theta_3 + \dot{\theta}_2^3 s\theta_3) + f_C(\ddot{\theta}_2 + \ddot{\theta}_3) \\ 0 \end{bmatrix} \tag{84} $$

where f_c is the position vector of the center of mass of Elbow link and its value is 0.35 m. So;

$$ {}^{3}\dot{v}_3^c = \begin{bmatrix} 0.46(\ddot{\theta}_2 s\theta_3 - \dot{\theta}_2^3 c\theta_3) - 0.35(\dot{\theta}_2 + \dot{\theta}_3)^2 \\ 0.46(\ddot{\theta}_2 c\theta_3 + \dot{\theta}_2^3 s\theta_3) + 0.35(\ddot{\theta}_2 + \ddot{\theta}_3) \\ 0 \end{bmatrix} $$

The accelerations of gravity expressed in the Elbow link frame is

$$ {}^{3}g = {}^{3}R_2\, {}^{2}g = \begin{bmatrix} -g_c s\theta_{23} & -g_c c\theta_{23} & 0 \end{bmatrix}^T \tag{85} $$

6.3 BACKWARD COMPUTATION

After calculating velocities and accelerations of links, the joint forces can be computed of one link at a time starting from the end-effector link and ending at the base link.

A method given in literature (Tsai, Lung-Wen, 1991) is used to compute inertia force and inertia moment exerted at the center of mass of link *i*.

$$ {}^{i}f_i^* = -m_i\, {}^{i}\dot{v}_{ci} \tag{86} $$

$$ {}^{i}n_i^{*} = -{}^{i}I_i \, {}^{i}\dot{\omega}_i - {}^{i}\omega_i \times ({}^{i}I_i \, {}^{i}\omega_i) \tag{87} $$

Where I is a inertia matrix of a rectangular bar of cross section $a \times b$ and length c.

$$ I_i = \frac{m}{12}\begin{bmatrix} b^2 + c^2 & 0 & 0 \\ 0 & c^2 + a^2 & 0 \\ 0 & 0 & a^2 + b^2 \end{bmatrix} $$

For Shoulder the value of *a, b* and *c* are 0.05, 0.05 and 0.46 m, respectively, so inertia matrix for Shoulder is

$$ I_2 = \frac{3.7}{12}\begin{bmatrix} 0.21 & 0 & 0 \\ 0 & 0.21 & 0 \\ 0 & 0 & 0.005 \end{bmatrix} $$

Above matrix can be simplified as

$$ I_2 = 1.47\begin{bmatrix} 1 & 0 & 0 \\ 0 & 1 & 0 \\ 0 & 0 & 0.02 \end{bmatrix} \tag{88} $$

For Elbow the value of *a, b* and *c* are 0.038, 0.038 and 0.764 m respectively, so inertia matrix for Elbow is

$$ I_3 = 0.22\begin{bmatrix} 1 & 0 & 0 \\ 0 & 1 & 0 \\ 0 & 0 & 0.005 \end{bmatrix} \tag{89} $$

Referring to Fig. 6.1, the force and moment balance equations about the center of mass of link i can be written as:

$$ {}^{i}f_i^{*} + {}^{i}f_{i,i-1} - {}^{i}f_{i+1,i} + m_i \, {}^{i}g = 0 \tag{90} $$

$$ {}^{i}n_i^{*} + {}^{i}n_{i,i-1} - {}^{i}n_{i+1,i} - ({}^{i}r_i + {}^{i}r_{ci}) \times {}^{i}f_{i,i-1} + {}^{i}r_{ci} \times {}^{i}f_{i+1,i} = 0 \tag{91} $$

Writing the Eqs. (90) and (91) in recursive forms, we obtain

$$ {}^{i}f_{i,i-1} = {}^{i}f_{i+1,i} - m_i\ {}^{i}g - {}^{i}f_i^* \tag{92} $$

$$ {}^{i}n_{i,i-1} = {}^{i}n_{i+1,i} + ({}^{i}r_i + {}^{i}r_{ci}) \times {}^{i}f_{i,i-1} - {}^{i}r_{ci} \times {}^{i}f_{i+1,i} - {}^{i}n_i^* \tag{93} $$

After computing the reaction force and moment in the *i*th link frame, they are converted into the (*i-1*)th link frame by the following transformations:

$$ {}^{i-1}f_{i,i-1} = {}^{i-1}R_i\ {}^{i}f_{i,i-1}, \tag{94} $$

$$ {}^{i-1}n_{i,i-1} = {}^{i-1}R_i\ {}^{i}n_{i,i-1}, \tag{95} $$

Eqs. (92) through (95) can be used to solve for ${}^{i}f_{i,i-1}$ and ${}^{i}n_{i,i-1}$ recursively. Starting from the end-effector link. For the end-effector link, ${}^{n}f_{n+1,n}$ and ${}^{n}n_{n+1,n}$ represent the end-effector output force and moment and are consider as known.

For the backward computation of RPAR, forces exerted on Elbow are first computed and then Shoulder. Assuming that there are no externally applied forces, ${}^{3}f_{4,3} = {}^{3}n_{4,3} = 0.$ Substituting ${}^{3}f_{4,3} = {}^{3}n_{4,3} = 0$ along with velocities and accelerations of the Elbow link obtained from the forward computations into Eqs. (86), (87), (92) and (93) for $i = 3$, we obtain

$$ {}^{3}f_3^* = -m_3 \begin{bmatrix} e(\ddot{\theta}_2 s\theta_3 - \dot{\theta}_2^3 c\theta_3) - f_C(\dot{\theta}_2 + \dot{\theta}_3)^2 \\ e(\ddot{\theta}_2 c\theta_3 + \dot{\theta}_2^3 s\theta_3) + f_C(\ddot{\theta}_2 + \ddot{\theta}_3) \\ 0 \end{bmatrix} $$

or

$$ {}^{3}f_3^* = -1.55 \begin{bmatrix} 0.46(\ddot{\theta}_2 s\theta_3 - \dot{\theta}_2^3 c\theta_3) - 0.35(\dot{\theta}_2 + \dot{\theta}_3)^2 \\ 0.46(\ddot{\theta}_2 c\theta_3 + \dot{\theta}_2^3 s\theta_3) + 0.35(\ddot{\theta}_2 + \ddot{\theta}_3) \\ 0 \end{bmatrix} \tag{96} $$

$$ {}^3n_3^* = -\frac{m_3 f^2}{12}\begin{bmatrix} 0 \\ 0 \\ \ddot{\theta}_2 + \ddot{\theta}_3 \end{bmatrix} $$

or

$$ {}^3n_3^* = -0.07\begin{bmatrix} 0 \\ 0 \\ \ddot{\theta}_2 + \ddot{\theta}_3 \end{bmatrix} \tag{97} $$

$$ {}^3f_{3,2} = m_3\begin{bmatrix} e(\ddot{\theta}_2\, s\theta_3 - \dot{\theta}_2^3\, c\theta_3) - f_C(\dot{\theta}_2 + \dot{\theta}_3)^2 + g_c s\theta_{23} \\ e(\ddot{\theta}_2\, c\theta_3 + \dot{\theta}_2^3\, s\theta_3) + f_C(\ddot{\theta}_2 + \ddot{\theta}_3) + g_c s\theta_{23} \\ 0 \end{bmatrix} $$

or

$$ {}^3f_{3,2} = 1.55\begin{bmatrix} 0.46(\ddot{\theta}_2\, s\theta_3 - \dot{\theta}_2^3\, c\theta_3) - 0.35(\dot{\theta}_2 + \dot{\theta}_3)^2 + g_c s\theta_{23} \\ 0.46(\ddot{\theta}_2\, c\theta_3 + \dot{\theta}_2^3\, s\theta_3) + 0.35(\ddot{\theta}_2 + \ddot{\theta}_3) + g_c s\theta_{23} \\ 0 \end{bmatrix} \tag{98} $$

$$ {}^3n_{3,2} = \begin{bmatrix} 0 \\ 0 \\ \frac{1}{3}m_3 f^2(\ddot{\theta}_2 + \ddot{\theta}_3) + \frac{1}{2}m_3 ef(\ddot{\theta}_2\, c\theta_3 + \dot{\theta}_2^3\, s\theta_3) + \frac{1}{2}m_3 g_c fc\theta_{23} \end{bmatrix} $$

or

$$ {}^3n_{3,2} = \begin{bmatrix} 0 \\ 0 \\ 0.3(\ddot{\theta}_2 + \ddot{\theta}_3) + 0.27(\ddot{\theta}_2\, c\theta_3 + \dot{\theta}_2^3\, s\theta_3) + 0.59 g_c c\theta_{23} \end{bmatrix} \tag{99} $$

Substituting the foregoing forces and moments obtained for Elbow link along with the velocities and accelerations of Shoulder link into Eqs. (86), (87), (92) and (93) for $i = 2$ and making use of Eqs. (94) and (95), we obtain

$$ {}^{2}f_2^* = -\frac{m_2 e}{2}\begin{bmatrix} -\dot{\theta}_2^3 \\ \ddot{\theta}_2 \\ 0 \end{bmatrix} $$

or

$$ {}^{2}f_2^* = -0.85\begin{bmatrix} -\dot{\theta}_2^3 \\ \ddot{\theta}_2 \\ 0 \end{bmatrix} \tag{100} $$

$$ {}^{2}n_2^* = -\frac{m_2 e^2}{12}\begin{bmatrix} 0 \\ 0 \\ \ddot{\theta}_2 \end{bmatrix} $$

or

$$ {}^{2}n_2^* = -0.06\begin{bmatrix} 0 \\ 0 \\ \ddot{\theta}_2 \end{bmatrix} \tag{101} $$

$$ {}^{2}f_{2,1} = m_3\begin{bmatrix} m_3\left[-e\dot{\theta}_2^3 - \frac{1}{2}f(\dot{\theta}_2+\dot{\theta}_3)^2 c\theta_3 - \frac{1}{2}f(\ddot{\theta}_2-\ddot{\theta}_3)s\theta_3 + g_c s\theta_2\right] + m_2(-\frac{1}{2}e\dot{\theta}_2^3 + g_c s\theta_2) \\ m_3\left[e\ddot{\theta}_2 - \frac{1}{2}f(\dot{\theta}_2+\dot{\theta}_3)^2 s\theta_3 + \frac{1}{2}f(\ddot{\theta}_2-\ddot{\theta}_3)c\theta_3 + g_c s\theta_2\right] + m_2(\frac{1}{2}e\ddot{\theta}_2 + g_c c\theta_2) \\ 0 \end{bmatrix} $$

or

$$ {}^{2}f_{2,1} = 1.55\begin{bmatrix} 1.55\left[-0.46\dot{\theta}_2^3 - 0.38(\dot{\theta}_2+\dot{\theta}_3)^2 c\theta_3 - 0.38(\ddot{\theta}_2-\ddot{\theta}_3)s\theta_3 + g_c s\theta_2\right] + 3.7(-0.2\dot{\theta}_2^3 + g_c s\theta_2) \\ 1.55\left[0.46\ddot{\theta}_2 - 0.38(\dot{\theta}_2+\dot{\theta}_3)^2 s\theta_3 + 0.38(\ddot{\theta}_2-\ddot{\theta}_3)c\theta_3 + g_c s\theta_2\right] + 3.7(0.2\ddot{\theta}_2 + g_c c\theta_2) \\ 0 \end{bmatrix} \tag{102} $$

and

$$
{}^{2}n_{2,1} = \begin{bmatrix} 0 \\ 0 \\ (\frac{1}{3}m_2e^2 + \frac{1}{3}m_3f^2 + m_3e^2 + m_3efc\theta_3)\ddot{\theta}_2 + (\frac{1}{3}m_3f^2 + \frac{1}{2}m_3efc\theta_3)\ddot{\theta}_3 - m_3efs\theta_3(\dot{\theta}_2\dot{\theta}_3 + \frac{1}{2}\dot{\theta}_3^2) \\ +\frac{1}{2}m_2g_cec\theta_2 + m_3g_cec\theta_2 + \frac{1}{2}m_3g_cfc\theta_{23} \end{bmatrix}
$$

or

$$
{}^{2}n_{2,1} = \begin{bmatrix} 0 \\ 0 \\ 0.55(1.6 + c\theta_3)\ddot{\theta}_2 + 0.27(1.1 + c\theta_3)\ddot{\theta}_3 - 0.54s\theta_3(\dot{\theta}_2\dot{\theta}_3 + \frac{1}{2}\dot{\theta}_3^2) \\ +0.85g_cc\theta_2 + 0.71g_cc\theta_2 + 0.59g_cc\theta_{23} \end{bmatrix} \tag{103}
$$

6.3.1 Joint Torque Equations

Actuator torques or forces, τ_i, are obtained by projecting the forces of constraint onto their corresponding joint axes: that is,

$$
\tau_i = {}^{i-1}n_{i,i-1}^{T}\,{}^{i-1}z_{i-1} \tag{104}
$$

So the required joint torques of Shoulder and Elbow is computed using the above Eq.

$$
\tau_2 = \left[(\frac{1}{3}m_2 + m_3)e^2 + m_3efc\theta_3 + \frac{1}{3}m_3f^2)\right]\ddot{\theta}_2 + (\frac{1}{2}m_3efc\theta_3 + \frac{1}{3}m_3f^2)\ddot{\theta}_3
$$
$$
- m_3efs\theta_3(\dot{\theta}_2\dot{\theta}_3 + \frac{1}{2}\dot{\theta}_3^2) + g_c\left[(\frac{1}{2}m_2 + m_3)ec\theta_2 + \frac{1}{2}m_3fc\theta_{23}\right]
$$

or

$$
\tau_2 = 0.55(1.6 + c\theta_3)\ddot{\theta}_2 + 0.27(1.1 + c\theta_3)\ddot{\theta}_3 - 0.54s\theta_3(\dot{\theta}_2\dot{\theta}_3 + \frac{1}{2}\dot{\theta}_3^2) + 0.59[2.7c\theta_2 + c\theta_{23}]g_c \tag{105}
$$

Similarly

$$\tau_3 = \left[(\frac{1}{2} m_3 efc\theta_3 + \frac{1}{3} m_3 f^2) \ddot{\theta}_2 + \frac{1}{3} m_3 f^2 \ddot{\theta}_3 + \frac{1}{2} m_3 efs\theta_3 \dot{\theta}_2^2 + \frac{1}{2} m_3 g_c fc\theta_{23} \right]$$

or

$$\tau_3 = \left[0.27(1.1 + c\theta_3) \ddot{\theta}_2 + 0.30 \ddot{\theta}_3 + 0.27 s\theta_3 \dot{\theta}_2^2 + 0.59 g_c c\theta_{23} \right] \quad (106)$$

6.4 RESPONSE OF SHOULDER AND ELBOW TORQUES

The values of $\dot{\theta}_2, \dot{\theta}_3, \ddot{\theta}_2$ and $\ddot{\theta}_3$ are calculated from the empirical values tabulated in Figs. 5.7 & 5.8 and substituted in Eqs. (105) and (106). After putting these values, the variations of Shoulder and Elbow torques $(\tau_2 \,\&\, \tau_3)$ with different values θ_2 and θ_3 are given in Figs. 6.3 and 6.4. The torques verses angle is plotted without considering the payload.

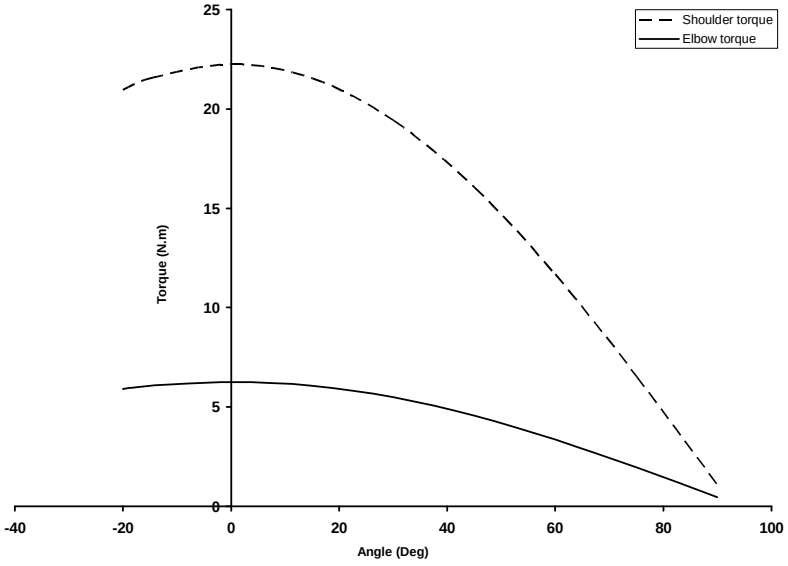

Fig.6.3: Variation of Shoulder and Elbow torques with Shoulder movement

Fig. 6.3 shows the variations of Shoulder and Elbow torques with different values of θ_2. The Shoulder and Elbow torques are maximum at 0° and decreases when the Shoulder moves up or down. The Elbow velocity ($\dot{\theta}_3$) and angle (θ_3) are set at 0°.

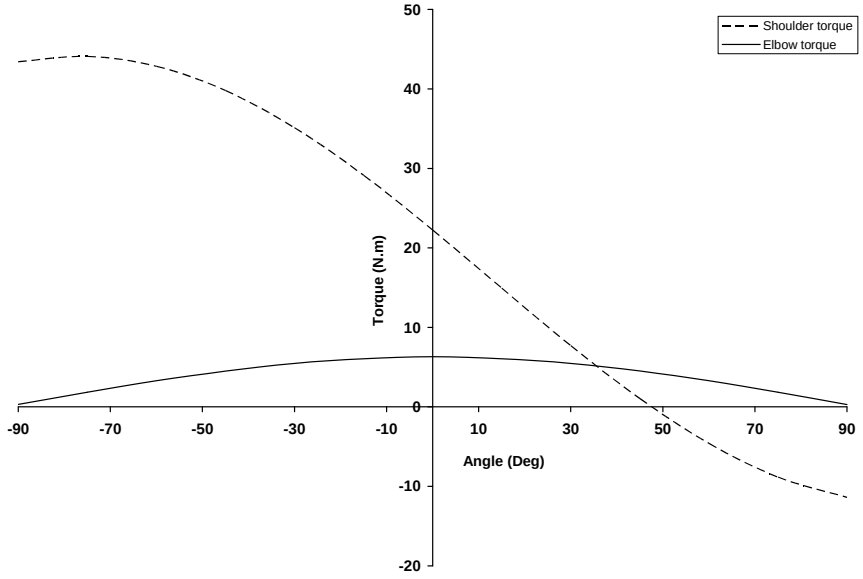

Fig.6.4: Variation of Shoulder and Elbow torque with Elbow movement

Fig. 6.4 shows the variations of Shoulder and Elbow torques with different values of θ_3. The Shoulder torque is maximum when Elbow angle or θ_3 is -90° and decreases when the Elbow moves up. The Elbow torque is maximum when θ_2 is 90° and decreases when the Elbow moves down. The Shoulder velocity ($\dot{\theta}_2$) and angle (θ_2) are set at 0°.

6.5 PAYLOAD CAPACITY OF RPAR

Payload capacity of RPAR was determined experimentally using a dummy load. The weight of the dummy load was increased gradually from 1.5 to 4.3 kg. The lifting ability of Shoulder, Elbow and gripping capacity of Gripper was tested with every

increased weight. It was observed that the Shoulder and Elbow can lift a maximum of 2.45 and 2.1 kg respectively, where as the Gripper can hold a maximum weight up to 4.3 kg. Therefore, the weight at which all the segments of RPAR work properly or the maximum payload capacity of RPAR is 2.1 kg.

6.6 VERIFICATION AND VALIDATION OF TORQUES RESPONSES

Shoulder and Elbow torques given by Eqs. (105) and (106) were validated by using different payloads. For a payload of 2.1 kg, variation of Shoulder and Elbow torques with Shoulder movement is shown in Fig. 6.5. Shoulder torque assumes maximum value of 47.25 N.m at $\theta_2 = 0$. Similarly, for a payload of 2.1 kg, the variation of Shoulder and Elbow torques with Elbow movement is shown in Fig. 6.6. Elbow torque reaches maximum value of 21.63 N.m at $\theta_3 = 0$. So, the maximum torques delivered to Shoulder and Elbow links are 47.25 and 21.63 N.m respectively.

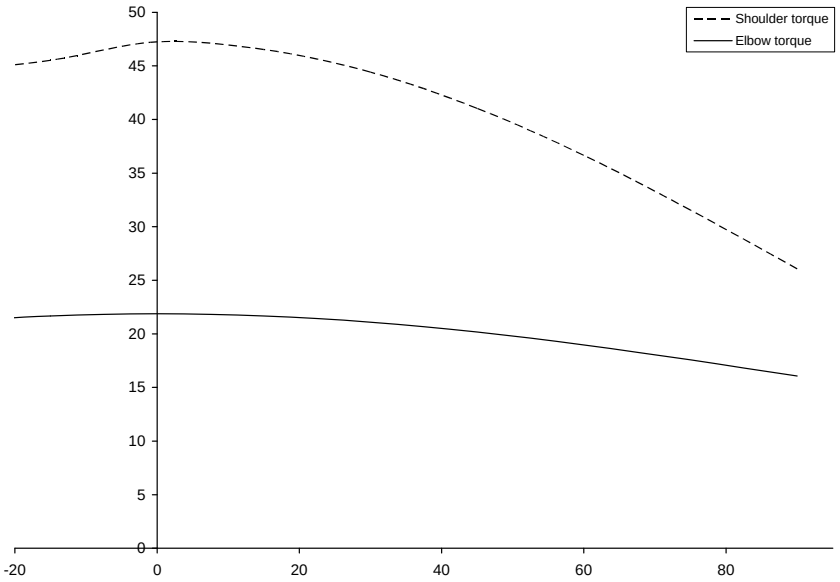

Fig.6.5: Variation of Shoulder and Elbow torques with Shoulder movement having a payload of 2.1 kg

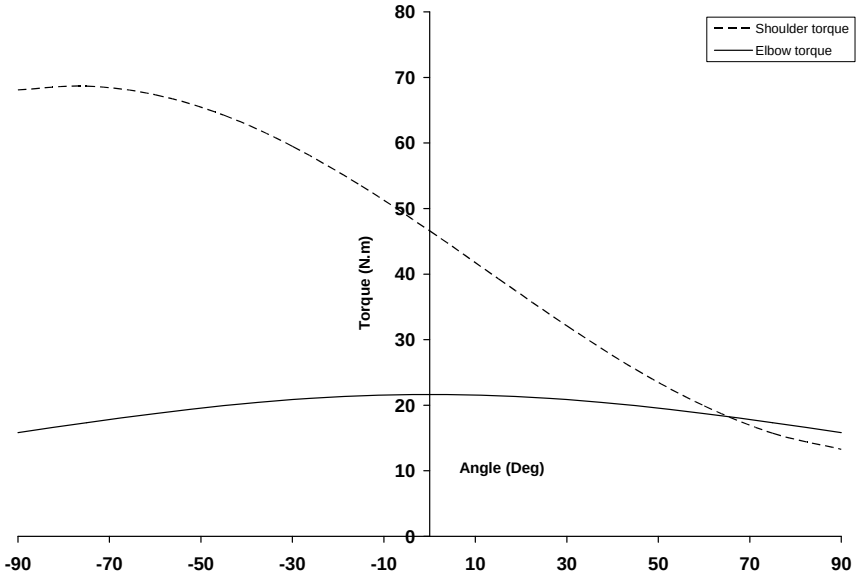

Fig.6.6: Variation of Shoulder and Elbow torques with Elbow movement having a payload of 2.1 kg

When the payload is increased up to 2.25 kg, the response of Shoulder and Elbow torques with Shoulder and Elbow movements are shown in Figs. 6.7 and 6.8. The maximum Shoulder stroke is -20° to 90°, whereas it lifted the payload from 30° to 90° only. Resultant Elbow torque is shown by solid line.

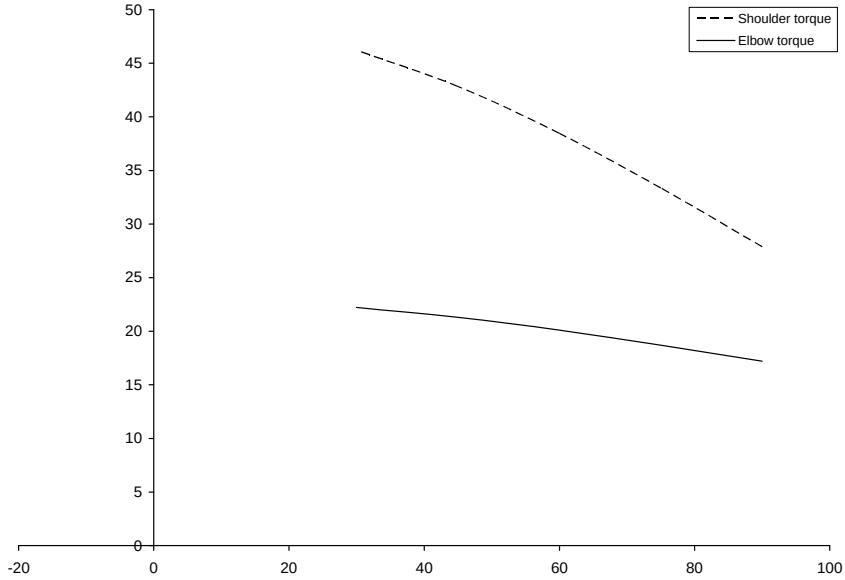

Fig.6.7: Variation of Shoulder and Elbow torques with Shoulder movement having a payload of 2.25 kg

Elbow lifted the payload of 2.25 kg from -90° to -45° and from 30° to 90° only as depicted in Fig. 6.8. The resultant Shoulder torque is shown by doted line.

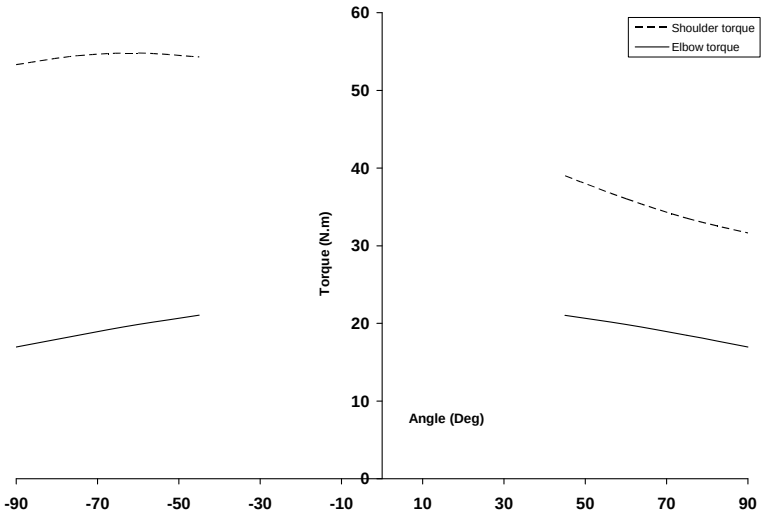

Fig.6.8: Variation of Shoulder and Elbow torques with Elbow movement having a payload of 2.25 kg

When the payload is increased up to 2.5 kg, the response of Shoulder and Elbow torques with Shoulder and Elbow movements are shown in Figs. 6.9 and 6.10. The Shoulder lifted the payload from 40° to 90° only. Resultant Elbow torque is shown by solid line.

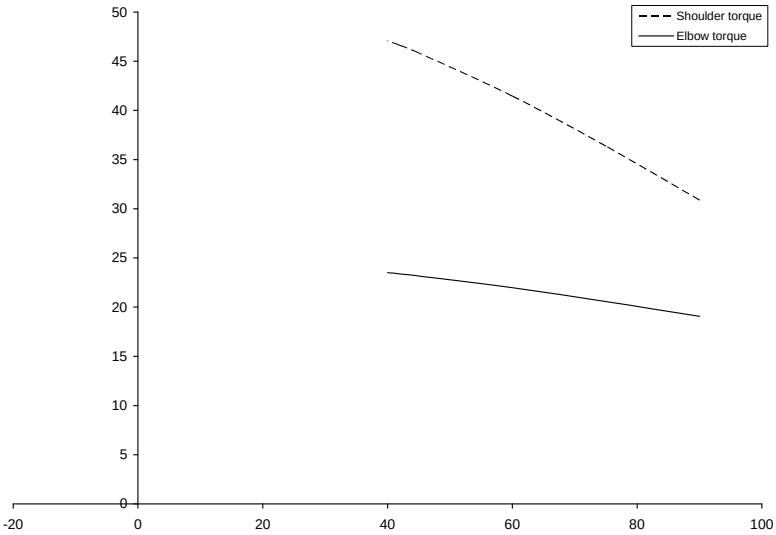

Fig.6.9: Variation of Shoulder and Elbow torques with Shoulder movement having a payload of 2.5 kg

The Elbow lifted the payload of 2.5 kg from -90° to -62° and from 60° to 90°. The resultant Shoulder torque is shown by doted line.

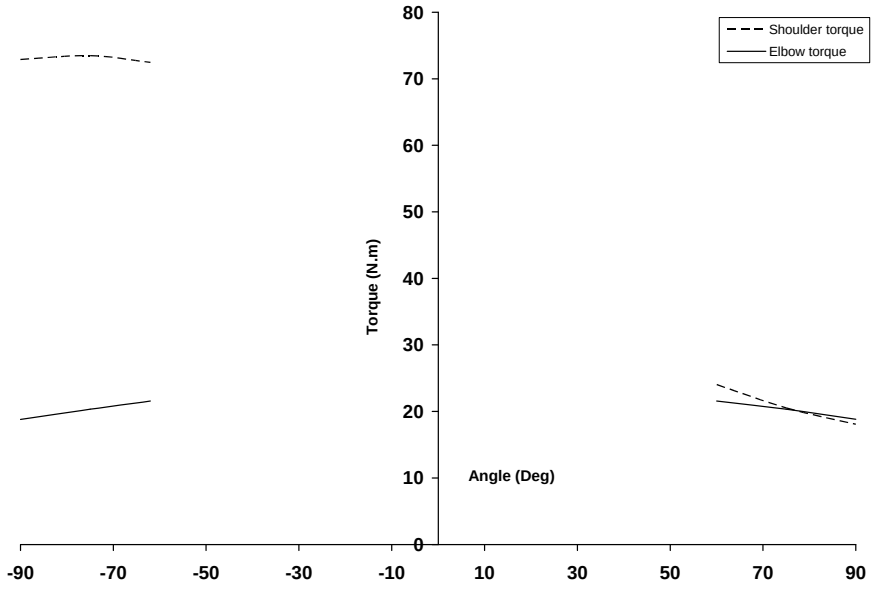

Fig.6.10: Variation of Shoulder and Elbow torques with Elbow movement having a payload of 2.5 kg

It is obvious from the aforementioned simulations and experimentation by using the dummy payloads that the maximum payload capacity of RPAR is 2.1 kg and if the payload is increased further, the RPAR segments (Shoulder and Elbow) unable to complete the maximum stroke.

6.7 CONCLUSION

This chapter presents the dynamics analysis of RPAR using the recursive Newton-Euler formulation. Only Shoulder and Elbow links of RPAR are analyzed for this study. The dynamics analysis provides the angular velocity, acceleration propagation, linear velocity, acceleration propagation, linear acceleration of the center of mass,

acceleration of gravity, inertia force and inertia moment exerted at the center of mass of Shoulder and Elbow links of RPAR. Behavior of torques or forces on the Shoulder and Elbow joints are simulated for different payloads and positions of Shoulder and Elbow links. The working of RPAR, validate and verify the simulation. The maximum payload capacity of RPAR was also determined.

CHAPTER

SEVEN

RADIATION EFFECTS ON ELECTRONICS AND ROBOTS

7.1 INTRODUCTION

Need of radiation hardening study became obvious in 1962 when the Telstar I satellite failed as a result of radiation in the Van Allen Belts (Peck 1963). Therefore, due to damaging effects of radiations, it is quite necessary to study the maximum radiation dose limit or stability tolerance of the electronic components. This limit is assumed as hardening limit of electronic circuitry. Finding this hardening limit is essential to determine the reliability and to get maximum performance of the devices.

This chapter presents brief summary of the radiation effects on the electronics and robotics as reported in the literature. The possible radiation sources are also discussed.

7.2 SOURCE OF RADIATION

The usage of digital circuits in space and aircraft applications revealed that cosmic rays and the radiation belt of protons and electrons, that surrounds each planet, are significant sources of Single Events Upsets (SEUs) (Johnston 2000). Before cosmic rays enter the Earth's atmosphere, they consist of about 89% protons, 10% α–particles and 1% heavier nuclei (Mckee et al; 1996). These particles reach energies of up to 10^{19}eV and have to be considered for space application design of electronic components. When these high energy particles under go collisions in the atmosphere, new particles such as high energy photons, electrons, protons, neutrons, muons, neutrinos and others are also created. The energies of these particles range from less than 1 eV to more then 10^{11} eV. For commercial aircraft applications, the high energy neutrons in the atmosphere are of higher interest than protons or heavy ions due to their greater penetrations. With the advent of smaller sizes of electronic components, the effects of cosmic rays are more and more corruptive.

Another source of radiations is the impurities in the package material of the chip (May and Woods; 1979). It contains uranium and thorium in part-per-million concentration. These materials are α–particle emitter. As the size of transistors and memory cells decreases, the effect/damage caused by α–particles emitted by packaging material becomes more important even for standard commercial applications.

Beside these above mentioned sources, radiation also originates from nuclear reactors, X-ray machines and particle accelerators. Finally, for military applications nuclear weapons have to be taken into account as they emit gamma and neutron radiation.

7.3 RADIATION INTERACTIONS

The primary ways in which the basic particles such as photons, electrons, neutrons, protons, high energy heavy ions and cosmic rays interact with matter are; (1) through the excitation of atomic electrons in matter which is commonly referred to as atomic or electronic excitation processes, (2) through nuclear interactions such as nuclear excitation, nuclear scattering (i.e., elastic or inelastic) and nuclear reactions, and (3) the breaking of chemical bonds in material via electronic excitation and/or nuclear reactions. The electrically charged particles (i.e. electrons, protons and high-energy heavy ions) have a much more probability of interaction with matter than do the neutral particles i.e. photons x-ray and γ-rays and neutrons. Indeed these latter particles must first create an energetic secondary charged particle i.e., an electron or a displaced lattice atom with sufficient kinetic energy to be stripped of its outer atomic electrons in order to ionize the material.

The unit primarily used in radiation effects that deal with ionization induced by γ–rays is *rad*. A rad is the amount of radiation which deposits 100 ergs of energy per gram of material. When dealing with particle radiation (protons, electrons, ions, α–particles and neutrons) the units are flux (number/cm^2.s) and fluence (number/cm^2).

The interaction probability for these processes is usually expressed in terms of an attenuation coefficient, μ, or the so-called "cross sections" for a given type of interaction. In the case where a cross section is used, the interaction (also called reaction) rate is given by

$$IR = RR = \left(\frac{\rho . N_A}{A} \right) \sigma_I \phi \qquad (107)$$

Where R R is the reaction rate (reactions per cm^3.s), N_A is Avagdro's Number, A is the atomic mass of the target atom/nucleus, ρ is the density, σ_I is the cross section for the given interaction and ϕ is the incident particle flux.

In the case of photons, the attenuation coefficient formalism is used. In this approach, the uncollided (no interaction) flux at a depth of penetration x, into a semi-infinite slab, is given by

$$\phi = \phi_o e^{-\mu x} \tag{108}$$

Where μ is the attenuation coefficient (sometimes the mass absorption coefficient, μ/ρ, is used in which case the depth of penetration is alternatively called aerial density and is ρx in units of gram/cm^2), x is the depth of penetration and ϕ_o is the incident flux (particles per cm^2.s).

7.3.1 Photons (x-ray and γ-rays) Attenuation

There are three primary processes that contribute to the attenuation of a photon beam in any material. These are (1) photoelectric absorption where an atom absorbs a photon, which leads to the emission of a photoelectron, (2) Compton scattering where the incident photon undergoes a scattering event with an atomic electron and (3) pair production where the incident photon produces a pair (i.e., an electron and a positron). This is a threshold reaction and interaction takes places at E >1.02 MeV. All the three process are E and Z dependent.

7.3.2 Energy Loss of Electrons and Protons in a Material

When protons and electrons pass though matter, they loss energy. For these particles in literature the term stopping power is used. It is denoted by dE/dx, and is a function of particle energy. From this type of data it is relatively straight forward, in the case of protons, to obtain the energy transfer at a depth of penetration. The proton stopping power consists of two contributions; that due to electronic excitations (This contribution is dominant at all but the lowest energies) and that due to nuclear interactions (i.e., nuclear reactions and elastic and inelastic scattering), which is dominant only at the lowest energies (i.e., at the end of the proton range) (Bennett and Posey; 1997).

The situation for electrons is much more complex due to large-angle scattering that they undergo when they interact with the atoms of a material. The energy deposition as a function of depth of penetration, normally called the depth-dose curve, increases quickly just inside the front surface of the material; peaks at a depth of about a third of the range, and then monotonically decreases until straggling sets in at the so-called extrapolated range.

7.3.3 Heavy Charged Particle Interactions

Heavy charged particles and protons can undergo nuclear reactions with lattice atoms. In almost all cases of potential robotic applications these reactions are not of practical significance. However, heavy charged particles, and to a lesser degree protons, can produce Single Event Effects (SEE) in silicon ICs. The heavy charged particles produce very high specific ionization track as they pass through the silicon. In some cases, the charge produced in the track and adjacent regions (i.e., if the minority carrier lifetime is long enough to collect this charge prior to recombination) is sufficient to change the charge state of a node within an IC. This causes an upset of the IC with the possibility of

improper functional operation. There is also the possibility of single event induced latch up in an IC or single event burnout. These processes would only be important for a space robotic system (Gossett et al; 1993). Neutrons have also been shown to be capable of producing both soft and hard errors in ICs by recoiling of a heavy nucleus (Fig. 7.1) (Mckee et al; 1996).

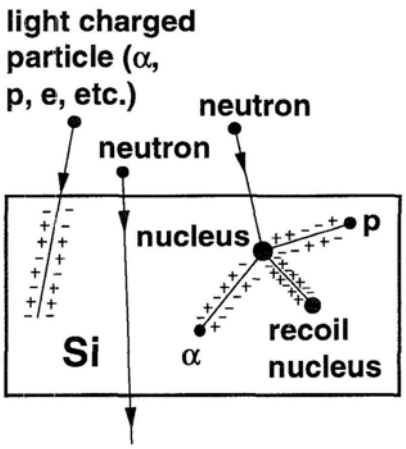

Fig. 7.1: Strikes of different particles on silicon which results in the creation of electron-hole pairs.

7.3.4 Neutron and Proton Displacement Damage

Neutrons and protons near the end of their range have a moderate-to-high probability of interacting with lattice atoms of a material and displacing them from their equilibrium position in the lattice structure to an interstitial location. In general, this creates an electrically active defect site; whether it is the interstitial site or the vacant lattice site left behind. These electrically active sites, often called defect sites, can produce changes in the electrical properties of metals, semiconductors, and insulators (Marshall et al; 1989).

Displacement-damage effects are cumulative effects and begin to be seen for fluences of about 10^{10} protons/cm^2 – about 6000 rad (Si) for 200 MeV protons and become more significant as the fluences increase. They may be important for devices to be used in more benign space radiation environments and definitely are important when exposed to harsher space, military and high-energy-physics radiation environments. Displacement damage effects are also a concern when performing SEU tests, as the repetitive measurements required to determine single-event cross sections may lead to cumulative displacement damage. The ionizing stopping powers for protons are too small to cause single-event upsets in all but the most sensitive devices, particularly at high proton energies. Neutrons have no charge, so there is no Coulomb elastic scattering. Therefore, at high energies, both displacement damage and single-event effects for protons and neutrons come from nuclear elastic and inelastic scattering processes. Only about 10% of the energy imparted by 200-MeV protons to recoiling nuclei by these processes goes to displacement damage. The remaining 90% goes into ionization and may lead to single-event upsets. (Charles 2003).

7.4 RADIATION EFFECTS

For the vast majority of robotic systems, the primary radiation driver is that of Total Ionizing Dose (TID), which refers to the amount of energy that ionization processes create and deposit in a material (such as semiconductor or insulator), when energized particles pass through it, causing ionization. This is especially true for systems based upon MOS-technology devices, although some bipolar ICs are sensitive to TID, especially for low dose rate (i.e., < 1 rad [Si]/s) situations. The effects on silicon can be transient as well as permanent in nature. Space robotic systems are an example of alternative applications

where displacement damage in bipolar devices and SEE in MOS-type devices may also be of practical importance (Bennett and Posey; 1997).

7.4.1 Total Dose Effects

The energy deposition giving rise to Total Ionizing Dose (TID) effects can be produced by photons, neutrons, electrons, protons, and high-energy heavy ions, although the most important of these for robotic applications are the photons. In most cases these are the gamma-rays emitted by radionuclides such as the fission products present in spent reactor fuel etc.

TID effects are also cumulative effects and occur in the dose range of 10^4–10^8 rad (Si). They are important considerations for exposure of semiconductor devices to harsh radiation environments such as those found in military and high-energy-physics applications. The ionizing stopping power is the basis of TID effects, which lead to the formation of oxide traps, interface traps, border traps, and device malfunction. (Charles 2003).

Ionization produces electron-hole pairs within insulators and semiconductors. The effect of the ionization on MOS devices depends upon the way that this charge is transported and trapped at the silicon-silicon dioxide interface. The net effect of ionizing radiation on MOS device oxides depends upon the oxide thickness, the field applied to the oxide during and after exposure, as well as trapping and recombination within the oxide. The manufacturing and processing techniques strongly affect the latter factor.

These TID effects can be time dependent due to the competing kinetics of the damage produced by the dose and the annealing of this damage. These time dependent effects can make for a very complex response for many modern ICs. An example of this

for MOS-type ICs is shown in Fig. 7.2 where the failure dose is presented as a function of dose rate.

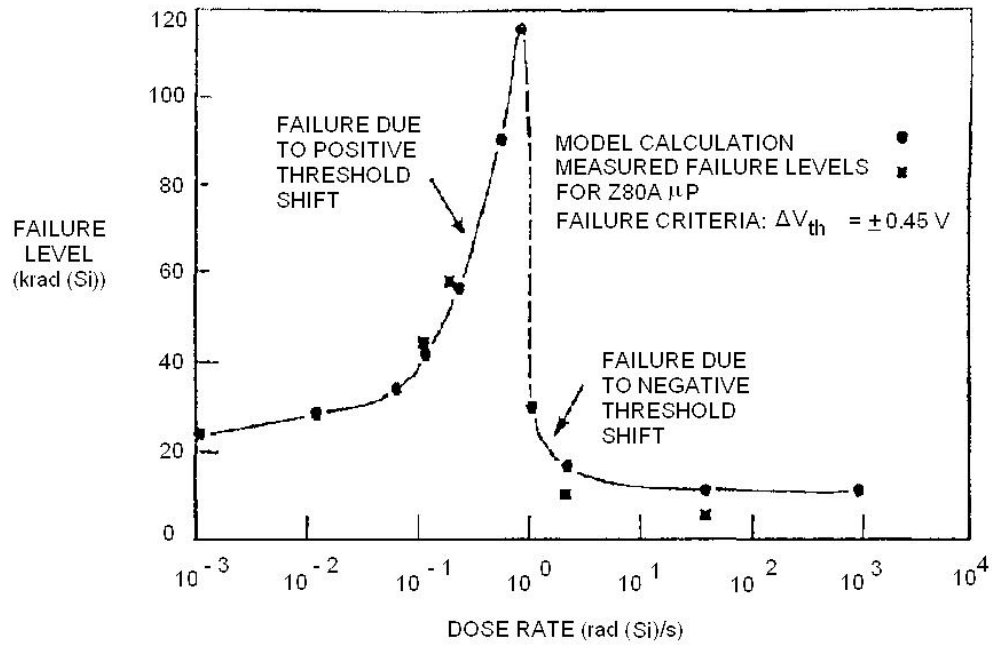

Fig. 7.2: IC Failure Level Dependency on Dose Rate (Johnston 1984).

Fig. 7.3 presents the threshold voltage shift as a function of dose for four different dose rates. These two figures give an indication of the complexity for such device types.

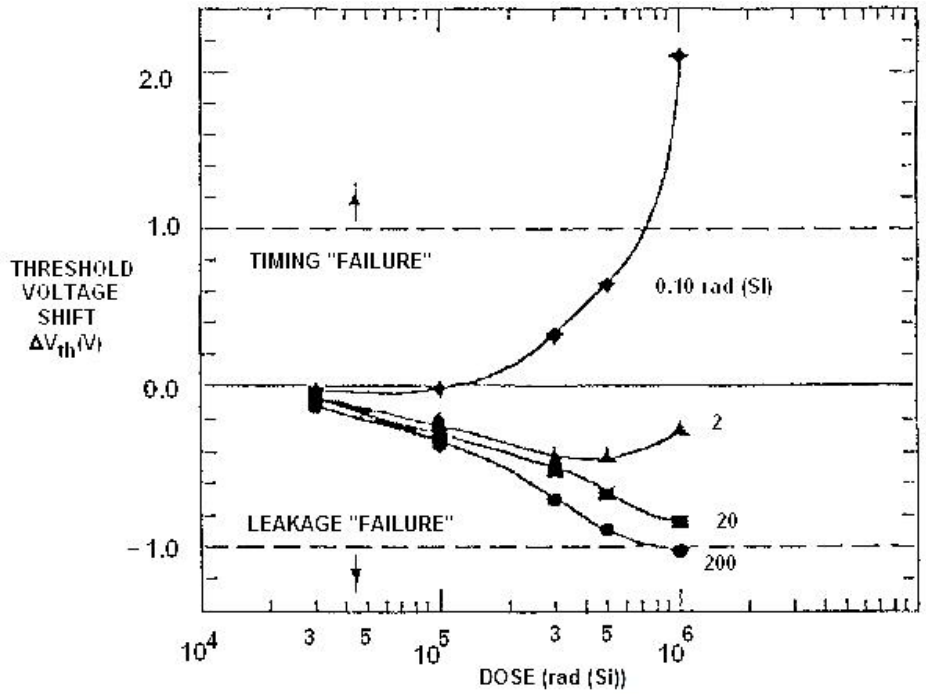

Fig. 7.3: Threshold-Voltage Shift vs. Dose at Varying Dose Rates (Winokur et. Al; 1986).

7.4.2 Dose Rate Effects

At low dose rate (i.e., much less than 1 x 10^3 rad[Si]/s) the kinetics of the damage, and subsequent annealing processes can lead to a very complex response. At higher dose rate (well above 1 x 10^6 rad[Si]/s) the primary response of interest is the upset of ICs with the possibility of device burnout at very high dose rates (i.e., greater than 1 x 10^{11} rad[Si]/s).

7.4.3 Neutron Fluence Effects

The properties of semiconductors that are the most sensitive to displacement damage are (a) the minority carrier lifetime of the material and (b) the mobility of the majority carriers. This latter property is also important for metals. Displacement damage, produced by neutron, leads to a decrease in the minority carrier lifetime and to a decrease in the mobility of both majority and minority carriers. Significantly more damage is

required to produce the mobility changes. Permanent radiation damage makes n-type material tend towards p-type and makes p-type material become higher resistivity p-type.

7.4.4 Single Event Effects (SEE)

Except for the applications of robotics in space, SEE are of only minor importance for the vast majority of robotic applications (Bennett and Posey; 1997). In the absence of protons and high-energy heavy ions, effects of this type can only be produced by neutrons. Although it was thought that high energy neutrons were required, the experimental data has shown that the epi-thermal neutrons can also be reasonably effective in producing SEE (Luera 1993). This has been attributed to certain types of impurities used to obtain n- and p-type doping. However, relatively high neutron fluences are required so that it should not be of practical concern for most robotic systems and applications. In spite of this low probability, the possibility of the existence of neutron-induced SEE should be addressed for radiation environments with a neutron component.

7.5 RADIATION SENSITIVITY OF ROBOTIC COMPONENTS

Radiation sensitivity of robotic system falls into the categories of (a) electronic components, (b) sensors and (c) material and miscellaneous components. The radiation vulnerability of electronic components (i.e., electronic subsystems, individual circuits, etc.) can be quantitatively assessed by considering the response of the constituent parts to the primary radiation effects. The incident radiation produces an effect in the materials comprising an electronic part. These effects are (1) Total Ionizing Dose (TID) produced by all the ionizing particle types, (2) neutron and/or proton induced displacement damage (gamma's and electrons can also produce displacement damage but not to the extent of the heavier particles and this damage is more readily anneals out) (Anouar et al; 1999) which

can be important for space and possibly fusion applications and (3) Single Event Effects (SEE), which can be produced by high-energy neutrons and space radiations.

7.5.1 Electronic Component

The electronic components or piece parts that are the most susceptible to radiation effects are the semiconductors, the semi-insulators and, in some cases, the insulators. The most important of these are the silicon family of piece parts. This large family can be divided into commercial (non-hardened) and hardened categories. Autonomous robotic systems must use the more sophisticated piece parts in order to satisfy their functional requirements, whereas manually controlled manipulator arms can get it by using less sophisticated part types. The radiation hardness of electronic piece parts depends upon the technology, fabrication process and function, and complexity of the part type. With the development of smaller process technology and higher performance, systems become increasingly sensitive to smaller amounts of radiations. Commercial (non-hardened) parts are generally more sensitive to radiation effects although some can be as hard as "hardened" parts of another technology. For robotic systems, the most important radiation effect is Total Ionizing Dose (TID), although displacement damage is also of importance for the space and possibly for the fusion applications. Single Event Effects (SEE) can also be important in the space environment.

7.5.2 Sensors

In many cases sensors are the part of the system most sensitive to radiation effects. In general this results from the fact that optical parts are designed to exhibit a reasonable response to low levels of incident radiation (i.e., infrared through visible into the ultraviolet and very low-energy X-ray regions). This category has a great deal of overlap with the

category of electronic components since many sensors include electronic piece parts; indeed some contain silicon sensing electronics such as the CCD chips of video cameras. On the other hand there are very radiation resistant sensors such as the electrostatic version of an ultrasonic rangefinder, which does not contain any semiconducting materials.

7.5.3 Materials and Miscellaneous Components

The final category contains materials from metals to insulators (e.g., kapton, polyethylene, etc.) and other non-semiconductor based electronic and electromechanical components such as servo-motors (AC and DC), batteries and many other items. Items included in this category are generally much harder than those in the previous two categories with possible exception of fiber-optic materials/components. The hardened version of these materials exhibits a greater radiation resistance than most of the radiation hardened semiconductor piece parts and/or sensors. Some effects of gamma radiation in commonly used materials are listed in Table 7.1.

Table 7.1: Effects of gamma radiation to commonly used materials.

Material		**Threshold Level (Gy)**	**Effect**
Ceramics	(mica)	5×10^7	Dimensional swelling and decrease in density
	(alumina)	5×10^{10}	
Plastics	(Teflon)	100	Cracking, blistering and embitterment.
Coatings	(vinyl on aluminum)	2.1×10^6	Cracking, blistering and surface flaking
	(styrene on steel)	8.7×10^6	
Adhesives	(neoprene-phenolic)	1×10^6	Damages the chemicals in adhesive & decreases the number of adhesive bonds
	(epoxy)	5×10^6	
Glass	(quartz)	1×10^7	Darkening
Magnets	(soft magnets)	1×10^6	Decrease in magnetic strength
Semiconductors	(Silicon)	1×10^4	Displacement damage, Increased leakage current
Resistors	(carbon film)	$10^4 – 10^7$	Chemical degradation causing a decrease in resistance.

7.6 CONCLUSIONS

The radiation sources and effects of radiations on various components used to manufacture robots have been reviewed. It is learnt that gamma rays, beta particles, neutrons and heavy charged particles such as protons and alpha particles are emitted from radioactive materials. Of these gamma rays, which are photons with very short wavelength, pose the greatest threat to electrical and electronic components onboard robots. Gamma radiation is capable of traveling many meters in air and readily penetrates most material, earning itself the name "penetrating radiation". Gamma rays have a very destructive effect on a number of materials used to build robots. Electrical parts such as transformers, motors, thermocouples, relays and circuit boards, which form vital components of a robot, may be severely damaged from exposure to gamma radiation. Houssay (2000) has detailed the effects of gamma rays and has referred tables with threshold values for various materials that are used in robotic systems. The effect of radiation from gamma rays is increased for long exposure time with close proximity to its source distance and the intensity of the source (quantity).

It is also learnt that the effects produce are function of dose rate, however, the TID is most important. It is therefore essential that a robot designed to work in radiation environment must be tested for vulnerability against radiations for TID.

CHAPTER

EIGHT

RADIATION HARDENING STUDY OF RPAR

8.1 INTRODUCTION

The RPAR was designed to work in low to moderate level ionization radiation field with total ionizing dose $\leq$ 9 Sv (900 rad). The damaging effects of radiation, as discussed in previous chapter compelled us to make it radiation hardened and study the stability tolerance of the electronic modules. These modules of RPAR are fabricated with commercial (non-hardened) components (given in Tables 3.1 & 3.2) mainly due to non-availability of hardened components in local market and cost effectiveness.

There are a few commercial components that can be as hard as "hardened" components such as relays. The relays have radiation hardness of the order of >500 krad (Vandegriff 1990). Therefore, relays were used to develop the RPAR as a radiation

hardened robot. The differential wheel assembly of RPAR is controlled by two RLMs or four relays. So that, in case of radiation damage to the control of articulated arm, the RPAR can be retrieved from the radiation field with the help of these relays. Also a 0.5 mm Lead jacket filled with mineral oil was used around the main electronic control of RPAR to minimize the damaging effects of radiation and to make it more reliable in ionizing radiation environments.

In order to assess the stability and performance of Radiation Protection Assistant Robot in medium level of ionizing radiation environments, radiation hardening study was carried out. This study determined the radiation hardening limit i.e. the integrated dose at which the RPAR can perform its tasks reliably and can be retrieved safely before it stuck due to radiation damage. This is essential to make sure that the RPAR is functioning within design specifications.

8.2 EXPERIMENTAL SETUP

The radiation hardening study of the developed RPAR was carried out at the Secondary Standard Dosimetry Laboratory (SSDL) of Health Physics Division, Pakistan Institute of Nuclear Science and Technology (PINSTECH), Islamabad, Pakistan. The laboratory is equipped with pneumatically controlled gamma ray sources. The irradiation and re-irradiation of modules can be controlled from a control room. It also contains two cross intersecting laser beams. The first laser beam is fixed on the wall, facing the gamma ray source and points directly into the centre of the gamma ray source. This beam is used to position the H-Bridge Module (HBM) in the center of radiation beam. The second laser beam intersecting the first beam at right angle is fixed on the side wall at a distance of 100 cm from the radiation source. After adjusting the HBM at 50 cm from the radiation source by moving the trolley towards the source, with the help of a telescope and the scale fixed

on the wall facing the laser beam 2, the HBM is placed at 50 cm from the radiation source (29 TBq, Cobalt-60) to get the maximum exposure. The Schematic diagram of the irradiation set up at SSDL is shown in Fig. 8.1.

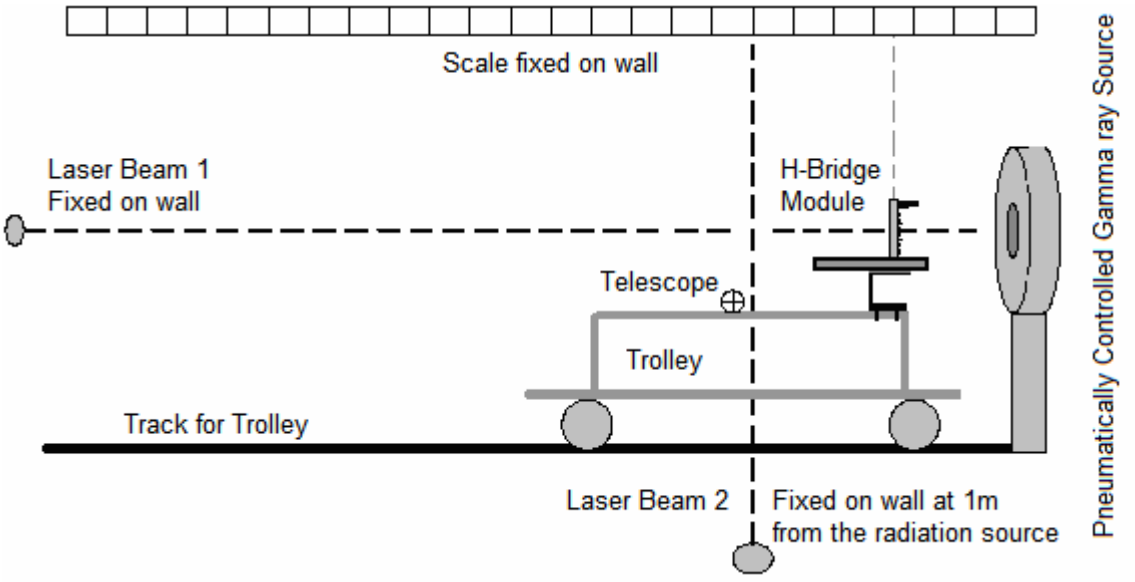

Fig. 8.1: Schematic irradiation set up at SSDL.

8.3 PROCEDURE FOR EXPOSURE

This experimental setup comprised of a 12 V DC power supply, geared motor. A multimeter was connected to observe the current behavior of the module during gamma radiation exposure. Shutter of the unit were opened completely so that the whole module got exposure as shown in Fig. 8.2. The dose rate on the module was 8.2695 mSv/s. The current was measured after every ten seconds. The total integrated dose was increasing by 82.695 mSv after ten seconds. The card was exposed for about 20 minutes in which it received a Total Ionizing Dose (TID) of about 10 Sv. This experiment was repeated with

other HBM and five RLMs. The current behavior responses of different modules in the radiation field are shown in Figures 8.3 to 8.9.

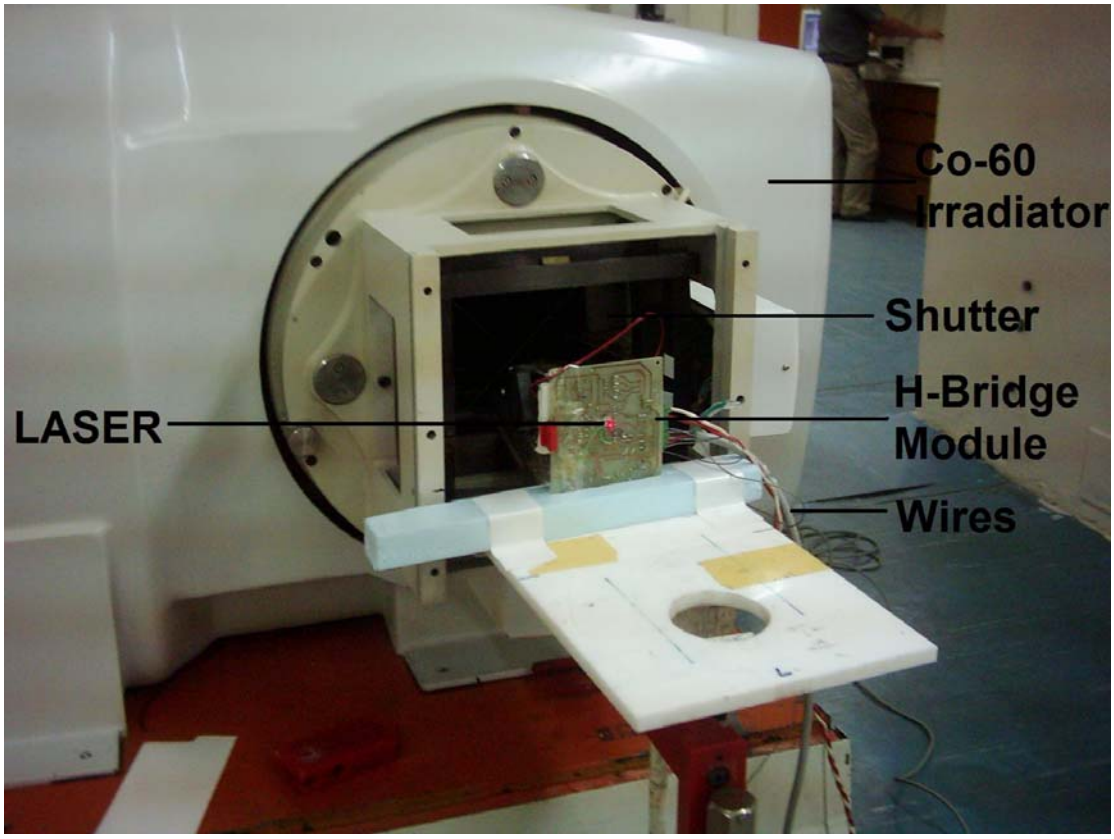

Fig. 8.2: Irradiation of HBM at SSDL, Health Physics Division, PINSTECH.

8.4 RESULT AND DISCUSSION

Fig. 8.3 shows the response of RLM of Gripper driving mechanism during irradiation. The current was monitored while the dose was increased up to 9.5 Sv. It is clear from this figure that there are no significant variations in current except for random variation, which is also negligible. The current is passing through the metallic contacts of relay and the integrated dose has not affected the contacts of metallic relay.

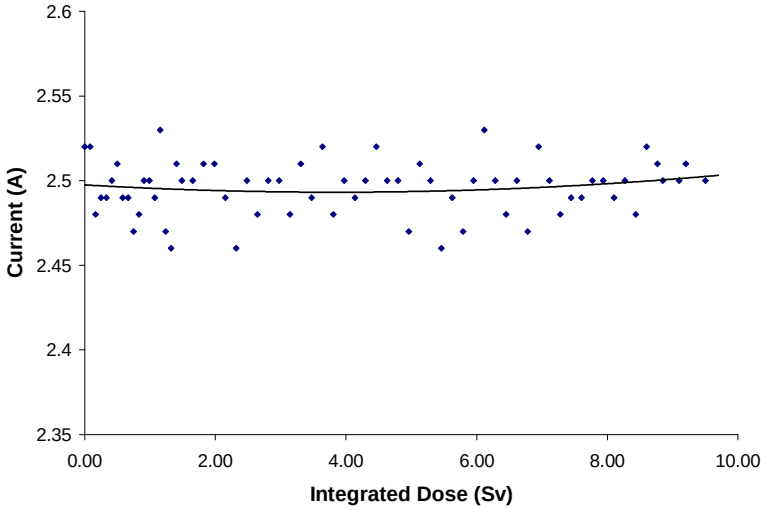

Fig. 8.3: Current behavior of Gripper's RLM with the integrated dose.

Fig. 8.4 shows the current response of HBM of Wrist as a function of integrated dose. The current increased from 2.37 to 2.47 A, when dose was increases to 9.1 Sv. There is a slight rise in final motor current. This rise comes to steady state and does not effect the normal operation of RPAR. This may be due to rise in temperature of the chip or production of free ions due to dose. Therefore, at dose up to 9.1 Sv, the module is working satisfactorily.

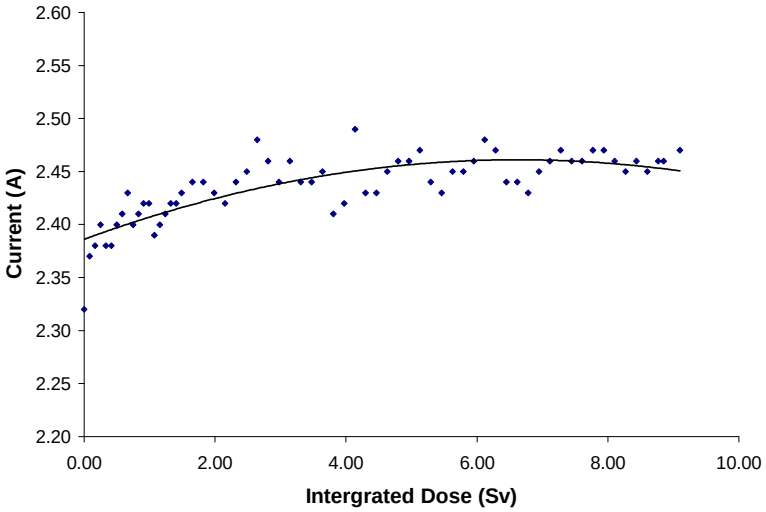

Fig. 8.4: Current behavior of Wrist's HBM with the integrated dose.

Fig. 8.5 shows the current response of Elbow's HBM as a function of integrated dose. The current increased from 2.4 to 2.51 A with TID up to 8.85 Sv. Final motor current is slightly greater than the initial motor current. This may be due to free ions produced due to irradiation or rise in temperature of the chip. The behavior of HBM of Wrist and Elbow are similar and these modules are working satisfactorily in the TID studied in this work, i.e. ~ 9 Sv.

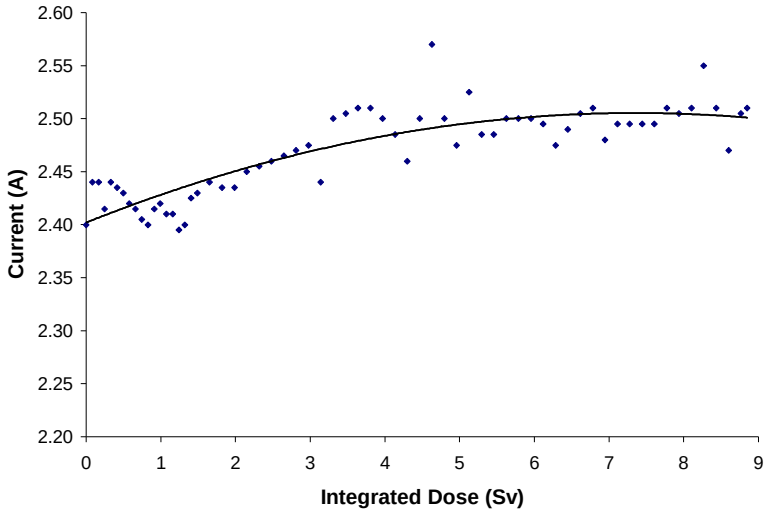

Fig. 8.5: Current behavior of Elbow's HBM with the integrated dose.

Fig. 8.6 shows the response of Relay Logic Module of Shoulder driving mechanism of Radiation Protection Assistant Robot. There was not variation in current and its average remained 2.46 A. The behavior of module is similar to other Relay Logic Modules. i.e. there is not any significant change in initial and final currents during irradiation. This module was exposed up to a total integrated dose of 9.2 Sv.

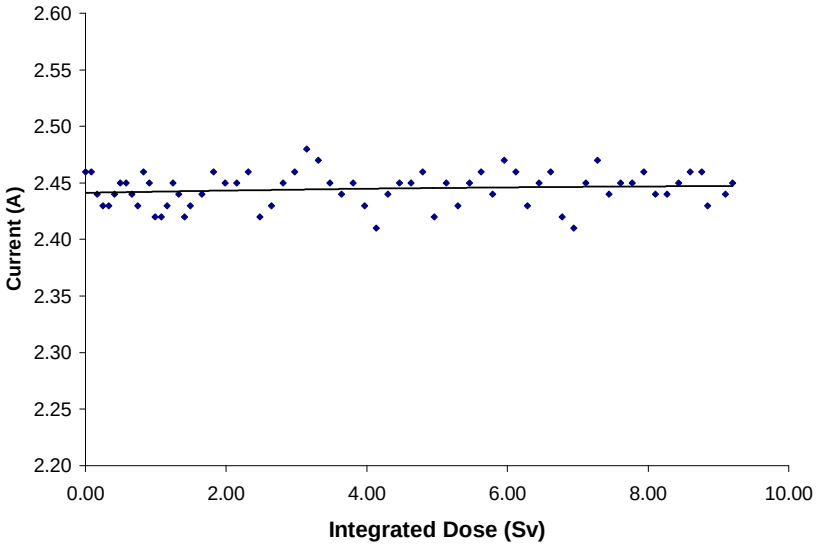

Fig. 8.6: Current behavior of Shoulder's RLM with the integrated dose.

Fig. 8.7 shows the response of Relay Logic Module of Waist driving mechanism of Radiation Protection Assistant Robot. The current was not found to vary. It remained about 2.35 A. The behavior of module is similar to other Relay Logic Modules. This card was found to work properly up to a total integrated dose of 9.5 Sv.

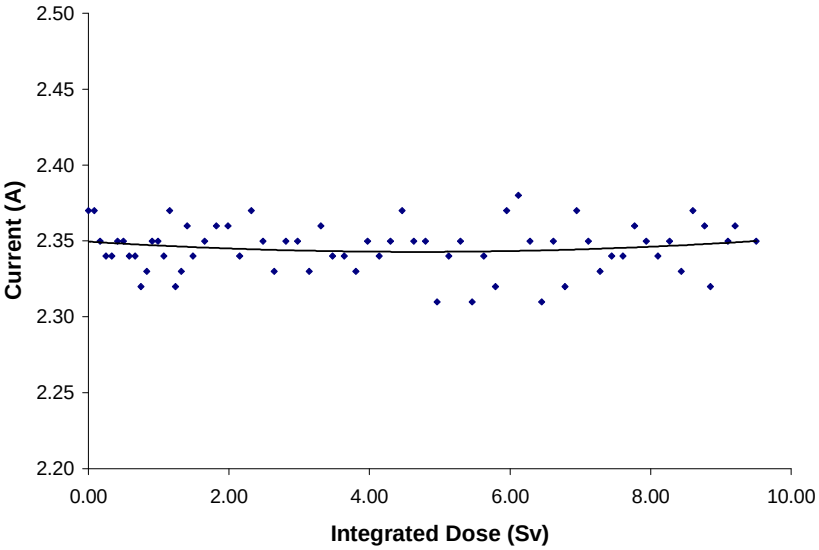

Fig. 8.7: Current behavior of Waist's RLM with the integrated dose.

Fig. 8.8 shows the response of Relay Logic Module of left Wheel's driving mechanism during irradiation. The current remained and the average value was 2.58 A. The behavior of module is similar to other Relay Logic Modules. This card was working satisfactorily up to a total integrated dose of 9.5 Sv.

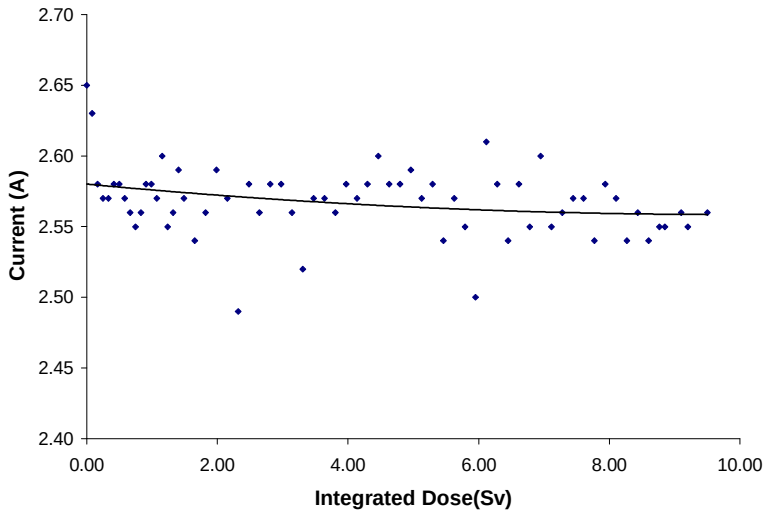

Fig. 8.8: Current behavior of left Wheel's RLM with the integrated dose.

Fig. 8.9 shows the response of Relay Logic Module of right Wheel's driving mechanism. The current remained constant at 2.71 A. There were random changes. This behavior is perfectly satisfactorily in the medium level irradiation i.e., up to 9.7 Sv.

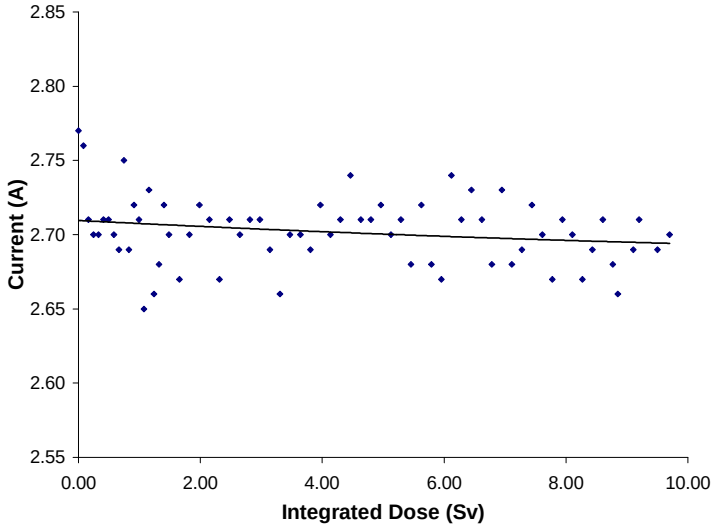

Fig. 8.9: Current behavior of right Wheel's RLM with the integrated dose.

8.5 CONCLUSION

This chapter presented the radiation hardening study of Radiation Protection Assistant Robot, designed and fabricated with locally available and non radiation hardened commercials components. The robot was exposed to a 29TBq ^{60}Co irradiation. The behavior of all the components remained essentially unchanged up to a dose of about 9 Sv. It may be noted that ideally, one may have irradiated the modules to even higher doses rates, however, it was not possible due to non-availability of stronger gamma sources.

It may also be pointed that when the irradiation was switched off, all the modules studied in this work restored the initial current. Therefore, it may be concluded that the irradiation up to 9 Sv has not produced any permanent effect on any module.

Furthermore, the maximum permissible dose is 20 mSv.y^{-1}. This means if the RPAR is working in gamma environment for one year and receive a dose of 9 Sv, then its worth is equivalent to 9×10^3 mSv/20 mSv/person = 450 persons.

CHAPTER
NINE

COST ANALYSIS OF RPAR

9.1 INTRODUCTION

During the last decades, the research and development in the category of mobile robots resulted in the appearances of many new mobile robots in a wide price range. Piperidis (2005) presented the survey of more then 56 up-to-date commercially available robotic vehicles. In Fig. 9.1, the price distribution for these commercially available mobile robots is presented. Almost half of them have a cost lower than US$1500. Complete Advance robotic systems for advance users and R &D purposes are available for US$10,000 to US$45,000 (Roboworld 2007 and Robosof 2007).

In the United States an average industrial robot cost the equivalent of US$115,000 in 1990. By 2001 the price had dropped to US$83,000. Prices in Europe were as low as

US$51,000 (USATODAY, 2002). A six-axis industrial robot developed by American company Adept cost about US$60,000 (Industrial Robotics, 2008).

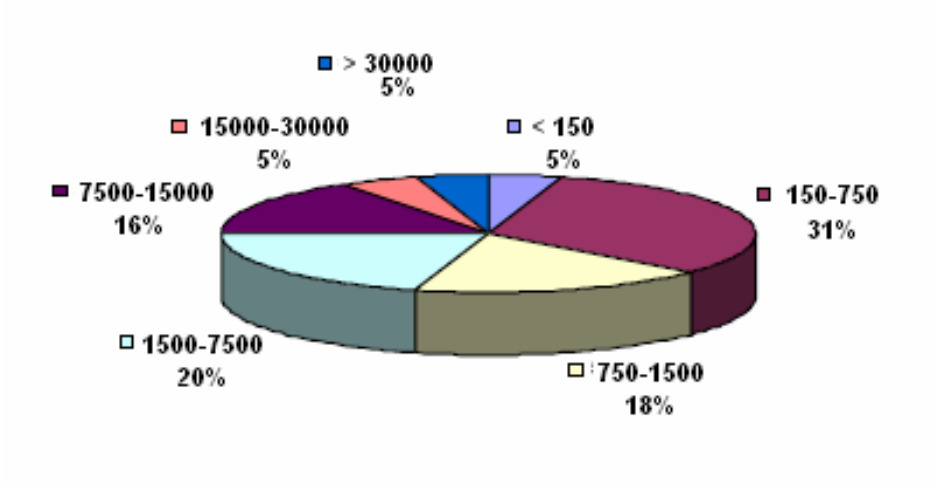

Fig.9.1: Prices (in US $) of the commercially available mobile robots.

The mobile robots, used for radiation environment are very expensive. Public Service uses a 700 pound Surbot-T machine for inspection of radioactive areas built by Remotec Inc. worth US$200,000 (Roman 1993). Minirover MK1 and MK2 built by Benthos Inc. were employed to work underwater. These robots cost from US$30,000 to US$50,000. (George 1990). The cost of Rosie used by U.S Department of Energy for Decontamination and Decommissioning was US$200,000 (ROSIE 1999) and Pioneer developed by RedZone robotics for Chernobyl reactor was US $ 3 million (Byron 1999).

RPAR has been designed and developed with off the shelf parts and locally fabricated machining parts. The main motivation to build locally is that such items are not easily available on import basis. Total cost of the RPAR is around Rs. 32,000 (US $500).

Cost of Laptop, Wireless assess point, tools and labor is not included in the total cost. Table 9.1 shows an item wise break down of the components used in RPAR.

Table 9.1: Item wise break down of Total cost.

Electronic/Electrical Components	QTY	Unit Cost (Rs.)	SUB-Total (Rs.)
H Bridge IC L298	02	100/-	200/-
IC 89C52	01	80/-	80/-
IC AD574A	01	100/-	100/-
IC HCC4529B	01	30/-	30/-
IC T820M	02	25/-	50/-
IC 74LS00	02	25/-	50/-
IC 4N25	30	20/-	600/-
IC 74LS245	01	25/-	25/-
IC 74154	01	35/-	35/-
IC 74LS367	04	25/-	100/-
IC 74LS11	02	25/-	50/-
IC 74LS04	01	25/-	25/-
IC 74LS07	01	25/-	25/-
IC 7805	03	25/-	75/-
Crystal 12 MHz	01	25/-	25/-
Push Switch, ST	07	10/-	70/-
Push Switch, DT	01	30/-	30/-
Two Way Switch	07	10/-	70/-
Transistor NPN C1384	02	10	20/-
Cable 8-pair	5y	40/-	200/-
Relay (5A DC 12V, SPDT)	02	30/-	60/-
Relay (10A DC 12V, DPDT)	05	50/-	250/-
FET (IRF640)	20	35/-	700/-
Bi-color LED 3.0 x 5.3mm Round	07	05/-	35/-
Connector 2 pins	10	10/-	100/-

Electronic/Electrical Components	QTY	Unit Cost (Rs.)	SUB-Total (Rs.)
Connector 6 pins	09	20/-	180/-
Connector 25 pins D type female	04	50/-	200/-
Connector 8 pins female	04	50/-	200/-
Connector 20 pins	03	50/-	150/-
Connector 15 pins	08	40/-	320/-
L298 Cooling Fan	02	50/-	100/-
Voltmeter 15V	01	350/-	350/-
Ammeter 20A	01	300/-	300/-
Automotive Ignition Switch.	01	150/-	150/-
Toggle Switch	01	50/-	50/-
Rechargeable battery 12V, 17Ah sealed lead-acid type	01	1200/-	1200/-
Limit Switches	15	50/-	750/-
Camera (Wireless)	01	2200/-	2200/-
Bread Board	10	70/-	700/-
Battery Charger	01	2000/-	2000/-
Voltage module 220V, 780 mA, +15 V 800 mA, and -15 V DC 800 mA.	01	500/-	500/-
Inverter 12 V to 220 V AC, 500 VA	01	1500/-	1500/-
Resistors, Capacitors, Diodes, LED, wires etc.	-	1000/-	1000/-
Total EEC			**14855/-**

Mechanical Components	QTY	Unit Cost (Rs.)	SUB-Total (Rs.)
DC geared motor	04	1000/-	4000/-
DC motor	03	800/-	2400/-
Speedo Meter Cable	01	250	250/-
Clutch Cable	01	70/-	70/-
Gripper	02	250/-	500/-

Mechanical Components	QTY	Unit Cost (Rs.)	SUB-Total (Rs.)
"O" Ring's	04	50/-	200/-
Nylon Wheel	02	150/-	300/-
Caster Wheel	01	150/-	150/-
Ball bearing 6200	02	100/-	200/-
Ball bearing 6203	04	100/-	400/
Worm Gear Set 1:30 ratio	01	500/-	500/-
Worm Gear Set 1:28 ratio	01	500/-	500/-
Worm Gear Set 1:100 ratio	01	1000/-	1000/-
Worm Gear Set 1:22 ratio	01	300/-	300/-
Spur Gear Set 1:7 ratio	01	200/-	200/-
Perspex Sheets	04	800/-	3200/-
MS Pipes, SS Sheets, rods etc.	-	2000/-	2000/-
Screws, Couplings, Connectors etc	-	2000/-	2000/-
		Total MC (Rs.)	**Rs. 17770/-**
		Grand Total (Rs.)	**32625/-**
		Grand Total (US $)	**494.72 or ~500**

9.2 COST BENEFIT ANALYSIS

For the future implementation of RPAR to be commercially viable, it must be a low cost machine. Furthermore it should have the potential to carry out all or most of the current tasks within the Reactor building or in any low radioactive environment. Some of these potential applications include radiation mapping, wipe testing of SRS, Transportation of radioactive materials produced for medical/agricultural applications etc.

As mentioned, the considerable economic and social costs related to the manual process of radiation work within a reactor building (especially labor costs and the human health risk, respectively) is more than balanced by the economic and social benefits of a

robot such as the RPAR. The benefits include, the less or limited employment of radiation workers, generation of radioactive waste (gloves, protective clothing, mask etc.) and the obvious reduction in human health hazards due to radiation.

The total cost of Radiation Protection Assistant Robot is very low as compared to available mobile robots for radiation assignments. The cost of RPAR is low because it is fabricated with non-hardened commercial components, ordinary or non conventional robotic parts and with cheapest labor.

This particular project has also commercial expectation; the initial development model has been designed to be used at PINSTECH. Such cost effective automation should therefore be relatively attractive to users. In addition to the cost consideration, all parts and material have been purchased from Pakistani distributors with nearly all of them being Islamabad based. Whilst this has been done to simplify the future manufacturing of the commercial product, the discerning Pakistani consumer was also considered. Finally, to enable the ease of reproduction, modification and replacement, almost all components are assembled from off the shelf parts or easily fabricated components.

It is also worth pointing out that the minimum wage of a radiation worker in Pakistan is about Rs. 6000/month, and maximum wage is about Rs. 18,000/month. Considering an average wage of Rs. 10,000/month, the annual salary is about Rs. 120,000/- per person, which is four times the cost of RPAR. Furthermore, RPAR can perform the work of almost 450 persons (Chapter 8) without endangering its performance. Therefore, it may be concluded that the use of robot such as RPAR is highly economical and also the humans can avoid radiation risk.

CHAPTER
TEN

WIPE TESTING OF SEALED RADIATION SOURCES USING RPAR

10.1 INTRODUCTION

Nowadays, growth in the demand of Sealed Radiation Sources (SRS) has increased due to their extensive application in high quality mass productions industry and other fields of bio and medical sciences. In industry, the main application of SRS is the non-destructive and fast quality control and material inspection. In nuclear medical centers and hospitals, the SRS are used for disinfection and sterilization of surgical and medical instruments, radio-imaging and radiotherapy. The SRS are also intensively used for radiation sterilization of a variety of food stocks items. Due to variety of uses, SRS are available with different made, types and activity. Because, all types of SRS are radioactive materials, therefore, frequent and strive monitoring is necessary for leakage/contamination during their use. The International Organization for Standardization (ISO) has classified standard

procedures (IOS 1992 and IOS 1999) for checking leakage and/or presence of loose radioactive contamination.

The standard leak test frequency ranges from six months to several years depending on the type and frequency of use. The SRS used for industrial radiography and other quality control and food stocks sterilization processes are of higher radiation strength; their leak test is recommended after six months (Leak Test 2008). Some SRS are used for small level sterilization in hospital and their leak test is recommended annually. The low strength SRS are used in level monitoring, moisture, soil and alignment gauges. For such SRS, the leak test is recommended after every 2 years. An integrity or leak test is not carried out for sealed source containing a radionuclide with a half-life of less than 30 days, liquid or gaseous radionuclide(s) or radionuclide with beta activity less than 185 MBq and/or gamma emitting material or not more than 185 kBq of alpha emitting material (Leak Test 2008). Sealed gaseous radionuclides are exempted from integrity testing because of the rapid escape of gases. The gaseous and liquid sealed radioactive sources are treated as radioactive materials (DOE 1994). The SRS used in smoke detectors and electron capture detector, and unsealed sources are not subjected to leak test. Similarly, electroplated sources are not tested with wipe test procedure. Furthermore, an indication of leakage is also obtained by checking the storage container for radioactivity (DOE 1999).

The wipe test is only suggested for long half-life gamma emitter radionuclides SRS. The wipe test equipment should be capable of detecting as low as 185 Bq of radioactive material on the test sample. Only record keeping is recommended when the wipe test indicates less than 200 Bq on SRS surface or 20 Bq on an equivalent surface of container (IAEA 1999). When a wipe test reveals the presence of leakage, the SRS is instantly withdrawn from the services and stored in a separate shielding container in secure interim storage. This is necessary to prevent the spread of radiological contamination. Moreover,

due to radioactivity the SRS handling represents a risk; hence specially designed hot cell, master-slave manipulators, special tools and equipments are required for SRS wipe tests.

In this study the Radiation Protection Assistant Robot (RPAR) has been utilized for the wipe testing. A total of five cylindrical SRS were subjected to wipe test. The radiation doses taken by RPAR were also measured as if it is a radiation worker conducting the test. By using a robotic arm, there is no need to follow the leak test procedures given by Thomas et al. (1975). The wipe tests were carried out by using Isopropyl alcohol and double-distilled de-ionized water.

10.2 MATERIAL AND METHODS

The RPAR has been designed and constructed to assist radiation workers in hazardous radiation environments (Zeb et al. 2007). It can be controlled manually through a remote consol or automatically through a task programme. The RPAR was used without any mechanical alteration or amendment in the present study. The RPAR picked and placed SRS directly from the shielding with the help of remote consol. The remaining procedure of wipe test, i.e. pressing and rolling over a wet cotton swab was carried out automatically with the help of a press and roll task programme. This programme is sufficient to wipe off thoroughly the external surface of SRS. When the programmed wipe test routine ended, the SRS was stored back in the shielding with the remote console. The whole operation was carried out in a hot cell with the help of an onboard RPAR'S WEB-Cam (Fig. 10.1), and a camera fitted inside the experimental room (Fig. 10.2).

Fig.10.1: View from onboard RPAR'S WEB-Cam

Fig.10.2: View from the camera fitted inside the experimental room

The swab holder mechanism consists of two perspex sheets with a polystyrene sheet, 3 mm thick, in between. The base tray has dimensions 110 × 60 × 5 mm. The swab

holder sheet (80 × 60 × 16 mm) at the top has a 1.5 millimeter deep cavity to hold a double folded wet cotton swab (20 × 20 mm). The polystyrene sheet provides the necessary flexibility to the swab holder sheet during testing. A list of the SRS used for the wipe testing is given in Table. 10.1.

Table 10.1: Lists of Sealed Radiation Sources

S. No.	SRS	Physical Form	Activity (MBq)
1.	^{60}Co	Cylindrical	87.4
2.	^{137}Cs	Cylindrical	4080
3.	^{137}Cs	Cylindrical	3140
4.	^{226}Ra	Cylindrical	1760
5.	^{226}Ra	Cylindrical	1660

10.2.1 WIPE-TEST WITH ISOPROPYL ALCOHOL

Five cotton swabs were prepared, one for each SRS. For each wipe test experiment the swab was moistened with analytical grade isopropyl alcohol (E. Merck, Germany), as the isopropyl alcohol moisten swab was found 100 times more efficient to wipe off the loose radioactive contamination compared to a dry swab (Ho and Shearer 1992). The wet cotton swab was placed in the cavity of the perspex tray. With the help of remote console of the RPAR a SRS was picked out of the shielding and was brought to a predefined position over the tray cavity. After adjusting a proper position of the RPAR gripper with the grabbed SRS, the press and roll task programme was started. This programme wiped the SRS five times over the wet cotton swab and rotated through 185 degrees at the same time. Each stroke consisted of two half strokes. In first half, the wiping was started from one side of the swab and continued towards the end with rubbing action. Then the subjected SRS was flipped over and second half was wiped in a similar way. The press and roll of SRS over the cotton swab is illustrated in Fig. 10.3. After completion of the task

programme for ten strokes, the wet cotton wipe was allowed to dry in open air. The dried smear was inserted and sealed in a small polystyrene sample counting vial with the help of forceps.

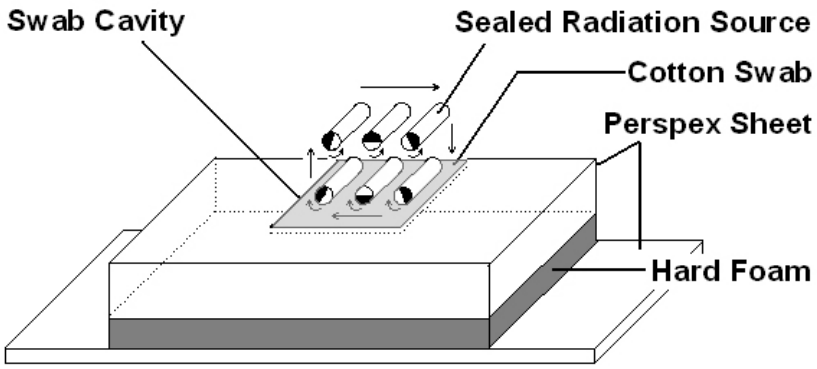

Fig.10.3: Press and roll of SRS over the cotton swab.

10.2.2 Wipe-Test with double distilled de-ionized water

The wipe test procedure was repeated with double distilled de-ionized water in a way similar to that of wipe test experiment with isopropyl alcohol. The wipes were allowed to evaporate till complete dryness and then inserted in small polystyrene counting vial.

10.3 MEASUREMENT OF RADIOACTIVITY

The measurement of leakage (radioactivity) was performed with a HPGe detector (Canberra Model AL-30) connected to a PC-based Intertechnique Multichannel Analyzer (MCA). "Intergamma, version 5.03" was used for data acquisition. The system has a resolution of 1.9 keV at 1332.5 keV peak of ^{60}Co and peak to Compton ratio of 40:1. The data files, containing γ-spectra were then used by our indigenously developed computer programme for activity calculations. In the calculation step background subtraction was applied for each swab.

10.4 RADIATION EXPOSURE RECEIVED BY RPAR

Each scrubbing stroke completed in 3 seconds. The RPAR conducted a single wipe test in about four minutes. To measure the radiation dose received by the RPAR, four thermoluminous dosimeters were used. Two dosimeters were mounted on the gripper and two were mounted on the waist segment.

10.5 RESULTS AND DISCUSSION

Each swab was subjected to gamma spectrometry for one hour. The spectrum shows only the background peaks. All the gamma spectra contained radionuclides originating from 238U and 232Th series, and from 40K. No radionuclide from any SRS was observed. The results indicate that all the wipe-tested SRS have no surface contamination and that the sources are leak tight and intact.

For all the SRS, the gripper and waist of RPAR received a total dose of 3.4 Gy and 208.9 mGy, respectively. The wipe testing was carried out in a hot cell. During this test, the operator remotely controlled the RPAR therefore, he did not receive radiation dose. The performance of the RPAR was found satisfactory in high radiation environment.

10.6 CONCLUSION

A robot having four degrees of freedom articulated robotic arm can perform wipe test on sealed radiation sources. The wipe testing is more convenient with a robot as compared to a master-slave manipulator inside hot cell. The master-slave manipulator has limited range and accessibility as compared to a mobile manipulator. The technique will protect the radiation workers from getting avertable ionizing radiation dose.

CHAPTER

ELEVEN

CONCLUSION AND FUTURE PROJECTS WITH RPAR

11.1 CONCLUSION

This thesis presented design and development of a Radiation Protection Assistant Robot using components available in local market. The mechanical, electrical/electronic, software design and developments have been handled single handedly as no such expertise are available in the country.

It has been designed and developed to assist radiation workers in those areas of nuclear installation that are beyond the safe approach for human. In a nuclear installation the congested work space and restricted time period is always problematic to work. This robot is expected to solve the problem to some extent.

Thesis presents detailed investigation and analysis of the kinematics and the manipulator Jacobian as it is the most important considerations to achieve better performance of a robotic device. The dynamics analysis of RPAR is presented using the recursive Newton-Euler formulation. This analysis also presented the behavior of torques or forces on the Shoulder and Elbow joints for different positions of Shoulder and Elbow segments. The results indicate that responses of torques satisfy design requirements in the anticipated workspace range of the articulated robotic arm of RPAR. Dynamics, kinematics and the manipulator Jacobian are also important for the maximum utilization of an articulated robotic arm system either with fixed or mobile platform.

Radiation hardening study was performed on different modules of RPAR to check their reliability in radiation field. The modules worked effectively up to a total integrated dose of 9 Sv (available in the country). Most of the modules remained unaffected and regained their original characteristics when the irradiation was switched off. Thus, RPAR can be used in low radiation environment for quite a long time. Its electronic modules were shielded with lead jacket filled with mineral oil to protect it from gamma and neutron radiations. This will further enhance its life.

Measurements have been carried out to compare the actual positioning and the calculated forward and inverse Kinematics. Repeatability range and payload capacity of RPAR was also measured. The results indicate a good agreement. The slight deviation and error in the position were due to physical errors such as less precise mechanical work and job accuracy, uncontrollable latch effect in the moving parts particularly in the gear modules etc. However, present study demonstrates that it is possible to develop a cost effective robotic device with most of the locally available commercial components. This is a successful step towards developing devices to assist radiation worker in a hazardous

radiation environment for safety and to avoid un-necessary radiation exposure risk. The robot is operational at PINSTECH for handling radioactive materials. It has been found to perform radiation mapping and wipe testing of sealed radiation sources.

The cost (US$500.00) of the robot is less than the three months salary of a radiation worker in Pakistan. Furthermore, it can perform work of more than 450 persons every year under the tested procedures.

11.2 FUTURE PROJECTS WITH RPAR

Design and development of an indigenous mobile robot is a tedious job especially in a developing country. Many features can be added to make it more reliable, accurate, effective and autonomous. It can also be modified for other tasks in hazardous chemical and biological environments. It can be used for fighting against terrorism after increasing its payload capacity for bomb disposal purposes. The possible modifications identified so far are as follow.

- Design and implement a digital controller to make its movements precise and control effective.
- Design of command protocol so that it can be operated over communication channels like wireless, Bluetooth etc
- Wireless RF controller can be used to make it wireless in a diameter of 2 km. This feature will be very helpful for handling radiation emergency and in bomb disposal task etc.
- Installation of sensors e.g. infrared, ultrasonic etc. will make the robot more intelligent, reliable and accurate.

However, all the above mentioned improvements are going to increase its cost.

REFERENCE:

Abel, E., and Watson, C. J. H., 1990, "A NEATER advance in active handling technology", *Nucl. Eng. Int.,* vol. 35, no. 430, pp.26.

Anderson, E. K., Robinson, C. W., and Heckendorn, F. M., 1992, "Specialized video systems for use in waste tanks, *"Proceedings, 40th Conference on Robotics and Remote Systems.* Chicago, Illinois, vol. 2, pp. 164-169.

Anouar, J., Aziz, Z., Zakia, E., Cosmo, C., and Shyam, M. K., 1999, "Displacement damages created by γ particles radiation in n type GaAs", *M. J. Condensed Matter*, vol. 2, no. 1, pp. 21.

Asada, H., and Slotine J. J., 1986, "*Robot Analysis and Control*", John Wiley & Sons, New York.

Bares, L. C., 1995, "Decommissioning? Why not use a robot?" *Nucl. Eng. Int.* vol. 40, o. 488, pp. 37-38.

Batanov, A. F., 1999, "The experience of application of remote control systems produced by Moscow state technical University for removal consequence of radioactive damages", *Proceedings, ANS 8th International Topical meeting on Robotics and Remote Systems.* Pittsburg, PA.

Bennett, P. C., and Posey, L. D., 1997, "*RHOBOT: Radiation Hardened Robotics*", SAND97-2405 UC-510, SANDIA Report, SNL, New Mexico, USA.

Boughman G., and Jones, S. L., 1992, "Robotic cleaning of radwaste tank nozzles", *Proceedings, 40th Conference on Robotics and Remote Systems.* Chicago, Illinois, vol. 2. pp. 68-72.

Burks, B. L., Armstrong, G. A., Butler, P. L., and Boissiere, P. T., 1991, "Combined long-reach and dexterous manipulation for storage tank applications," *Proceedings, 39th Conference on Robotics and Remote Systems.* San Francisco, California, pp. 139-144.

Byrd, J. S., 1995, ARISS: A Mobile Robot Inspector, in: *Proceedings of the ANS 6th Topical on Robotics & Remote Systems*, Monterey, CA.

Byrd, J. S., and Pettus, R. O., 1996, "A robotic inspector for low-level radioactive waste", *Proceedings of the 2nd Specialty Conference on Robotics for Challenging Environments,* Albuquerque, New Mexico, pp. 276-282.

Byron, Spice., 1999, "U.S. robot in Ukraine for continuing cleanup at ruined Chernobyl reactor", . http://www.post-gazette.com/healthscience/19990430pioneer2.asp.

(Accessed on 24th October 2008).

Carignan, C., and Howard R., 2000, "A partitioned redundancy management scheme for an eight-joint revolute manipulator", *Journal of Robotic Systems,* vol. 17, No.9, pp. 453-468.

Charles, C. Foster., 2003, "Total Ionizing Dose and Displacement Damage Effects in Microelectronics", *Materials Research Society Bulletin*, pp. 136-140.

Corke, P. I., 1996, "A robotics toolbox for MATLAB", *IEEE robotics & Automation Magazine*, vol. 3, No. 1, pp. 24-32.

Cox, D. J., 1999, "Requirements for modular dyal-arm robot architecture for use in deactivation and decommissioning tasks", *Proceedings, ANS 8th International Topical meeting on Robotics and Remote Systems*. Pittsburg, PA.

Critchlow, Arthur J., 1985, "*Introduction to Robotics*", Macmillan publishing company, New York.

Denavit, J., and Hartenberg, R. S., 1955, "A Kinematics Notation for Lower Pair Mechanisms Based on Matrices", *Journal of Applied Mechanics,* vol. 77, pp. 215-221.

Department of Energy. 1994, *Implementation Guide for Occupational Radiation Protection*: Sealed Radioactive Source Accountability and Control; G-N 5400.9/M1 - Rev. 1.

Department of Energy, 1999, *Sealed radioactive source accountability and control guide*. USA. DOE G 441.1-13.

Desbats, P., Andriot, C., Gicquel, P., Viallesoubranne J. P., and Souche, C., 1999, "Using industrial robots in nuclear fuel reprocessing facilities force feedback teleoperation control", *Proceedings, ANS 8th International Topical meeting on Robotics and Remote Systems*. Pittsburg, PA.

Desbats, P., Toubon, H., and Piolain, G., 2004, "Status of Development of Remote Technologies Applied to COGEMA Spent Fuel Management Facilities in France", *Proceedings of ANS 10th International topical meeting in robotics and remote systems for hazardous environment,* Gainesville, Florida, USA.

D'Souza, A., Vijayakumar, S., and Schaal, S., 2001, "Learning Inverse Kinematics", In *Proceedings of International Conference on Intelligent Robots and Systems,* IEEE/RSJ, Maui, Hawaii, USA.

Fryatt, A., 1994, "Radiation-tolerant robots improve nuclear maintenance", *Nucl. News.* pp.54.

Gebel, A., and Fontcuberta, P., 1994, "Equipment for the recovery of U.D.O.s from storage and reactor pools", *Proceedings, 42nd Conference on Robotics and Remote Systems.* New Orleans, Louisiana, vol. 1, pp. 87-94.

George. H., 2007, The Service Robot Lumbers Off the Drawing Board http://query.nytimes.com/gst/fullpage.html?res=9C0CE4D9123AF931A2575BC0A966958260&sec=&spon=&pagewanted=all (Accessed on 27th December 2007).

Gerriets, W., 1992, "TROD cleans up at Nine Mile Point 1", *Nucl. Eng. Int.* vol. 37, no. 452, pp. 32-34.

Glass, S. W., Levesque, M. L., Engels, G. J., Klahn, F.C., and Fairbrother, D.B., 1999, "Underwater robotic tools for nuclear vessel and pipe examination", *Proceedings ANS 8th International Topical Meeting on Robotics and Remote Systems.* Pittsburgh, P.A.

Glassell, R. L., Killough, S. M.., Lioyd, P. D., Love, L. J., Randolph, J. D., Hoesen, S. D. Van., Blank, J. A. B., Burks, L., DePew, R. E., Glover, W. H., Falter D. D., and Vesco, D. P., 1999, "Use of the modified light duty utility arm to perform nuclear waste cleanup of underground waste storage tank at Oak Ridge National Laboratory", *Proceedings, ANS 8th International Topical meeting on Robotics and Remote Systems.* Pittsburg, PA.

Gossett, C. S., Hughlock, B. W., Katoozi, M., LaRue, G. S., and Wender, S. A., 1993, "Single Event Phenomena in Atmospheric Neutron Environments", in: *IEEE Trans. on Nuclear Science,* vol. 40, Issue 6, Part 1-2, pp. 1845-1852.

Griebenow, B. L., Selleck, C. B., Strope, L. A., and Burke, J. B., 1991, "Imaging, inspection, and characterization systems for underground storage tank remediation", *Proceedings, 39th Conference on Robotics and Remote Systems.* San Francisco, California, pp. 145-150.

Griebenow, B. L., Conner, C. C., and Christenson, C., 1992, "Remote inspection of underground storage tanks", *Proceedings, 40th Conference on Robotics and Remote Systems.* Boston, Massachusetts, vol. 1, pp. 84-88.

Hazen, F. B., 1994, "Robotics for waste storage inspection: a user's perspective", *Proceedings, 42nd Conference on Robotics and Remote Systems.* New Orleans, Louisiana,. vol. 1, pp. 147-154.

Hendrich, K., Wiese, H., and Katzenmeier, G., 1999, "One year ahead of remote dismantling of the German prototype spent fuel reprocessing plant Karlsruhe", *Proceedings, ANS 8th International Topical meeting on Robotics and Remote Systems.* Pittsburg, PA.

Ho, S. Y., and Shearer, D. R., 1992, Radioactive contamination in hospitals from nuclear medicine patients. *Health Phys.* 62:462-466.

Houssay, L. P., 2000, *Robotics and Radiation Hardening in the Nuclear Industry*, M. Sc. Thesis, University of Florida.

IAEA, 1996, "*International Basic Safety Standards for Protection against Ionizing Radiation and for the Safety of Radiation Sources*", Safety Series No. 115, IAEA, Vienna.

IAEA, 1999, "*Radiation Protection and Safety in Industrial Radiography*", Safety Reports Series No. 13.

Iborra, A., Pastor, J. A., Álvarez, B., Fernández, C., Fernández-Meroño, J. M., 2003, Robots in Radioactive Environments, *IEEE Robotics and Automation Magazine,* 10 (4), 12-22.

Industrial Robots., 2008, "Learn about Industrial Robots", http://www.learnabotrobots.com/industrial.htm.

(Accessed on 22 January 2008).

International Organizations for Standardization, 1992, *Radiation Protection - Sealed Radioactive Sources - Leakage Test Methods*, ISO 9978.

International Organizations for Standardization, 1999, *Radiation protection - Sealed radioactive sources - General requirements and classification*, ISO 2919.

Ivanov, A., Ivanov, A., Borovoi, A., and Kluchnikov, A., 1999, "Main results of using of remote controlled systems inside the Chernobyl "sarcophagus" rooms and some unsolved problems", *Proceedings, ANS 8th International Topical meeting on Robotics and Remote Systems*. Pittsburg, PA.

Jaquish, W. R., Shen, E. J., and Yount, ad, J. A., 1991, "Robotic Technology demonstration program for underground storage tank remediation", *Proceedings, 39th Conference on Robotics and Remote Systems,* San Francisco, California, pp. 133-138.

Johnston, A. H., 1984, "Super recovery of total dose damage in MOS devices", *IEEE Trans. on Nucl. Sci.,* vol. NS-31, no. 6, pp. 1427-1433.

Johnston, A. H., 2000, "Radiation Damage of Electronic and Optoelectronic Devices in Space", *4th International Workshop on Radiation Effects on Semiconductor Devices for Space Application,* Tsukuba, Japan.

Kathren RL, editor., 1980, *A guide to Reducing Radiation Exposure to as Low as Reasonably Achievable (ALARA).* Washington D. C.: Division of Operational & Environmental Safety; Contract No.:EY-76-C-06-1830. Prepared for U.S. Department of Energy, Assistant Secretary for Environment.

Kimura, M., Okano, H., and Shimada, H., 1995, "The 15 cm inspection robot", *Nucl. Eng. Int.* vol. 40, no. 495, pp.52-53.

Leak Test, 2008, Directorate Radiation Control (DRC). Department of Health. www.doh.gov.za/department/radiation/codeofpractice/radionuclides/leaktests.pdf. (Accessed on 24th April 2008).

Luera, T. F., 1993, Personal Communication, *SNL, Dept.* 9363.

Malaugh, J., and Monaghan, D., 1994, "CECIL lances Bruce's boilers", *Nucl. Eng. Int.* vol. 39, no. 476, pp.23-25.

Marian, F. A., and Rowan H. T., 1987, "The Cost-Benefit of Robotic Devices in Nuclear Power Plants", *Public Service Electric and Gas Company,* New Jersey, USA.

Marshall, P. W., Dale, C. J., Summers, G. P., Wolicki, E. A., and Burke, E. A., 1989, "Proton, neutron and electron-induced displacement damage in germanium", *IEEE Transactions on Nuclear Science,* vol. 36, Issue 6, pp. 1882 – 1888.

Mavroidis, C., Dubowsky, S., Drouet, P., Hintersteiner, J., and Flanz, j., 1997, "A systematic error analysis of robotic manipulators: application to a high performance medical robot", *Proceedings of the IEEE Int. Conference of Robotics and Automation*, Albuquerque, New Mexico, pp. 980–985.

May, T. C., and Woods, M. H., 1979, "Alpha-Particles Induced Soft Errors in Dynamic Memories", in: *IEEE Trans. on Electron Devices*, vol. 26, Issue 1, pp. 2-9.

Meggiolaro, M., Dubowsky, S., Mavroidis, C., 2005, "Geometric and Elastic Error Calibration of a High Accuracy Patient Positioning System", *Mechanism and Machine Theory*, Vol. 40, No. 4, pp. 415-427.

McKee, W.R., McAdams, H.P., Smith, E.B., McPherson, J.W., Janzen, J.W., Ondrusek, J.C., Hyslop, A.E., Russell, D.E., Coy, R.A., Bergman, D.W., Nguyen, N.Q., Aton, T.J., Block, L.W., Huynh, V.C., 1996, "Cosmic Ray Neutron Induced Upsets as a Major Contributor to the Soft Error Rate of Current and Future Generation DRAMs" in: *IEEE Intl. Reliability Physics Symposium, 34th Annual Proc.*, pp. 1-6.

Mittal, R. K., and Nagrath, I. J., 2005, "*Robotics and Control*", Tata McGraw-Hill Publishing, New Delhi.

Murchie, B., and Reinhardt, M., 1995, "Plucking a loose weld rod from the depths of a boiler", *Nucl. Eng. Int.* vol. 40, no. 487, pp.26-27.

Newman Tools Inc., 2007, Neolube No. 2: Lubricant Colloidal Graphite in Isopropanol. http://www.newmantools.com/chemicals/neo2pds.htm (Accessed on 6 September 2007).

Noakes, M. W., 1999, "Dual arm work module development and applications", *Proceedings, ANS 8th International Topical meeting on Robotics and Remote Systems*. Pittsburg, PA.

Nucl. Eng. Int., 1990, "Robots deliver real benefits for PSE&G", vol. 35, no. 435, pp.120-121.

Nucl. Eng. Int., 1992, "Franco-Us co-operate on Cobra/Aramis", vol. 37, no. 452, pp.39.

Nucl. Eng. Int., 1994, "Making tracks to clean-up after accidents", vol. 39, no. 476, pp. 26.

Nucl. Eng. Int., 1996, "MACS makes maps of contamination", vol. 41, no. 503, pp.18-20.

Nucl. Eng. Int., 1998, "Cleaning up a spent resin spill", vol. 43, no. 529, pp.20-22.

Orwantschke, D., 1995, "Dismantling Niederaichbach. A lesson in remote-controlled decommissioning, *Nucl. Eng. Int.* vol. 40, no. 493, pp.16-18.

Peck, D. S., 1963, "Surface effects of radiation on transistors", *Bell Syst. Tech. J.,* vol. 42. pp. 95.

Piperidis. S., 2005, *Design and Implementation of the ALE robotic Vehicle*, Master Thesis, Technical University of Crete, Dept. of Production Engineering and Management.

Premier Technology Inc., 2007, Mineral Oil Filled Windows. http://www.premiertechnology.cc/premier/RadiationShieldingWindows.cfm (Accessed on 6 September 2007)

Reinhardt, M., Barbito, K., and K. Baughman., 1997, "Going a bundle on steam generator inspection and cleaning UBIB & UBHC", *Nucl. Eng. Int.* vol. 42, no. 518, pp.38-41.

Rizzo, J., 1991, "Small underwater/land robotic vehicles and related technology", *Proceedings, 39th Conference on Robotics and Remote Systems.* San Franciso, California, pp. 10-15.

Roboworld,2007, http://www.roboworld.com.sg/roboshop/product_list.aspx?Category=Adance+Robotics, (Accessed on 27th December 2007).

Robosoft, 2007, http://www.robosoft.fr/eng/sous_categorie.php?id=1029, (Accessed on 27th December 2007).

Roman, H. T., 1993, Robotic applications in PSE&G's nuclear and fossil power plants, *IEEE Transaction on Energy Conversion, Newark*, NJ, vol. 8(3), PP 584-592.

Rosen, D., 1999, "Reducing critical path IVVI time through the use of submersibles", *Proceedings, ANS 8th International Topical meeting on Robotics and Remote Systems.* Pittsburg, PA.

ROSIE, 1999, *Mobile Robot Worksystem, OST #1799*, Innovative Technology Summary, Report DOE/EM-0429, US. Department of Energy.

Schreiner, S. I., 1994, "Internal pipe inspection devices for use in radiation survey application", *Proceedings, 42nd Conference on Robotics and Remote Systems.* Washington, D. C., vol. 2, pp. 16-21.

Schemf, H., 1994, "Houdini: in-tank mobile cleanup robot", *ASCE Specialty Conference on Robotics for Challenging Environments*, Albuquerque, New Mexico, pp. 286-295.

Slifko, A., Catalan, M., and Denmeade, T., 1999, "PIONEER, a robot for structural assessment, of the Chernobyl shelter", *Proceedings, ANS 8th International Topical meeting on Robotics and Remote Systems.* Pittsburg, PA.

USATODAY., 2008, "Robots poised to make way from tech fringes to mainstream life", http://www.usatoday.com/tech/news/techinnovations/2002-10-02-robot-future_x.htm, (Accessed on 22nd January 2008).

Thomas, J., Pasternack, B. S., Bohning, D. E., and Vacirca, S. J., 1975, Methods for reducing exposure to personnel leak-testing sealed radium sources. *Health Phys.* 28:111-121.

Tsai, Lung-Wen., 1999, "*Robot Analysis: the mechanics of serial and parallel manipulators",* John Wiley & Sons Inc., USA.

Vandegriff, K. U., 1990, Designing equipment for use in radiation environments *ONRL/TM-11175.*

Weber, P. J., and Vanecek, C. W., 1990, "SIMON combines radiation hardness with computer power", *Nucl. Eng. Int.* vol. 35, no. 430, pp. 34-38.

Wiesman, R. M., 1992, "GRI's internal inspection system for piping network", *Proceedings, 40th Conference on Robotics and Remote Systems*. Chicago, Illinois, vol. 2, pp. 109-115.

Willis, W. D., Anderson, M. O., and McKay, M. D., 1999, "The remote underwater characterization system", *Proceedings, ANS 8th International Topical Meeting on Robotics and Remote Systems*. Pittsburgh, PA.

Winokur, P. S., Sexton, F. W., Schwank, J. R., Fleetwood, D. M., Dressendorfer, P. V., Wrobel, T. F., and Turpin D. C., 1986, "Total-dose radiation and annealing studies: implications for hardness assurance testing," *IEEE Trans on Nucl. Sc*i., vol. 33, no. 6, pp. 1343-1351.

Wolovich, W. A., 1987, "*Robotics: Basic Analysis and Design*", CBS college publishing, New York.

Xia, Y., and Wang, J., 2000, "A Dual Neural Network for Kinematics Control of Redundant Robot Manipulators", *IEEE Transactions on systems, man, and cybernetics, part b: cybernetics,* vol. 31, no.1.

Zeb, J., Rashid, F., Iqbal, N., and Ahmed, N., 2007, A simple and low cost radiation protection assistant robot for multipurpose tasks. *Proceedings of National Conference on Information and Communication Technologies (NCICT-2007)*; Bannu, pp. 81-87.

APPENDIX-A

SPECIFICATIONS of RPAR

Axis		*Waist*	*Shoulder*	*Elbow*	*Wrist*
Joint		Rotary	Rotary	Rotary	Rotary
Actuator		DC motor	DC motor	DC motor	DC motor
Stroke (deg)		195	110	180	210
Speed (deg/sec)	*(Up/CCW)*	5.42	4.32	11.61	18.94
	(Down/CW)	6.09	6.11	17.65	17.43
Stroke cycle time (sec)	*(Up/CCW)*	35.98	25.46	15.50	11.09
	(Down/CW)	32.02	18	10.19	12.05
Safe Gripping range (max)		12.0 cm			
Total operational time		85 minutes			
Reach		122.50 cm			
Payload		2100 g			
Power Supply		12 V DC/17Ah Battery			
Power consumption		50.76 watts			
Gross weight		55.6 kg			
Speed of Mobile Platform		24.4 cm/s			
Radiation Hardening Study		Up to 9.2 Sv			